THE HONG KONG POLYTECHNIC UNIVERSITY

Department of Electrical Engineering

Probabilistic Small Signal Stability Analysis for Power Systems with Plug-in Electric Vehicle and Wind Power Integration

HUANG HUAZHANG

A thesis submitted in fulfillment of the requirements for the degree of Doctor of Philosophy

August 2012

CERTIFICATE OF ORIGINALITY

I hereby declare that this thesis is my own work and, to the best of my knowledge and belief, it reproduces no material previously published or written nor material which has been accepted for the award of any other degree or diploma, except where due acknowledgement has been made in the text.

_____ (Signed)

_____Huazhang Huang___ (Name of student)

Abstract

Small signal stability analysis (SSSA) is one of the most significant tools for evaluating the rotor angle stability issue of power system operation and control, especially in interconnected power networks. Due to the rapid increase of renewable energy sources, especially wind power, integration of these new kinds of generations result in new impacts on dynamic stability of power system; these effects need to be considered and estimated by SSSA more carefully. The mainstreaming devices adapted in wind farms are fixed-speed induction generator (FSIG) and double-fed induction generators (DFIG) based wind energy conversion systems (WECS), which have controllability by a bidirectional converter, thus providing flexible operation.

This thesis is devoted to study the damping performance of power system impacted by WECS and also damping enhancements from WECS. As the mechanical torque oscillations from wind turbine model were not taken into account before, impacts from wind shear and tower shadow are focused upon and relevant estimations are made first. A damping enhancement with neural network and adaptive fuzzy control theory is proposed to improve the operational performance with such oscillations.

By taking advantage of the controllable type WECS, a power oscillation damper (POD) has been implemented in the decoupled control system of DFIG.

Parameters of the POD are optimized by a widely used algorithm, which with shorter optimization time can provide higher quality solutions, i.e. the modified particle swarm optimizer (MPSO). Its performance has been evaluated by eigenvalues of electro-mechanical oscillation modes in the system from SSSA and also transient simulations for observing the power angle differences and electrical power torque of synchronous generators.

However, wind power is acknowledged as a stochastic source. The power output of a wind farm is undispatchable and difficult to be completely and accurately predicted. An analytical method based probability theory for probabilistic SSSA is proposed in this thesis for accounting for the variation of wind farm power output when designing damping controllers for DFIG-based WECS. The coordination with other damping controllers in the system such as power system stabilizers (PSS) for synchronous generators also has been studied. Case study results confirm that damping control scheme by the proposed method can consistently enhance system stability with synchronous machines and DFIG-based WECSs, under a wide range of operating conditions of DFIG.

Recently, with the fast development of plug-in electric vehicles (PEVs) and large rating chargers allocated in charging stations, the potential storage capability of battery based PEVs is planned to work in coordination with wind farms. The joint effects of these two new establishments on rotor angle stability are intended to be studied. Similar to wind power, PEV is also a kind of stochastic source. It is significant to consider stochastic effects of both on power

system stability. In this thesis, a simulative method with high efficiency, quasi Monte-Carlo (QMC) based probabilistic SSSA method is proposed to evaluate the damping impacts. Negative damping effect found in the system, from PEVs, is proven by both the study of different scenarios and individual analysis. Compared to commonly using simulative method Monte Carlo simulations (MCS), QMC can provide a more reliable result with a shorter computational time.

List of Publications

Journal paper:

1. Huazhang Huang and C.Y. Chung, "Coordinated damping control design for DFIG-based wind generation considering power output variation," *IEEE Trans. Power Syst*., vol. 27, no. 4, pp. 1916-1925, Nov. 2012.
2. Huazhang Huang, C.Y. Chung, K.W. Chan, and Haoyong Chen, "Quasi-monte carlo based probabilistic small signal stability analysis for power systems with plug-in electric vehicle and wind power integration," *IEEE Trans. Power Syst., Submitted.*
3. Huazhang Huang and C.Y. Chung, "Adaptive neuro-fuzzy controller for SVC to damp out wind energy conversion system oscillation," *IET Proc.- Generat. Transmiss. Distrib., Accepted.*

Conference paper:

1. Huazhang Huang and C.Y. Chung, "Design of a power oscillation damper for DFIG-based wind energy conversion system using modified particle swarm optimizer," in *Conf. of Sixth Asia Modeling Symposium* (*AMS*), Indonesia, May, 2012.

Acknowledgements

I would like to express my sincere gratitude to Dr. C.Y. Chung, my chief supervisor in the Department of Electrical Engineering, The Hong Kong Polytechnic University. His supervision and guidance have helped me overcome all obstacles during the PhD study. This work could not have been completed without his vast knowledge and the encouragement he gave me. And my co-supervisor Prof. K.P. Wong, I have benefited so much from his invaluable suggestions and guidance.

I appreciate my colleagues and classmates contribution in terms of useful suggestions on the research. I also acknowledge the emotional support my family provided during my study in Hong Kong.

The studentship support from the Department of Electrical Engineering and Research Office is gratefully acknowledged.

Table of Contents

List of Figures

List of Tables

List of Symbols

a	Tower radius
A	Area swept by the turbine blades
c_i	Center of Gaussian function
c_n	Center of the hidden nodes
C_ρ	Power coefficient of wind turbine
f_i	Constant value in zero-order Sugeno fuzzy model
H	Elevation of rotor hub
K	Gain of compensation
M	Coefficient, $M=1+\alpha(\alpha-1)R^2/8H^2$
m_i	Merge of Gaussian function
n	Number of compensation stages
N	Number of hidden nodes
p	Number of poles
pf	Penalty factor for preventing overshoot
P_M	Mechanical power of wind turbine
r	Gear box ratio
R	Radial distance from rotor axis
t	Time
T_1, T_2,T_3, T_4	Time constant of compensation
T_M	Mechanical torque of wind turbine

T_W	Time constant of wash-out filter
V_H	Wind speed at hub height
V_{ws}	Equivalent wind speed caused by wind shear
V_{ts}	Equivalent wind speed caused by tower shadow
w_0	Biasing term
w_i	Firing strength of a rule
w_n	Weights between the hidden layer and output
x	Distance between blade origin and tower midline
x_p	Input of Gaussian function in RBF network
α	Empirical wind shear exponent
β	Pitch angle of blades
η	Learning rate
θ	Azimuthal angle of the turbine blade
θ_b	Azimuthal angle of one blade, the other two have a deviation value of 120 °
λ	Tip speed ratio
ρ	Air density
σ_n	Width of the hidden nodes
ω_s	Synchronous speed in rad/s
ω_T	Rotational speed of wind turbine
d	Direct axis
q	Quadrature axis

r	Rotor
s	Stator
v	Voltage
R_s	Stator resistances
R_r	Rotor resistances
i	Current
w_s	Stator electrical speed
w_r	Generator rotor speed
ψ	Flux linkage
L_s	Self-inductance of the stator windings
L_r	Self-inductance of the rotor windings
L_m	Mutual inductance between stator and rotor windings
ψ_{qr}, ψ_{dr}	Rotor flux linkage
e_d, e_q	Direct and quadrature axis voltage behind the transient reactance
i_{dr}, i_{qr}	Rotor currents
X	Open circuit reactance equal to $w_s L_s$
X'	Transient reactance equal to $w_s(L_s - L_m^2/L_r)$
T_0	Rotor open circuit time constant equal to L_r/R_r
$2H$	Moment of the inertia
T_m	Mechanical torque

T_e	Electrical torque
V_w	Wind velocity
K_{px}	Proportional gains
K_{ix}	Integral gains
w_{ref}	Reference generator rotor speed
σ	Real part of eigenvalue
ω	Imaginary part of eigenvalue
f	Oscillation frequency
ζ	Damping ratios
ζ_s	Acceptable damping ratio
PF_1, PF_2	Penalty factors
l	Total number of electromechanical oscillation modes
w	PSO momentum or inertia coefficient
c_1, c_2	Parameters determine how far a particle will move during one iteration
$rand_i()$	Random numbers between 0 and 1
K	Shape parameters of Weibull distribution
C	Scale parameters of Weibull distribution
p_{rated}	Rated power
V_{ci}	Cut-in speed
V_{rs}	Rated speed

V_{co}	Cut-off speed
a_i	Regression constants identified by curve fit tools
V	Nodal voltages
S	Nodal injections
λ	Eigenvalues
μ	Expectation
σ^2	Variance
J_λ	First order derivative matrix $\partial\lambda_k/\partial V_i$ of eigenvalue λ
$npss$	Total number of PSSs
e_a, e_b and e_c	Source voltages
e_d, e_q	Input voltages in the synchronous rotating frame
i_d, i_q	Input currents in the synchronous rotating frame
i_b	Input current of battery
i_d^*, i_q^*	Reference values for decoupled current variables
U_{dc}^*	Reference value for dc side voltage
i_1	Current flowing in the resistor R_1
C_1R_1	Time constant
Q_e	Extracted charge
θ	Electrolyte temperature
θ_a	Ambient temperature
C_θ	Battery thermal capacitance

R_θ	Battery thermal resistance
P_s	Thermal power generated internally in the battery
μ_P	Expectation selected from data of base case
σ_P	Standard deviation
erf^{-1}	Inverse error function
r	Uniformly distributed variable
D	Daily driving distance
D_{max}	Maximum distance
t_s	Serviced time
T_μ	Mean in exponential distribution
$P_{EV,i}$	Instant power demand
λ_μ	Expected value in Poisson distribution
N	Total number of PEVs
M	Lowest integer
$a_k(n)$, h_j	Either 0 or 1
$\oplus$	Bit-by-bit exclusive-or operator
v_k	So-called direction number
F	Primitive polynomials
Φ_i	Right eigenvector
PF_{ki}	Participation factor, a measure of the relative participation of the *k*th state variable in the *i*th mode
$F(\varsigma_i)$	CDF of ς_i

σ	Standard deviation
s	Skewness
k	Kurtosis

List of Abbreviations

ANFIS	Adaptive Neuro-Fuzzy Inference System
AVR	Automatic Voltage Regulation
CDF	Cumulative Distribution Function
CSWT	Constant Speed Wind Turbine
DCC	Direct Current Control
DDSG	Direct Drive Synchronous Generator
DFIG	Doubly Fed Induction Generator
EV	Electric Vehicle
FACTS	Flexible AC Transmission Systems
FDLF	Fast Decoupled Load Flow
GA	Genetic Algorithms
GSC	Grid Side Converter
LDS	Low Discrepancy Sequences
MCS	Monte-Carlo Simulations
MPPT	Maximum Power Point Tracking
MPSO	Modified Particle Swarm Optimization
OLTC	On-Load Tap Changer
PDF	Probability Density Function
PEV	Plug-in Electric Vehicle
PF	Participation Factor

PI	Proportional Integral
POD	Power Oscillation Damper
PSAT	Power System Analysis Tool
PSO	Particle Swarm Optimization
PSS	Power System Stabilizer
PSSSA	Probabilistic Small Signal Stability Analysis
PWM	Pulse-Width Modulation
QMC	Quasi-Monte Carlo
RSC	Rotor Side Converter
SCIG	Squirrel Cage Induction Generator
SDC	Supplementary Damping Controller
SG	Synchronous Generators
SMIB	Single Machine Infinite Bus
SOC	State-Of-Charge
SRF	Synchronous Rotating Frame
SSSA	Small Signal Stability Analysis
TSRC	Tip-Speed Ratio Control
VSWT	Variable Speed Wind Turbine
WECS	Wind Energy Conversion Systems

Chapter 1 Introduction

1.1 Background

Since the world-wide energy crisis in the 1970s, environmental pollution and energy shortages have become perennial problems for the modern civilized society. With the growing environmental awareness and the sense of crisis, governments are making efforts to develop their own energy policies, resulting in new opportunities in areas such as wind, solar, tidal and geothermal energy. These developments have been reshaping the electric power industry in a manner that is giving rise to new opportunities, as well as challenges, mainly in terms of the need for development of sustainable energy. Since the mid-1980s, application of wind energy conversion technology has attracted universal attention. With rapid development of modern science and technology, new types of wind turbines like aerodynamics, aerospace technology and high capacity power electronics, besides Wind Energy Conversion Systems (WECS) have considerably developed in the past three decades.

According to official data, wind power capacity has grown at an average annual rate of 22% from 1990s onwards. From 1997 to 2002, worldwide installed capacity of wind power reached 32,039 GW of which 7,231 GW of new capacity was added in 2002 alone. At the end of 2011, worldwide nameplate capacity of wind-powered generators was 238 GW, representing a growth of 41 GW over the

preceding year.

The majority of WECS are erected with an extended electricity grid such as substations and transmission lines, in order to be connected to the power grid. Wind power penetration in modern power systems has significantly increased. The behavior of power systems is largely determined by the behavior and interaction of the types of generators that are connected to it. When a large number of WECS are connected to a system and they replace a substantial fraction of the output of conventional synchronous generators, they start to affect various aspects of the system's behavior.

In WECS, generators are different from the conventional synchronous generator traditionally used in power plants. Other types of generators such as Squirrel Cage Induction Generator (SCIG), Doubly Fed Induction Generator (DFIG) and Direct Drive Synchronous Generator (DDSG) are grid coupled by a power electronics converter. For normal operation of an electric power system, it is essential that generation and load are balanced and the small signal stability of the system is assured. Therefore, much attention has been paid to WECS impact on power system's small signal stability.

The future technologies related to Hybrid Electric Vehicles (HEV) or Electric Vehicles (EV) constitutes the most feasible alternatives to reduce greenhouse gases emissions from automobiles. Plug-in Hybrid Electric Vehicles (PHEV) or Electric Vehicles (PEV) and Vehicle-to-grid (V2G) concepts are the recent inventions. Financial and environmental implications of advancements in

technologies for battery and hybrid-electric power and concerns related to energy security have resulted in increasing interest in these concepts. It is expected that by 2030, the penetration of PEVs will be 25%, which would represent a large additional load on power systems [Hadley, 2007]. According to the Electric Power Research Institute (EPRI), PEVs would be recharged during off-peak hours overnight. Total power generation needs to be increased by 60% to fulfill the extra load demand if 50% of all vehicles on the roads are replaced with EVs by 2050. With increase of penetration level of PEVs, demand management of power systems may not be so simple as to accommodate networks which do not have automatic controls and enough spare capacity. The related topic of V2G integration is worth further research.

1.2 Literature Review

1.2.1 Damping Performance Influenced by WECS

Prof. Kundur [Kundur, 1994] efficiently applied Small Signal Stability Analysis (SSSA) to power system. This work is extended to study the impact of large-scale wind power generation on system oscillation [Slootweg, 2003]. The effect of wind power on oscillations is investigated by gradually replacing power generated by the synchronous generators by power from either constant or variable speed wind turbines, while observing the motion of eigenvalues through the complex plane. It is concluded that in most cases, an increase in frequency and damping of power system oscillations was observed. This observation is

caused by a relative reduction in size of synchronous generators which engage in power system oscillation. Further, it also shows that Constant Speed Wind Turbine (CSWT) damps oscillation more than Variable Speed Wind Turbine (VSWT) due to the damping effect of the SCIG utilization.

Modal characteristics of oscillation modes of a two-area, four-machine power system, when a wind farm replaces one of the generators, have been analysed [Sanchez-Gasca, 2004]. The results of this investigation are in accordance with Slootweg's results and show that the modal characteristics were not influenced by WECSs since the inherent characteristic of WECSs lead to the absence of speed and angle state variables associated with local mode and inter-area mode.

Factors like grid configuration, load and wind power integration are also considered [Mendoça, 2005]. An automatic algorithm is used to search the space formed by such parameters and generate a representative set of possible operational conditions. The oscillation modes are then calculated for each operation point. Some of these points of operation are subjected to a deeper analysis and the movement of oscillation modes on the complex plane is revealed.

SCIG for CSWT is investigated with infinite bus to illustrate its characteristics [Lopez, 2008]. Under the conditions of changes of wind and load demand, it shows no oscillation behavior and the CSWT system is stable.

The impact of increase in output of WECS on the damping performance of

the New Zealand power system was assessed [Vowles, 2008]. A comparison is made between two scenarios: the original base case having no WECS and after replacing synchronous generators with an equivalent WECS. Then the sensitivity of the system damping performance to the type of WECS technologies, type of voltage control, variation in wind farm output and level of system loading is assessed.

A large test system representing the Midwestern portion of the U.S. interconnection was used, converting the DFIG machines into equivalent conventional synchronous machines, to evaluate the sensitivity of eigenvalues with respect to inertia [Gautam, 2010]. The results indicated both detrimental and beneficial impacts of increased DFIG penetration for small signal stability related performance, which actually depends on the point of common coupling of DFIG into the network.

1.2.2 Damping Performance Enhanced by WECS

A novel control scheme for a DFIG was first proposed and has since been implemented to provide support in power system operation [Huges, 2005]. It shows that this controller provides a DFIG-based wind farm with operational and control compatibility with conventional power stations, the ability to contribute to voltage support and recovery following network faults, the ability to provide a Power System Stabilizer (PSS) capability that improves overall system damping, and the capability of contributing short-term frequency support following loss of

network generation. Later, they proposed a more standard PSS for a wind turbine employing a DFIG [Huges, 2006]. It is claimed that this PSS from DFIG can significantly make a contribution to system damping, i.e. a DFIG-based wind farm can make to enhance network damping. The performance capabilities are even superior to those provided by synchronous generator with Automatic Voltage Regulation (AVR) and PSS. Then when the DFIG-based wind farm is subjected to mechanical power variations due to tower shadow and wind turbulence, the relative capabilities of PSS based on stator power, rotor speed and network frequency as input signal, are investigated via simulation studies [Huges, 2008].

Power systems with high penetration of wind power usually require long-distance transmission to export wind power to the market. Inter-area oscillation is an issue in long-distance transmission. Extant research has concentrated on damping of the inter-area mode in interconnected power system. A variable speed windmill control system has been proposed to damp inter-area power system oscillations [Ledesma, 2007]. Frequency deviation signal has been implemented as PSS input and designed for a variable-speed wind power converter for damping oscillations [Gallardo, 2008]. A two-area system that suffers from poor inter-area oscillation damping along with a wind farm in the area that exports power is investigated. A control scheme is developed for the DFIG with Rotor Side Converter (RSC) to damp inter-area oscillations [Miao, 2009].

The existing control system applied in DFIG is also considered to enhance system damping. It is stated that under certain penetration levels of wind power in the system (not necessarily large), for which the voltage control loop of DFIG will reduce damping. Then the modulation of active power generation of wind turbines is a powerful tool to introduce additional damping to inter-area oscillations through a simple wind PSS design [Tsourakis, 2009]. The general trend for increased oscillation damping is verified in the case of a large interconnected system encompassing Southeastern Europe for a projected high level of wind penetration in Greece. For the same system, it is also shown that low-damping voltage oscillations are possibly introduced by the voltage control mode of DFIG, which can be adequately damped by properly adjusting control parameters.

Coordinated tuning of the original DFIG system controller and damping controller to enhance the damping of oscillatory modes is presented using bacterial foraging technique [Mishra, 2010]. The results of both eigenvalue analysis and the time-domain simulation studies are presented to elucidate the effectiveness of the tuned controllers in the DFIG system. Later, they focus on the impact of a damping controller on super-synchronous/sub-synchronous modes of operation for the DFIG-based WECS. It is observed that when the tuning of the controllers is done at any sub-synchronous speed, the system is stable for all modes of operations. However, as this study is based on Single Machine Infinite Bus (SMIB) DFIG system, conclusions cannot be extended to

multi-machine DFIG-based WECS system. Recently, the method of eigenstructure assignment has been proposed for the design of a controller for a WECS scenario in Northern Scotland [Kshatriya, 2010]. The designed controller serves the combined purpose of a conventional PSS and an active damping controller in order to contribute to both network and shaft damping.

1.2.3 Damping Performance Influenced by EV Charging

The usage of PEV has been recognized as a promising means not only to reduce emissions by automobiles but also to relieve operational problems caused by the intermittent characteristic of wind energy [Kempton, 2005]. In [Li, 2012], a hierarchical control algorithm which integrates PEV charging and wind energy scheduling is presented. This work has explored the controllable nature of PEV charging to accommodate the intermittent wind energy. Besides, the possibility of applications of PEVs to system frequency regulation and stability enhancement has been validated [Yang, 2012; Han, 2010 and 2011]. Due to various advantages of PEVs, its large-scale application is under consideration in America [Patten, 2011] and Denmark [Larsen, 2008].

Modeling of battery for PEV is a significant concern before making analysis. [Ceraolo, 2000; Barsali, 2002] have been presented about models of electrochemical batteries suitable for use in electrical engineering, especially for analysis of electric power systems with batteries. A genetic battery model using only state-of-charge as a state variable is chosen in order to accurately reproduce

the manufacturer's curves for the four major types of battery chemistries: Lead-Acid, Lithium-Ion (Li-Ion), Nickel-Cadmium (NiCd) and Nickel-Metal-Hydride (Ni-MH) [Tremblay, 2007]. For Li-ion batteries, new equivalent-circuit model is found by the method of electrochemical impedance spectroscopy [Buller, 2005], but it is more suitable for power electronic applications. For Ni-MH battery, one basic equivalent-circuit model structure including hysteresis voltage is presented [Feng, 2008], which can be applied for the estimation of battery state-of-charge. Based on a remapped variant of the well-known Randle's lead-acid model, [Gould, 2009] presented a novel adaptive battery model which allowed improved modeling capabilities and estimates parameter of dynamic circuit parameters accurately. For accounting all dynamic characteristics of the battery, from open-circuit voltage, current, temperature, cycle number and storage time-dependent capacity to transient response, a comprehensive electrical battery model is proposed [Chen & Rincon-Mora, 2006].

As PEVs will be an important part of future power systems, effects of EV charging on stability and control need full investigation. Prof. Islam analyzed the impact of dynamic PHEV loads in a SMIB system through SSSA and time-domain simulation [Islam, 2010]. Prof. Das modeled power demand of PHEVs as a constant power load (CPL) and showed the possibility of reducing damping and causing instability due to the increasing penetration of PEVs [Das, 2008].

1.3 Motivation of This Research Work

1.3.1 Handling Stochastic Characteristic of Wind

Wind power has its own peculiarities. Generation is variable, relatively non-dispatchable and less predictable than most other types of generation. Wind velocity is a stochastic phenomenon that is continuously changing in direction and speed. It is important to note that wind adds both variability and uncertainty to the net power balance of a power system, the power load flow thus operating conditions.

The conventional methodology to assess SSSA is to study only the worst scenario or a few scenarios. However, the basic weakness of this deterministic analysis is that it cannot respond to, nor reflect, the stochastic nature of power system behavior introduced caused by wind power integration. With a high level of wind power penetration, a single power flow solution can no longer describe the possible system states in a representative way. To fulfill the requirement of small signal stability under different operating conditions, research works have attempted to account for the uncertainties. From the viewpoint of engineers and system planners, the assessment of this variability is necessary for planning of system stability enforcements such as PSSs tuning for conventional synchronous generators.

Moreover, the operational modes of a DFIG-based WECS, including sub-synchronous, normal and super-synchronous, are determined by wind

velocity. It is necessary to study the efforts of damping controller under different modes and optimize it to achieve the best performance.

1.3.2 Damping Control Coordinate with Other Controllers

Besides PSSs for conventional power plants, Flexible AC Transmission Systems (FACTS) devices with Supplementary Damping Controller (SDC) are also applied to enhance system stability. Particularly in multi-machine system, when conventional power plants with PSSs are shut down and replaced by newly built wind farms, the remaining damping controllers may not provide sufficient damping for inter-area oscillations. PSS for DFIG-based WECS erected in wind farms may be one of the useful solutions.

However, with application of DFIG equipped with PSS, every PSS may affect all electro-mechanical oscillation modes to some extent. Sequential addition of new stabilizers disturbs previously assigned eigenvalues and that may cause destabilization due to lack of coordination, especially in multi-machine systems. To improve overall system performance, the coordination between PSSs for different types of generators needs to be studied. Computational intelligence algorithm or linear/nonlinear programming may be appropriate for conducting this work.

1.3.3 Stability Analysis Including EV Charging

Integration of WECSs and PEVs result in new impacts on system stability

these need to be investigated carefully. DFIG affects the dynamic behavior of the systems [Gautam, 2009]. Besides, PEV chargers have rectifiers to provide regulated dc voltage supply at a fixed load. Since considering PEV as a constant impedance or constant power load may not be sufficient for analysis, it is clear that an urgent research on detailed PEV modeling for SSSA is needed.

Wind is known as a stochastic source; power output of wind farm is thus undispatchable. On the other hand, usage of vehicles also shows stochastic characteristics due to the different driving times and distances [Qian, 2011] and, therefore, state-of-charge of the battery is a random factor when the PEV plugs into the grid. Under these randomized nodal injections, load flow and operational state vary from time to time, so a method is needed to account for their stochastic behavior in system analysis.

Probabilistic methodologies are well suited to study stochastic problems and they have been successfully used in rotor angle stability studies. However, power output of a wind farm is a mixed random variable which is continuous between values of zero and the rated power, but discrete at values of zero and rated power. Analytical methods such as convolution calculation [Villanueva, 2011], point estimate method (PEM) [Su, 2005] and first-order second-moment method (FOSMM) [Chung, 2003] cannot be applied to this profound nonlinearity problem with different combinations of variables. Among the simulative methods, quasi-Monte Carlo (QMC) is proved to handle probabilistic problems with higher efficiency than Monte Carlo simulations (MCS) [Singhee, 2010]. Compared to

MCS, deterministic data are sampled by Sobol sequences in QMC, which is advanced over pseudorandom sequences in MCS. Based on the randomized model representing nodal power injections of PEVs and WECSs, and a new sampler formed by QMC with Sobol sequences, a novel probabilistic small signal stability analysis (PSSSA) method is proposed.

1.4 Thesis Organization

Chapter 1 provides the background of the small signal stability issues in power systems with wind power integration and EV charging. New methodologies proposed in this thesis are also introduced.

Chapter 2 proposes an adaptive neuro-fuzzy controller for SVC, used in power networks integrated with WECS. Due to wind shear and tower shadow, a periodic pulse reduction in mechanical torque captured from wind energy results in WECS active power oscillations. The proposed method can address this oscillation problem.

Chapter 3 presents a method to design a POD for DFIG-based WECS, operating with voltage control loop. Modified PSO is used to tune all parameters of damping controller to achieve the desired performance.

Chapter 4 proposes a novel control design method for coordination and synthesis of damping controllers for conventional synchronous generators and DFIG-based WECS in multi-machine power systems to alleviate the impacts of stochastic WECS on stability performance.

Chapter 5 proposes a QMC-based PSSSA method to estimate the entire dynamic effects on power system from new establishments including PEVs charging stations and wind power generation.

Chapter 6 presents overall conclusion of the work in this thesis and future research directions.

Chapter 2 Adaptive Neuro-Fuzzy Controller for SVC to Damp Out Wind Energy Conversion System Oscillation

2.1 Introduction

Previous studies [Slootweg, 2003; Sanchez-Gasca, 2004; Mendonca, 2005] have shown that grid integration of wind power generation does not bring much negative impact to power network. However, characteristics of three-blade wind turbines such as wind shear and tower shadow produce a cyclical pulse reduction in torque as each blade passes the support tower, called 3p oscillation [Thiringer, 2001; Dolan, 2006]. For example, in the case of a normal synchronous speed induction generator, the 3p frequency can be calculated as: $3 \cdot 2\omega_s/rp \approx 10.59 rad/s = 1.69$Hz. In this case, 3 is the number of turbine blades, ω_s is $2\pi 50$ in Europe, r is 1:44.5 and p is four. Current rotational speeds of three blade turbines induce the frequency of these pulses within a range close to the local area mode oscillation frequency of a power network, which induces power oscillation of synchronous generators [Cidras, 2002].

The influence of torque oscillation from three-blade WECSs have been investigated by [Larsson, 2002; Hughes, 2008; Fadaeinedjad, 2009], who concluded that wind shear and tower shadow affect the generated power and voltage, thus possible remedies should be found to maintain the performance. A

mathematical model of 3p oscillation induced by wind shear and tower shadow will be established, which is suitable for time-domain simulation. However, since the relationship with rotational speed of wind turbine blade is not constant, the oscillation frequency changes with time. For example, WECSs' initial angles are different and the oscillation frequency varies between 3p and 3*n*p, where *n* is the number of WECSs in wind farm. Also, DFIG-based WECSs are equipped with a Maximum Power Point Tracking (MPPT) controller to capture the maximum wind energy, which means the rotation speed varies according to stochastic wind speed.

Generally SVC provides voltage support to wind farm, especially when the FSIG-based WECS is used, which absorb a large amount of reactive power from the system and then lead the low voltage problem at the point of common coupling. The artificial intelligence-based methods have been implemented to design adaptive supplementary damping controller. Especially theory about fuzzy logic shows good potential in enhancing the damping condition of system, when the controller is tuned by neural network. Previous studies show the adaptive control theory has been successfully used in power system dynamic control, such as PSS and FACTS. [You, 2003] applied adaptive neuro-fuzzy theory to design a novel PSS for a multi-machine system. [Mohagheghi, 2007] proposed a neuro-fuzzy external controller for STATCOM using in a 12-Bus system. This online tuning of controller parameters strategy was proven effective in providing damping control to power system. The design of present controller is based on

the linearized transfer function model at a particular operating point, it may not provide a satisfy performance over a wide range of operating conditions. As in this chapter, the controller is design for a local SVC and wind farm, due to the random nature of wind, oscillation content includes magnitude and frequency are vary. In consideration of previous problems, this chapter proposes an adaptive neural network theory to implement a damping controller for the wind farm's SVC. Firstly, for simpler topology and the capability for faster learning (than feed-forward networks), Radial Basis Function (RBF) neural network has been applied to provide the predicted value of input signal and to help online tuning of controller parameters [Ramakrishna, 2007]. Then the Adaptive Neuro-Fuzzy Inference System (ANFIS) theory [Jang, 1993] is used to implement a controller which provides a damping signal in the SVC internal control system to damp the oscillations.

2.2 Mathematical Models

2.2.1 Concepts of Wind Shear and Tower Shadow

Distribution of wind speed over the swept area of turbine blade is generally assumed to be constant. But actually wind velocity profiles closest to the ground level are different from those at the top of the blade travel, which alternately produce corresponding air flow and power effects on the turbines. Fig. 2.1 illustrates variations caused by different heights; from lowest level to top of blade travel, there is a gap of about 4.4m/s when wind speed is about 14m/s at

the turbine hub height. Wind velocity usually rises with height and this type of variation is termed as wind shear [Heier, 1998].

In addition to the vertical speed gradient, tower shadow also causes fluctuations in torque and hence power during blade rotation. As demonstrated in Fig. 2.2, wind blows in front of the tower, it is redirected and then total power capture drops when the blades pass the tower. Therefore, the mechanical torque from wind turbine is presented as an oscillation behavior. This effect depends upon the number of blades, height of the turbine and positioning of the rotor, i.e. upwind or downwind of the tower [Heier, 1998].

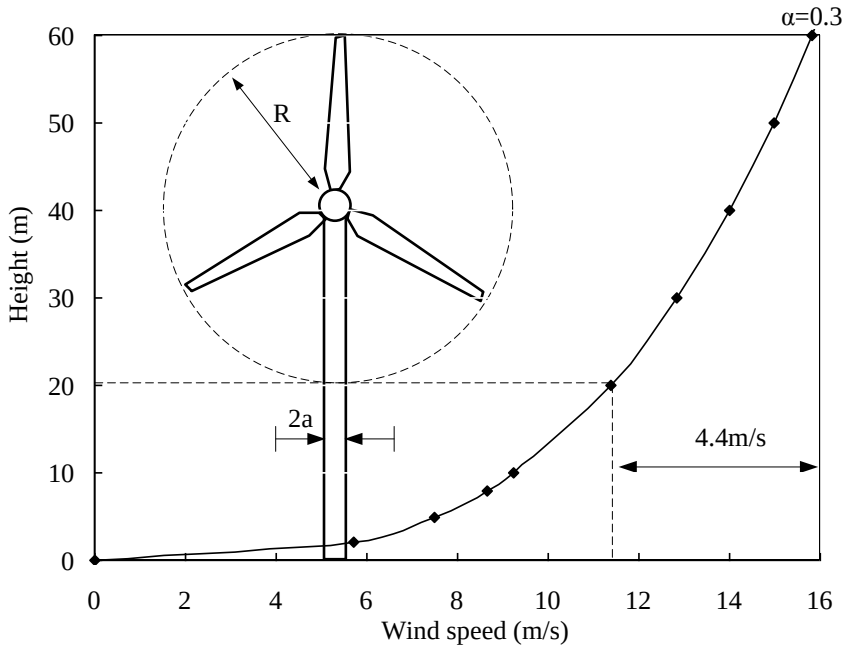

Fig. 2.1 Wind speed vertical profile effort

The mechanical torque variation due to wind shear and tower shadow is illustrated in Fig. 2.3.

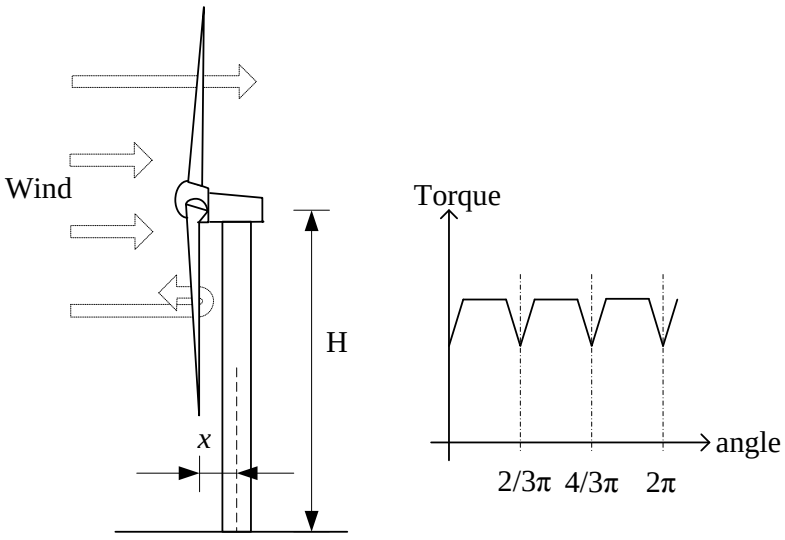

Fig. 2.2 Tower shadow effects on wind turbines

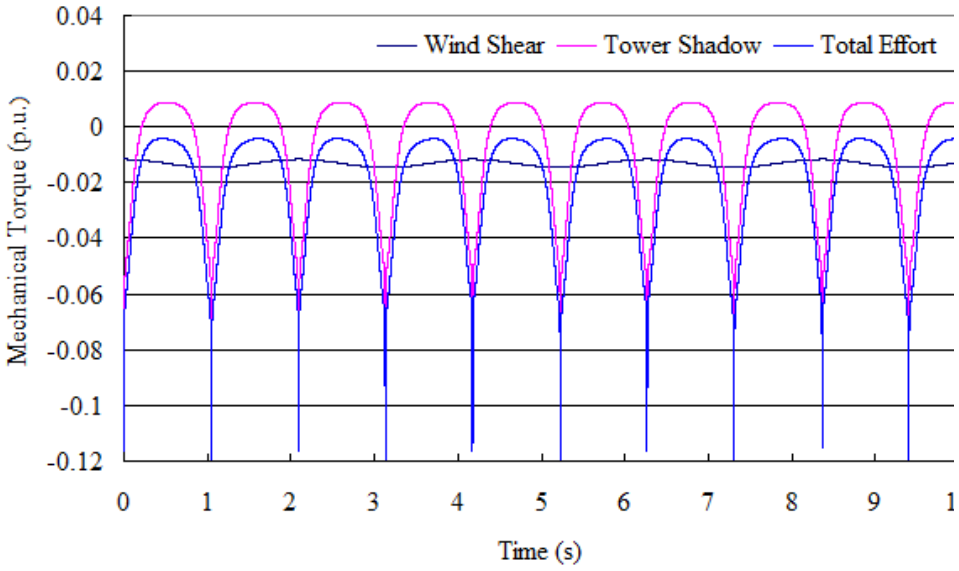

Fig. 2.3 Torque variation due to wind shear and tower shadow

It can be found that the effort of tower shadow is more dominant than wind shear. The total effect reduces the mechanical torque by almost 0.12 p.u. at the worst situation. The most harmful situation is that tower shadow and wind shear influence on turbine torque can excite the turbine at a frequency close to power network natural oscillation. Mathematical model of wind shear and tower

shadow can be modified for time domain simulation; the equivalent wind speed is represented as follows:

$$V_{ws} = V_H[\frac{\alpha(\alpha-1)}{8}(\frac{R}{H})^2 + \frac{\alpha(\alpha-1)(\alpha-2)}{60}(\frac{R}{H})^3\cos 3(\theta+\omega_T t)] \tag{2.1}$$

$$V_{ts} = \frac{M\cdot V_H}{3R^2}\sum_{b=1}^{3}[\frac{a^2}{\sin^2(\theta_b+\omega_T t)}\ln(\frac{R^2\sin^2(\theta_b+\omega_T t)}{x^2}+1) - \frac{2a^2R^2}{R^2\sin^2(\theta_b+\omega_T t)+x^2}] \tag{2.2}$$

2.2.2 Wind Turbine (Aerodynamic) Model

By using models mentioned in 2.2.1, 3p oscillations can be taken into the conventional aerodynamic model of wind turbine. The mechanical torque capture from wind is generally expressed as:

$$T_M = P_M / \omega_T = \frac{1}{2}\rho A C_\rho(\lambda,\beta) V_H{}^3 / \omega_T \tag{2.3}$$

Therefore, the new normalized equivalent mechanical torque, combined with the effects of tower shadow and wind shear, is as follows:

$$T_M^* = T_M \times \left(1+\frac{2}{M\cdot V_H}[V_{ws}+V_{ts}+(1-M)V_H]\right) \tag{2.4}$$

Eq. (2.1)-(2.4) could be used in the time-domain simulation. Then the total effect of all WECSs in the same wind farm must be considered.

2.2.3 Synchronization of WECSs

To a wind farm, synchronization of WECSs does not mean running at network synchronous speed ω_s, which indicates that WECSs operate at exactly

the same rotor speed. Rather, when the torque oscillation is studied here, synchronization means blades of WECSs pass in front of the tower simultaneously (Fig. 2.4).

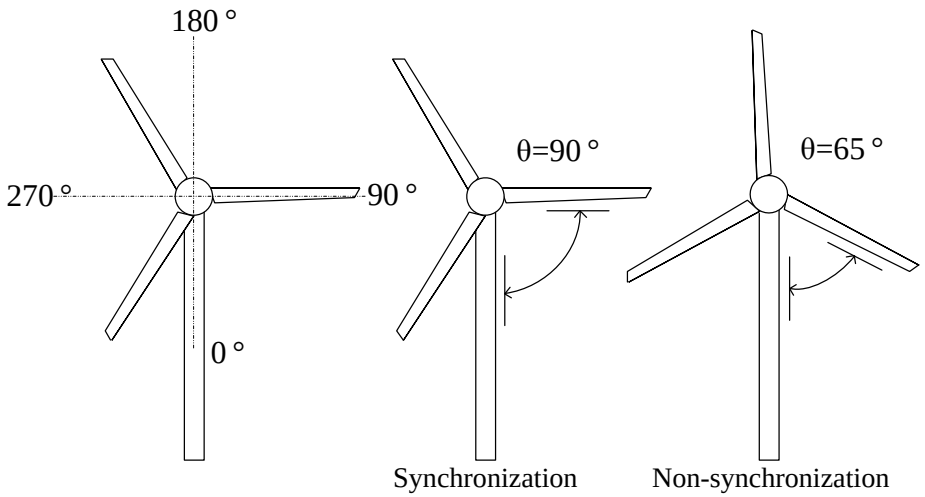

Fig. 2.4 Synchronization and non-synchronization phenomenon of WECSs

Synchronization seems possible when the wind turbines are identical and operate under similar conditions. If these conditions are given and different wind turbines work at the same speed, then after a very short time, their blades will tend to pass in front of the towers at the same time. This phenomenon is already observable in complex simulations [Cidras, 2002]. Data analyses of turbines also show that the motion of the turbine blades is not strictly random and turbines do synchronize [McSwiggan, 2008]. Considering WECSs are operating continuously, except when the winds stop blowing, synchronization should be the main situation most of the operating time.

Therefore, the 3p oscillation effect on the wind farm's power output is amplified by the synchronization of the WECSs. This situation is most harmful

for power system operation since the frequency is close to natural frequency of the system. In this chapter, WECSs in the wind farm are assumed to be running under synchronization and the initial azimuthal angle of different WECSs' blades is assumed to be the same in the simulation.

2.3 Control System Design

The structure of the proposed control system shown in Fig. 2.5 consists of two subsystems: identifier for the system and ANFIS controller. The system identifier is represented for a third-order ARMA model of the system and feedback the input at time step *t+1* to tune the parameters of the ANFIS controller.

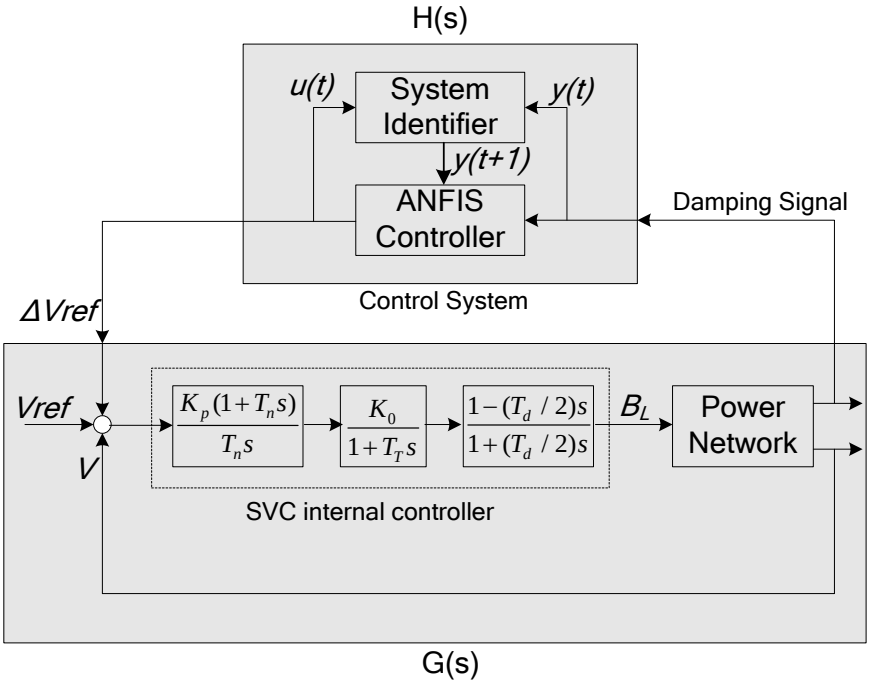

Fig. 2.5 The schematic diagram of control loop

2.3.1 Residue Method

In this chapter, the parameters of lead/lag compensator, used for comparison with the proposed control system, are adjusted by the residue method [Pagola, 1989; Yang, 1998]. An electrical network is a high-order nonlinear system. In order to obtain a linearized system for analysis, linearization has been applied when the model operates at the steady-state point. Thus, the linearized model of power network can be described by the following state equations:

$$\begin{cases} \dot{X}(t) = AX(t) + BU(t) \quad X(0) = X_0 \\ Y(t) = CX(t) \end{cases} \tag{2.5}$$

Fig. 2.5 shows the transfer function of the close-loop system, where:

$$G(s) = C(sI - A)^{-1}B \tag{2.6}$$

is the open-loop system transfer function (for description of SVC internal controller please refer to [Kundur, 1994]) ; and

$$H(s) = K \cdot \frac{T_w s}{1 + T_w s} \cdot \left(\frac{1 + T_1 s}{1 + T_2 s} \right)^n \tag{2.7}$$

is the transfer function of lead/lag compensation; parameters are decided by the residue method and modal sensitivities since the residue method can allow measurements of observability and controllability. Details of the design approach for adjusting K, T_1, T_2 and n can be found in [Pagola, 1989; Yang, 1998].

2.3.2 Identification

The form of the identifier model is as follows:

$$y(t+1) = \theta(t) \cdot \psi(t) + e(t) \tag{2.8}$$

where $\theta(t) = [a_1\ a_2\ a_3\ b_1\ b_2\ b_3]$ is the parameter vector which can be updated by the network, $\psi(t) = [y(t)\ y(t\text{-}1)\ y(t\text{-}2)\ u(t)\ u(t\text{-}1)\ u(t\text{-}2)]^T$ is the variable vector, y is the candidate input signal of different time steps, u is the output of the controller and $e(t)$ is the error. A RBF network is applied for identification. As shown in Fig. 2.6, the network consists of two layers: one hidden layer comprising radially symmetric basis functions and an output layer. The hidden layer nodes consist of a parameter vector called centers. Each node calculates the Euclidean distance between the center and the network input vector and then the result is passed through a Gaussian function. The overall input-output sequence of the RBF network is given by:

$$y = w_0 + \sum_{n=1}^{N} w_n \exp\left(-\frac{\left\|x_p - c_n\right\|}{\sigma_n^{\,2}}\right) \tag{2.9}$$

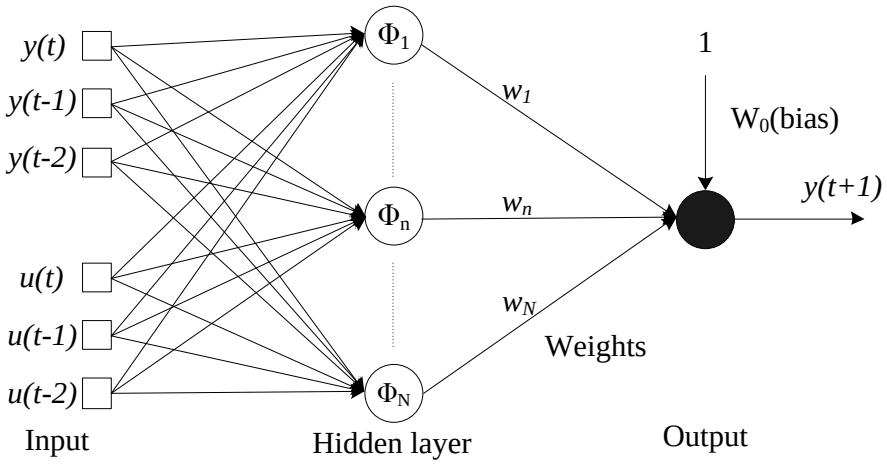

Fig. 2.6 The structure of RBF neural network

The Widrow-Hoff learning algorithm is used to update the centers and weights simultaneously during the training [Demuth, 1998]. The RBF hidden node is added at a time when the network's mean square error satisfies the

minimum value. The following steps are repeated until error $e(t)$ is minimized:

Step a) The input vector is fed in the network and then error is found after each period;

Step b) Add a new hidden node with center equal to that vector;

Step c) The linear weights are updated using Widrow-Hoff algorithm.

RBF network is trained to represent the nonlinear model of the system, especially when WECSs operate under non-synchronization condition; fast tracking ability of RBF is needed for the higher frequency oscillation.

2.3.3 ANFIS Control

The fuzzy inference system having two inputs y_1, y_2 and one output u is considered. For a zero-order Sugeno fuzzy model, Fig. 2.7 illustrates the corresponding equivalent ANFIS architecture, where functions of nodes in the same layer are similar, as described below.

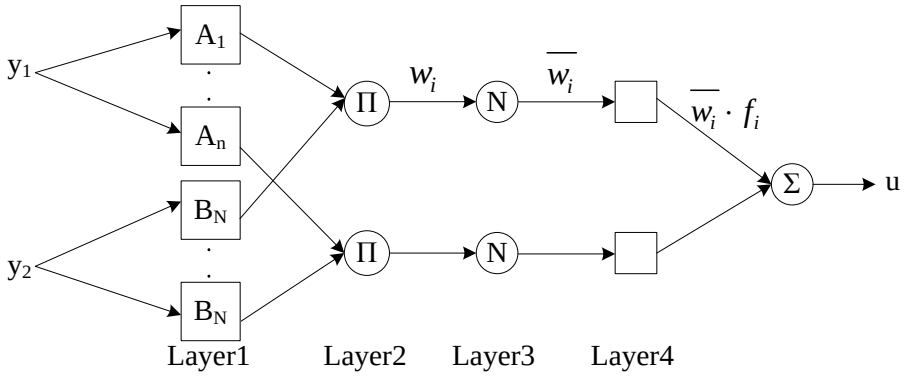

Fig. 2.7 The structure of ANFIS controller

The nodes of layer 1 are adaptive nodes with output defined by the Gaussian function:

$$w_i(y) = \exp\{-[(y - c_i)/m_i]^2\} \tag{2.10}$$

In other words, outputs of this layer are the degree to which the given y satisfies either linguisitc label A_i or B_i. In layer 2 every node is a fixed node; label Π means multiple inputs and sends the product out.

$$w_i = \mu_{Ai}(y_1) \times \mu_{Bi}(y_2) \tag{2.11}$$

In layer 3 each node is a fixed node labeled N, to normalize firing strengths. The *i*th node calculates the proportion of the *i*th rule's firing strength to the total of all rules' firing strengths:

$$\overline{w_i} = w_i / \sum_{i=1}^{N} w_i \tag{2.12}$$

In layer 4 every node is an adaptive node with a function:

$$u_i = \overline{w_i} f_i \tag{2.13}$$

The output of the controller is the sum of output of every node in layer 4. Thus an adaptive network has been constructed, which acts as an adaptive controller.

2.3.4 Training Algorithm

In the proposed control system, parameters of the fuzzy controller, such as membership functions (c_i, m_i) and the consequent parameters (f_i) are adjusted on the basis of the performance. The objective of renewing parameters inside the fuzzy inference system is to minimize a cost-to-go function:

$$J(t) = \frac{1}{2} \times [y(t+1)^2 + pf \cdot u(t)^2] \tag{2.14}$$

Here parameters are adjusted by a gradient descent learning algorithm; each

of them is updated in the negative gradient direction of the objective function $J(t)$, taking c_i as example:

$$c_i(t) = c_i(t-1) - \eta \cdot \frac{\partial J(t)}{\partial c_i} \tag{2.15}$$

$$\frac{\partial J(t)}{\partial c_i} = \frac{\partial J(t)}{\partial u(t)} \cdot \frac{\partial u(t)}{\partial c_i} = [y(t+1) \cdot \frac{\partial y(t+1)}{\partial u(t)} + pf \cdot u(t)] \cdot \frac{\partial u(t)}{\partial c_i} \tag{2.16}$$

In Eq. (2.16), $\partial y(t+1)/\partial u(t)$ can be obtained by the system identifier:

$$\frac{\partial y(t+1)}{\partial u(t)} = \sum_{n=1}^{N} \left(2 \frac{c_{i,n} - x_i}{\sigma_n{}^2} \cdot \exp - \sum_{i=1}^{N} \left(\frac{x_i - c_{i,n}}{\sigma_n} \right)^2 \right) \tag{2.17}$$

And

$$\frac{\partial u(t)}{\partial c_i} = \sum_{j=1}^{n} \left(\frac{\partial u(t)}{\partial \overline{w_j}} \cdot \frac{\partial w_j}{\partial c_i} / \sum_{i=1}^{N} w_i \right) = \frac{2(y - c_i)}{m_i^2} \cdot \sum_{j=1}^{n} f_j \cdot \overline{w_j} \tag{2.18a}$$

where i means ith membership function; j means ith membership function participates in jth fuzzy rule, and m_i and f_i, have similar rules and change the last term of Eq. (2.16) by the following:

$$\frac{\partial u(t)}{\partial m_i} = \sum_{j=1}^{n} \left(\frac{\partial u(t)}{\partial \overline{w_j}} \cdot \frac{\partial w_j}{\partial m_i} / \sum_{i=1}^{N} w_i \right) = \frac{2(y - c_i)^2}{m_i^3} \cdot \sum_{j=1}^{n} f_j \cdot \overline{w_j} \tag{2.18b}$$

$$\frac{\partial u(t)}{\partial f_i} = \overline{w_i} \tag{2.18c}$$

The whole control system training steps are as follows:

Step a) Sample $y(t)$ and $u(t)$ with initial ANFIS controller;

Step b) Update parameter vector $\theta(t)$ of the identifier;

Step c) Obtain predicted value of $y(t+1)$ by the identifier, tune the membership functions and the consequent parameters in the ANFIS controller through (2.15)-(2.18).

2.4 Simulation Result

To validate the proposed damping controllers, a simulation study was performed on a two-area four-machine system [Kundur, 1994] with a wind farm, shown in Fig. 2.8.

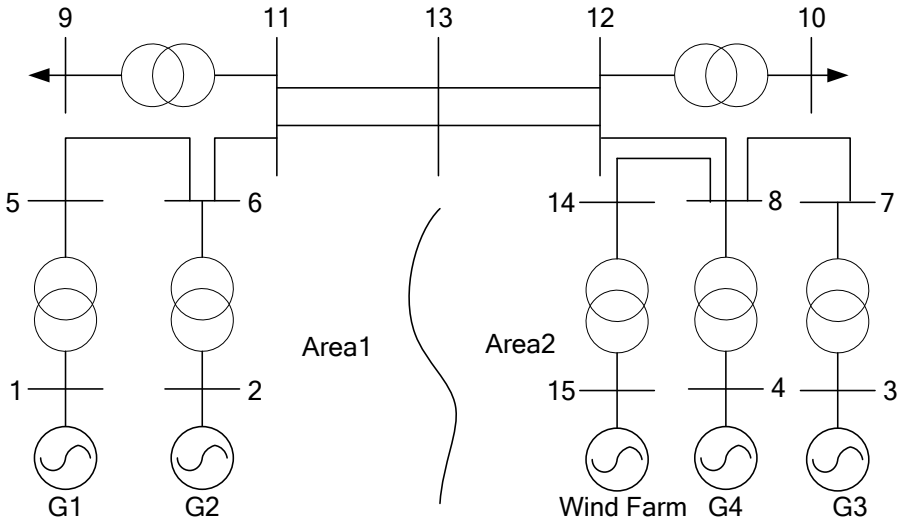

Fig. 2.8 The diagram of modified two-area four-machine system

Each equivalent generator represents a group of strong couple, operating at similar condition generators. synchronous generators are provided with standard governor and excitation control. Both G2 and G4 were equipped with Prof Kundur's $\Delta\omega$ PSS and thus the original system is stable. Parameters of this system can be found in Appendix. G4 has an original capacity of 900MVA and is reduced to the rating of 360MVA, replaced by a wind farm; therefore, wind power penetration is about 10% of total power network capacity. The random nature of wind speed is represent by wind turbulence then its effect on the mechanical torque is taken into account in the simulations. The parameters of

WECSs are given below. A SVC is employed for reactive power compensation to the wind farm, connected at Bus 8. In this way, effects of the 3p oscillation from wind farm on other generators and effectiveness of the proposed control system can be investigated.

Table 2.1 Parameters of wind farm

Wind shear and tower shadow parameters:	
α	0.3
R	20(m)
H	40(m)
a	0.85(m)
x	2.9(m)
Wind Energy Conversion System parameters:	
Nominal capacity	60 (MVA)
Line-to-line voltage	575(V)
Nominal system frequency	60(Hz)
Stator resistance	0.004843(p.u.)
Stator leakage inductance	0.1248(p.u.)
Rotor resistance	0.004377(p.u.)
Rotor leakage inductance	0.1791(p.u.)
Magnetizing inductance	6.77(p.u.)
Inertia constant	5.04
Friction factor	0.01
Number of poles	4

Time-domain simulations with MATLAB Simulink are performed on the test system. Fig. 2.9 illustrates the response of 4-machine in the system. Due to the wind farm torque oscillation, low frequency oscillations of local modes have been induced. It should be noted that when the simulation comes to about 80s, the power angle of G1 versus G4 turned to be 180 degree, the system became unstable (simulation stopped). The oscillations cannot be restrained by PSS installed; their influence on generators is not less than those without PSS, as

shown in Fig. 2.9.

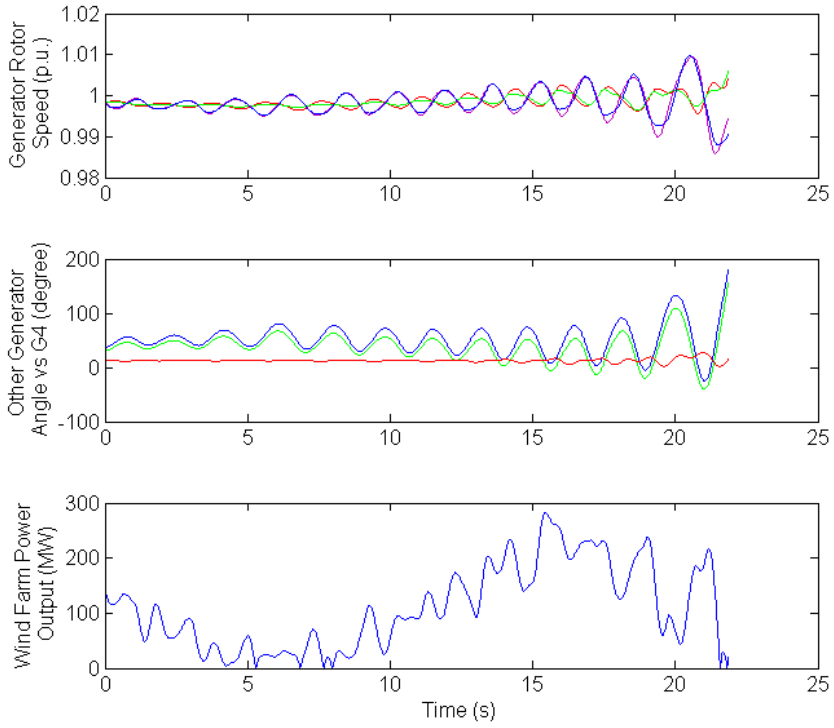

Fig. 2.9 Influence of wind farm variation without damping controller

Then a supplementary control scheme is used to improve this phenomenon. Initially the input signal of damping controller is determined as active power of wind farm P_{wf}, which shows good controllability and observability from residue calculation. According to residue method, in order to enable the weak damping mode eigenvalue to be more negative, parameters of lead/lag compensation controller based on signal ΔP_{wf} can be calculated as:

$$H(s) = 0.2 \cdot \frac{10s}{1+10s} \cdot \left(\frac{1+0.5s}{1+0.0507s} \right)^2 \tag{2.19}$$

Fig. 2.10 illustrates the dynamic response of synchronous generators and wind farm under SVC combined with lead/lag compensation. From the plots, it

can be observed that additional control can keep the system operation stable.

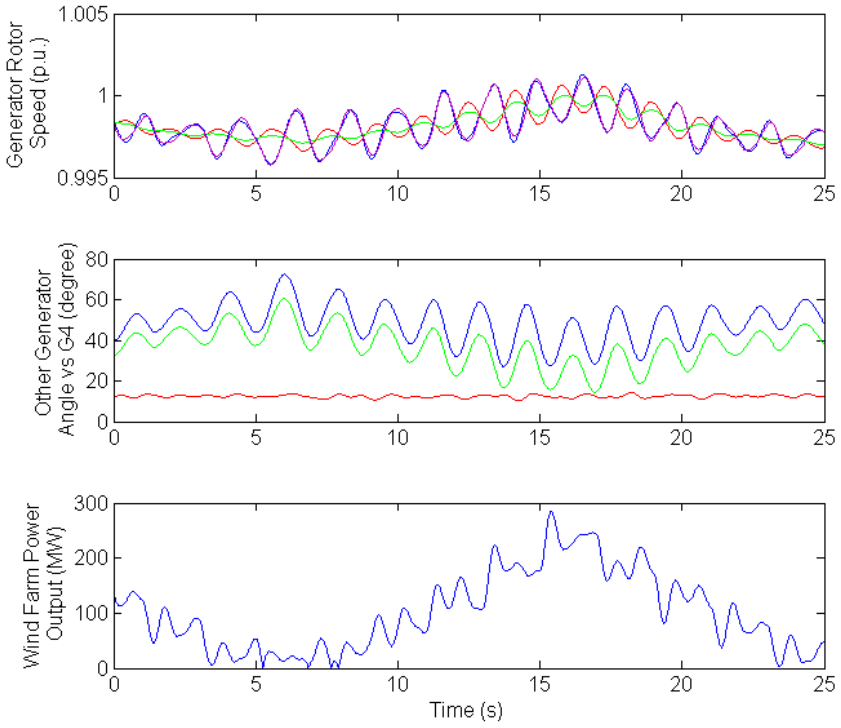

Fig. 2.10 Influence of wind farm variation with lead-lag compensation

Then the effectiveness of adaptive neuro-fuzzy control can be explored. Fig. 2.11 shows the speed deviation of synchronous generators under synchronous operation of WECSs. It demonstrates that the proposed controller can effectively decrease the speed deviation from wind farm output oscillation faster than lead/lag compensation. In Fig. 2.12, the injected reactive power from SVC and the controlled bus voltage are further confirm the performance of proposed method.

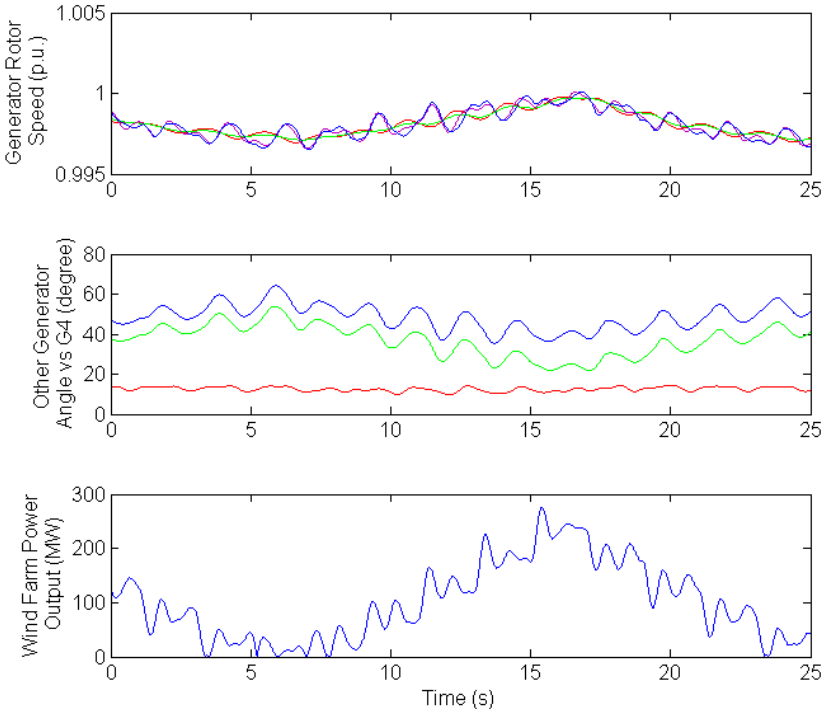

Fig. 2.11 Influence of wind farm variation with proposed controller

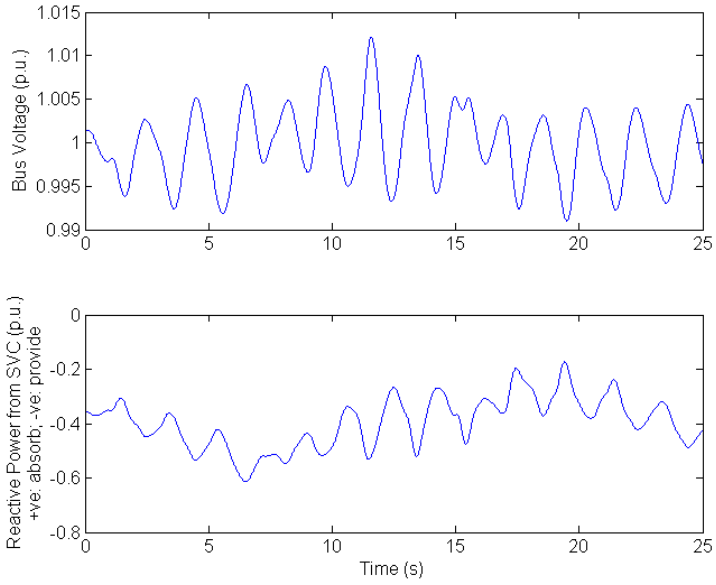

Fig. 2.12 Controlled bus voltage and reactive power of SVC

2.5 Summary

Wind shear and tower shadow cause torque oscillation of WECSs and then become active power oscillation of wind farm, which can induce low frequency oscillation modes of power system. The influence is extreme and becomes greater when WECSs in the wind farm operate at synchronization. Simulation results prove that without proper remedies the system becomes unstable.

An adaptive neuro-fuzzy controller is proposed for damping control. Radial basis function neural network is used for representing a third-order ARMA system model, and predicting the next time step input for online parameter tuning. The adaptive neuro-fuzzy inference system based controller is proposed to stabilize the output power and the system. Simulation results show that the proposed controller can damp WECS oscillation more effectively, compared to conventional lead/lag compensation.

Chapter 3 Design of a Power Oscillation Damper for DFIG-based Wind Energy Conversion System Using Modified Particle Swarm Optimizer

3.1 Introduction

Nowadays, DFIG has been widely used in WECS due to efficient power generation form wind, besides, the low cost and flexible control. The use of DFIG improves the phenomenon of absorbing reactive power from power grid [Akhmatov, 2005] and achieves some network support such as providing voltage support and damping control. DFIG with PSS or POD is proven to contribute to system dynamic and transient stability. Robust control theory and intelligent algorithms can be applied to improve performance of PSS for DFIG.

In PSS design, a parameter usually participates in more than one oscillation mode and, therefore it is difficult to define the specified gradient information for the parameters during the process of optimization. Genetic Algorithms (GA) have been widely used as optimization tools since they do not require gradient information of an objective function, only its value and hence they are easily implemented. GA has been applied in [Bomfim, 2000; Zhang, 2000] to simultaneously tune damping controllers in power systems. However, when

handling the highly epistatic objective functions, in which optimized parameters are strongly correlated, efficiency of GA deteriorates. Also GA cannot avoid the shortcoming of premature convergence which reduces its search ability. Unlike GA, Particle Swarm Optimization (PSO) [Eberhart, 1995; Kennedy, 1995] has reinforced global and local exploration abilities and has been found to be efficient when applied to complex optimization problems [Abido, 2002]. The nonlinear and noncontinuous optimization problems with continuous variables can be easily solved by PSO. It is considered robust to control parameters and computationally efficient. In a shorter calculation time, this technique generates high-quality solutions and has more stable convergence characteristics than other stochastic methods [Zhao, 2005]. Moreover, a Modified Particle Swarm Optimizer (MPSO) was proposed by [Shi, 1998], which has been widely applied and has been cited over 400 times. Therefore, in this chapter, the parameters of POD for DFIG are intended to be optimized by MPSO.

3.2 Mathematical Model

3.2.1 DFIG Model

The variable speed constant frequency generator has a structure similar to the wound rotor induction generator. During operation, the rotor and stator currents are considered as outputs, instead of inputs. Both active and reactive power are assigned positive values if they are fed into the network. The transient model decoupled in the reference frame using direct (d) and quadrature (q) axis

representation in per unit can be obtained as in [Ekanayake, 2003; Almeida, 2004]. In these equations, subscripts *r* and *s* stand for rotor and stator, respectively:

$$\begin{cases} v_{ds} = -R_s i_{ds} - w_s \psi_{qs} + \dot{\psi}_{ds} \\ v_{qs} = -R_s i_{qs} + w_s \psi_{ds} + \dot{\psi}_{qs} \end{cases} \tag{3.1a}$$

$$\begin{cases} v_{dr} = R_r i_{dr} - (w_s - w_r)\psi_{qr} + \dot{\psi}_{dr} \\ v_{qr} = R_r i_{qr} + (w_s - w_r)\psi_{dr} + \dot{\psi}_{qr} \end{cases} \tag{3.1b}$$

where v is the voltage, R_s and R_r are stator and rotor resistance, respectively, i is the current, w_s is the stator electrical speed, w_r is the generator rotor speed, and ψ is the flux linkage. Since stator transients are very fast, it is possible to neglect the last terms of (3.1a). When the *q*-axis is assumed to be 90 ° ahead of the *d*-axis for the generator at synchronous speed and the *q*-axis is chosen to align with the stator voltage vector, flux linkage can be defined as

$$\begin{cases} \psi_{ds} = -L_s i_{ds} + L_m i_{dr} \\ \psi_{qs} = -L_s i_{qs} + L_m i_{qr} \end{cases} \tag{3.2a}$$

$$\begin{cases} \psi_{dr} = L_r i_{dr} - L_m i_{ds} \\ \psi_{qr} = L_r i_{qr} - L_m i_{qs} \end{cases} \tag{3.2b}$$

where L_s and L_r represent the self-inductance of the stator and rotor windings, respectively, and L_m is the mutual inductance between stator and rotor windings. The transient voltage can be written by the terms of rotor flux linkage ψ_{qr} and $\psi_{dr.}$

$$\begin{cases} e_d = -\dfrac{w_s L_m}{L_r}\psi_{qr} \\ e_q = \dfrac{w_s L_m}{L_r}\psi_{dr} \end{cases} \tag{3.3}$$

where e_d and e_q are the direct and quadrature axis voltage behind the transient

reactance, respectively. Then, by substituting flux linkage formulas (3.2) and (3.3) into (3.1) to eliminate rotor currents (i_{dr} and i_{qr}), the relationship between stator current and transient voltage can be obtained as:

$$\begin{cases} v_{ds} = -R_s i_{ds} + X' i_{qs} + e_d \\ v_{qs} = -R_s i_{qs} - X' i_{ds} + e_q \end{cases}$$
$$\begin{cases} \dot{e}_d = -\frac{1}{T_0}[e_d - (X - X')i_{qs}] + (w_s - w_r)e_q - w_s \frac{L_m}{L_r} v_{qr} \\ \dot{e}_q = -\frac{1}{T_0}[e_q + (X - X')i_{ds}] - (w_s - w_r)e_d + w_s \frac{L_m}{L_r} v_{dr} \end{cases} \quad (3.4)$$

where X is the open circuit reactance equal to $w_s L_s$, X' is the transient reactance equal to $w_s(L_s\text{-}L_m^2/L_r)$, and T_0 is rotor open circuit time constant equal to L_r/R_r. Similar to synchronous generator, the swing equation is given by

$$\dot{w}_r = \frac{1}{2H}(T_m - T_e) \quad (3.5)$$

where $2H$ is the moment of inertia, T_m is the mechanical torque and T_e is the electrical torque calculated as

$$T_e = e_q i_{qs} + e_d i_{ds} \quad (3.6)$$

Finally, the DFIG can be represented by the third-order dynamic model in (3.4)-(3.5).

3.2.2 Wind Turbine Model

The mechanical torque in the wind turbine is given by the following equation

$$T_m = \frac{P_m}{w_t} = \frac{1}{2}\rho A V_w^3 C_\rho(\lambda, \theta) / w_t \quad (3.7)$$

where P_m is the mechanical power, w_t is the wind turbine rotor speed, ρ is air density, V_w is the wind velocity, A is the area swept by the blades, C_ρ is power

coefficient of the wind turbine, which is a function of tip speed ratio λ and pitch angle of blades θ. The tip speed ratio is defined as

$$\lambda = \frac{w_t R}{V_w} \tag{3.8}$$

where R is the length of the blade. It can be noted in (3.7) that the mechanical power captured from wind can reach the highest efficiency if C_ρ is maximized.

3.2.3 Control System

A general schematic of the DFIG, bidirectional converter and controllers is illustrated in Fig. 3.1.

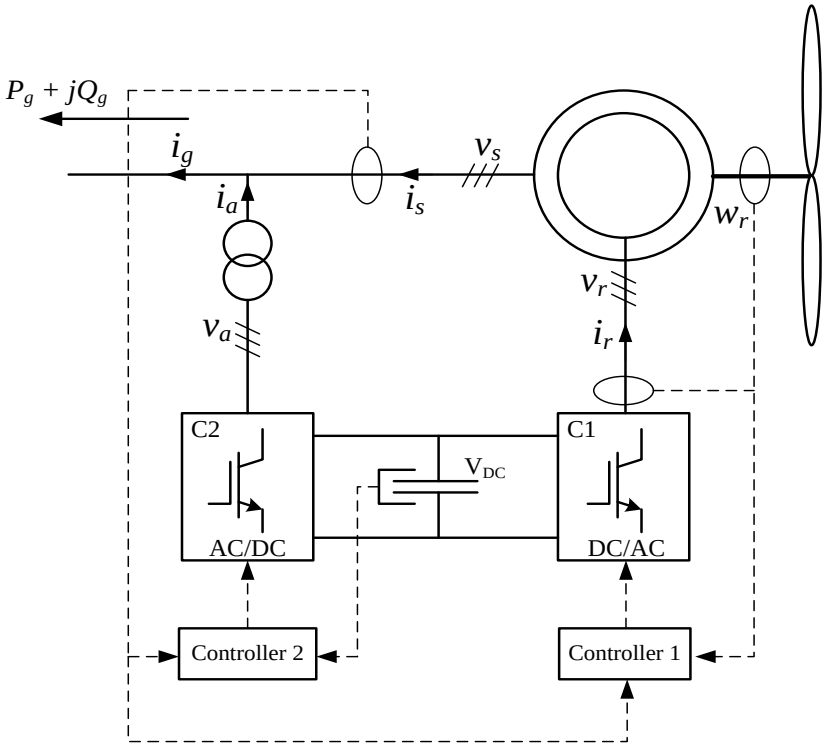

Fig. 3.1 Basic configuration of DFIG-based WECS

The RSC (C1) controls injected rotor voltage so that electromagnetic torque of the DFIG can follow the reference speed. It can also provide voltage support and reactive power control. The GSC (C2) keeps the dc link voltage constant.

Here, converter C1 is considered as a voltage source injected into the rotor; and converter C2 is modeled as a current source. To realize the rotor speed and terminal voltage, decouple control of converter C1 operates in a stator-flux *d-q* axis reference frame controlled by Controller 1 (Fig. 3.2). The control loops are with the PI controllers, where K_{px} and K_{ix} are proportional and integral gains, respectively.

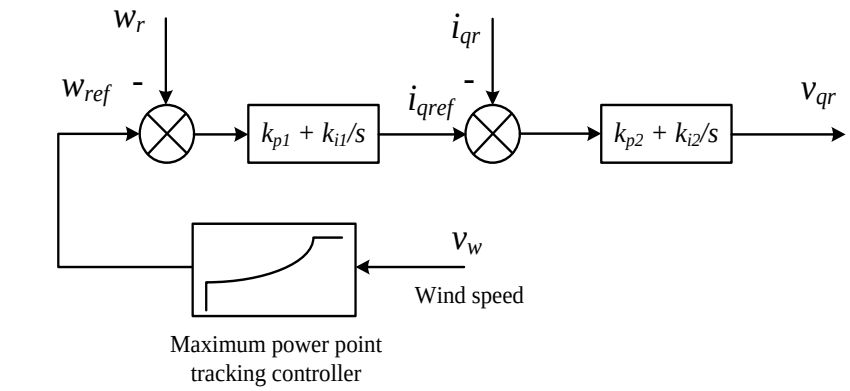

(a) Speed control loop

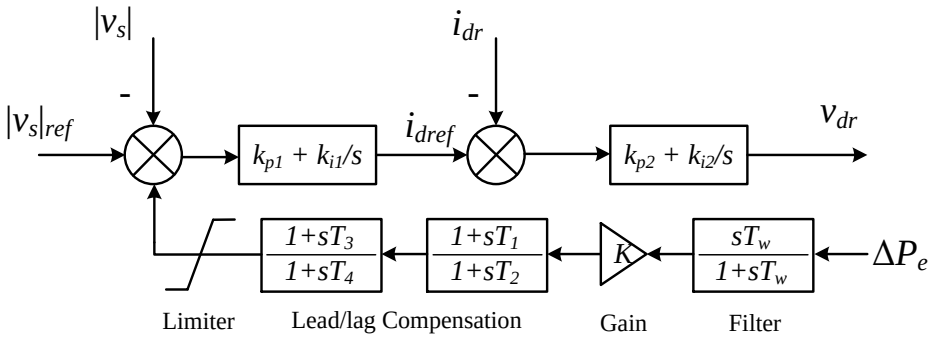

(b) Voltage control loop

Fig. 3.2 Speed and voltage control schemes for DFIG

Rotor speed is controlled by the *q* component of injected voltage v_{qr}. The reference turbine rotor speed is obtained by a MPPT controller, as illustrated in Fig. 3.2a. Many MPPT techniques have been developed and a look-up table based algorithm is commonly used. One commercially employed look-up table MPPT is Tip-Speed Ratio Control (TSRC) which typically requires

measurements of wind speed V_w. By using a look-up table of optimal tip-speed ratio, which is pre-determined from experimental simulations, reference generator rotor speed w_{ref} can be obtained when V_w is measured by an anemometer. The rotor speed error (deviation between the desired and the actual value) passes through PI controllers to get the desired i_{qr} and finally v_{qr}.

The terminal voltage control is as shown in Fig. 3.2b. Similar to speed control, terminal voltage error passes through PI controllers to get the desired i_{dr} and finally v_{dr}. The voltage controller may get saturated due to its limited ability to regulate power factor of wind farm. One solution is provision for external power factor compensation such as a capacitor bank, to enhance power factor regulation capability. Also, On-Load Tap Changer (OLTC) can be used to improve the dynamic range of DFIG itself. OLTC of a local transformer can be coordinately used to ensure the DFIG rotor current is controlled within a defined operating range: when i_{dr} is negative and has been limited, the tap is up; when i_{dr} is positive and has been limited, the tap is down [Cartwright, 2004]. This can reduce the possibility of exceeding a control limit in the event of a change in system operating condition.

3.2.4 Power Oscillation Damper

The basic configuration of POD consists of three blocks: a signal washout block (filter), a gain block and a phase compensation block. The signal washout block serves as a high-pass filter. When time constant T_w is high enough, steady

changes of input signal do not modify the terminal voltage. The gain K determines the improvement of damping by the PSS and phase compensation block is used to achieve the desired phase compensation. Stabilizer output limits are also needed and set as ±0.2 p.u. to prevent the PSS from countering the normal action. Since WECSs are far from load areas in general, variations in their terminal voltages have only a slight effect on bus voltage of loads. Therefore, although terminal voltages of WECSs may deviate slightly from their reference values due to integration of PSS into the voltage control loop, their impacts on voltage of load buses are limited. This is analogous to the principle of PSS for synchronous generator. Therefore, in this work, the POD is integrated into the voltage control loop (Fig. 3.2b). In a typical POD, the parameters are as follows:

- K: Gain of the compensation, typically K is in the range of 0.1 *p.u.* to 100 *p.u.*;
- T_w: time constant of wash-out filter, typically selected as 10s;
- T_1, T_2: time constants of phase compensation, and T_3=T_1, T_4=T_2, typically they are in the ranges of 0.1s to 1s and 0.001s to 0.1s respectively.

Stator electrical power has been widely used for PSS of synchronous generator so DFIG stator electrical power is employed as its input signal. Moreover, compared to other candidate signals such as slip or network frequency, it can avoid the impact of wind shear and tower shadow (as mentioned in Chapter 2) and maintain regular performance [Huges, 2008]. Therefore, stator electrical

power is the most suitable input signal for POD of DFIG.

3.3 Optimization Procedure

This section explains the application of PSO to solve problems related to tuning of for POD parameters. This chapter describes tuning of gain K and time constants T_1 (T_3) and T_2 (T_4) of POD for DFIG in order to explore the best performance for the system damping control.

3.3.1 Problem Formulation

Small signal stability is generally understood as the ability of a power system to restore to original stable operation condition, after being subjected to disturbance that leads to a gradually increasing change of one or more of the state variables of the power system. In this chapter, small signal stability problems for DFIG-based WECS and its influence on the whole interconnected power system is investigated with SSSA [Kundur, 1994]. SSSA makes good use of linear techniques to find useful information about the inherent dynamic characteristic of WECS.

Eigenvalues obtained by SSSA in complex forms must exist as a pair of conjugate eigenvalues, in the form of

$$\lambda_k = \alpha_k \pm j\omega_k \tag{3.9}$$

where the suffix k denotes the kth mode and each pair belongs to a corresponding electromechanical oscillation mode. Moreover, it is known that the real part of

the complex conjugate denotes the damping effect in that oscillation mode, while the imaginary part gives oscillation frequency in that mode. Frequency and damping ratio ζ of each oscillation are given by:

$$f_k = \frac{\omega_k}{2\pi} \tag{3.10}$$

$$\zeta_k = \frac{-\alpha_k}{\sqrt{\alpha_k^2 + \omega_k^2}} \tag{3.11}$$

To summarize, eigenvalues in complex forms are the major concern in SSSA. In this chapter, a tuned POD is applied in the DFIG-based WECS to improve damping ratios and real parts of eigenvalues related to electromechanical oscillatory modes so that the overall system stability can be enhanced. In other words, with the application of POD, real parts of complex eigenvalues should be shifted to be as negative as possible to improve damping ratios of damped oscillations. At the same time, no complex eigenvalues with positive real parts are allowed to survive in the system because all oscillation modes must be surely damped and none of them should be swinging in increasing amplitude with respect to time.

The optimization problem is a composite set of two eigenvalue-based objective functions, comprising the desired real part and damping ratio of lightly damped and undamped electromechanical modes, as follows:

$\zeta_k \geqslant \zeta_s$: Acceptable damping ratio ζ_s, which ensures that the *k*th eigenvalue with damping ratio (ζ_k) has sufficient damping and considerable stability margin;

$\alpha_k \leqslant \alpha_s$: α_k, the real part of the *k*th eigenvalue, should be placed in the region that lies on the left-side of a specified value, α_s.

Therefore, the objective function can be represented as follows:

$$\min \quad J = PF_1 \cdot \sum_{k=1}^{l} \sum_{\xi_k \le \xi_s} \left|\xi_k - \xi_s\right| + PF_2 \cdot \sum_{k=1}^{l} \sum_{\alpha_k \ge \alpha_s} \left|\alpha_k - \alpha_s\right| \tag{3.12}$$

where PF_1 and PF_2 stand for the penalty factors and l is the total number of electromechanical oscillation modes.

3.3.2 Modified Particle Swarm Optimizer Algorithm

PSO is a population-based optimization technique where the population comprises particles (solutions in this case). The system is initialized with a population of random solutions and each solution is assigned a randomized velocity, as follows:

$$\begin{aligned} x_m^{(n)}[] &= [K_m^{(n)}, T_{1,m}^{(n)}, T_{2,m}^{(n)}] \\ v_m^{(n)}[] &= [v_{k,m}^{(n)}, v_{t1,m}^{(n)}, v_{t2,m}^{(n)}] \end{aligned} \tag{3.13}$$

where $x_m^{(n)}[]$ stands for the position of *m*th particle during *n*th iteration ($x_m^{(0)}[]$ stands for initial population). $v_m^{(n)}[]$ stands for velocity of the *m*th particle during *n*th iteration ($v_m^{(0)}[]$ stands for initial velocity). The fitness of each position is defined as *fit*(). The objective function in (3.12) is used as the fitness function in PSO optimization with SSSA. Each particle keeps tracking its coordinates in hyperspace and its best value (i.e. the best fitness it has achieved so far) is called *pbest*. The global version of PSO keeps tracking the overall best value and its position, obtained by any particle(s) in the population, called *gbest* [Eberhart, 1995; Kennedy, 1995]. Until the best solution is found or iterations are completed, the velocity and position of particles is adjusted by the following

formula:

$$v_m^{(n+1)}[] = v_m^{(n)} + c_1 * rand_1() * (pbestx_m^{(n)}[] - x_m^{(n)}[]) + c_2 * rand_2() * (gbestx_m^{(n)}[] - x_m^{(n)}[]) \quad (3.14a)$$

$$x_m^{(n+1)}[] = x_m^{(n)}[] + v_m^{(n+1)}[] \quad (3.14b)$$

Acceleration parameters c_1 and c_2 determine how far a particle will move during one iteration. $rand_i()$ is a random number between 0 and 1. For different problems, the balance between local and global search ability is different. Considering this, an inertia weight or momentum was brought into Eq. (3.14a) by [Shi, 1998], as shown in Eq. (3.15):

$$v_m^{(n+1)}[] = v_m^{(n)} * w + c_1 * rand_1() * (pbestx_m^{(n)}[] - x_m^{(n)}[]) + c_2 * rand_2() * (gbestx_m^{(n)}[] - x_m^{(n)}[]) \quad (3.15)$$

where w plays the role of balancing global and local search. It can be a positive constant or even a positive linear or nonlinear function of time. Then the objective function in (3.12) is used as the fitness functions in MPSO optimization with SSSA.

3.3.3 Solution

Tuning of parameters of POD may be done as follows (the flowchart is shown in Fig. 3.3):

Step 1) Select the initial position $x_m^{(0)}[]$ and velocity $v_m^{(0)}[]$ for each particle. The initial position $x_m^{(0)}[]$ should be within a reasonable region for the SSSA as described in Section 3.2.4. Velocities $v_m^{(0)}[]$ are selected randomly.

Step 2) The position of each particle $x_m^{(n)}[]$, i.e. all parameters of POD, is

fed into the SSSA to obtain the specified eigenvalue $\lambda_k=\alpha_k+j\beta_k$, the real part for each oscillation mode and its damping ratio ξ_k. Fitness value from (3.12) determines the local best position $pbest\_x_m^{(n)}[]$ and the global best $gbest\_x_m^{(n)}[]$ for each particle. The best position is defined as the best particle with the smallest fitness achieved so far.

Step 3) Update the local best position $pbest\_x_m^{(n)}[]$ and global best position $gbest\_x_m^{(n)}[]$ at each iteration, as follows:

$$pbest\_x_m^{(n)}[]=\begin{cases} x_m^{(n)}, if \quad fit(x_m^{(n)}) \le fit(x_m^{(n-1)}) \\ pbest\_x_m^{(n-1)}, if \quad fit(x_m^{(n)}) > fit(x_m^{(n-1)}) \end{cases} \tag{3.16}$$

Global best position $gbest\_x_m^{(n)}$ is the local best position having the smallest fitness. Then the positions and velocities are updated by (3.15) and (3.14b), for all particles.

Step 4) Repeat *Steps 2*) and *3*) until total iterations are completed or the stability constraints are not violated.

Stop optimization when total iteration is complete or global best position have zero fitness, and choose values at the global best position as the final values of parameters of POD.

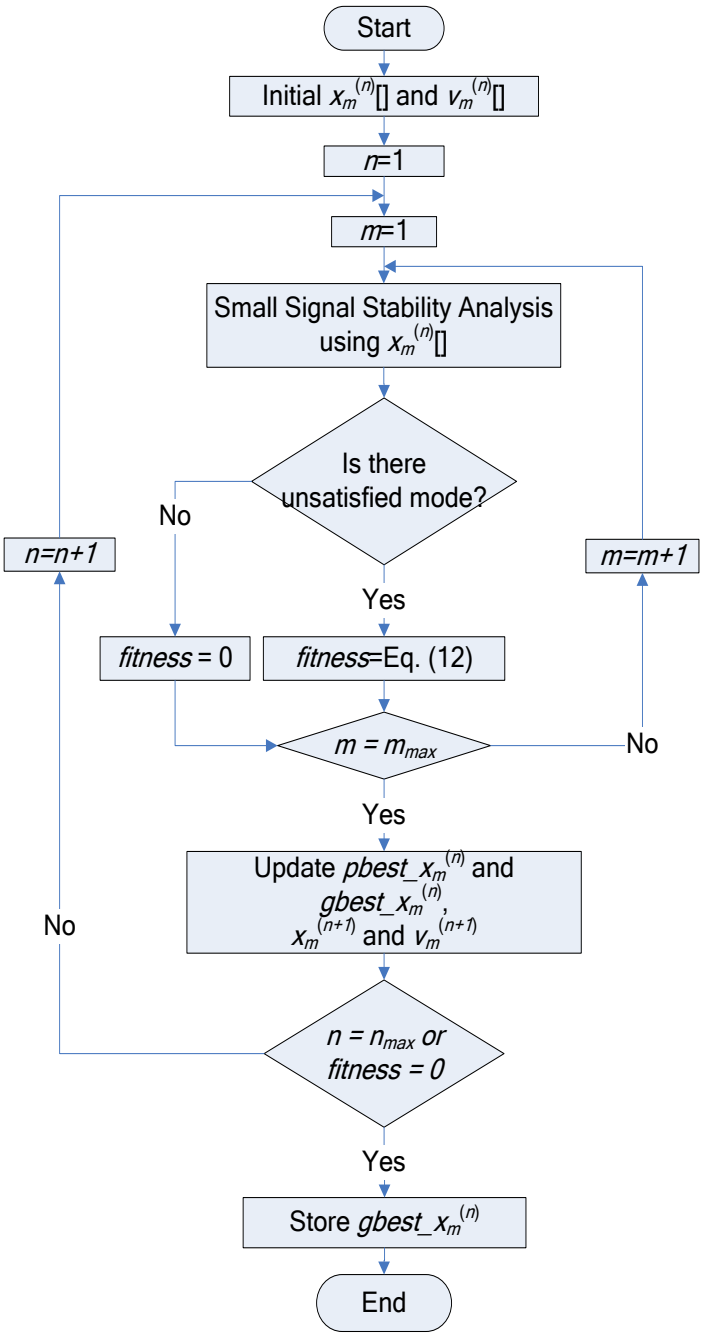

Fig. 3.3 Optimization procedure of POD parameters

3.4 Case Study

[Kundur, 1994] proposed the system shown in Fig. 3.4, consisting of two similar areas connected together by two transmission lines. All synchronous generators are identical with a common rating of 900 MVA, using the standard

third-order model. In Area 1, a DFIG-based WECS wind farm with rated capacity of 200MW is connected to the network while load of system is increased 200MW. The parameters of 2MW DFIG-based WECS can be found in Table 3.1.

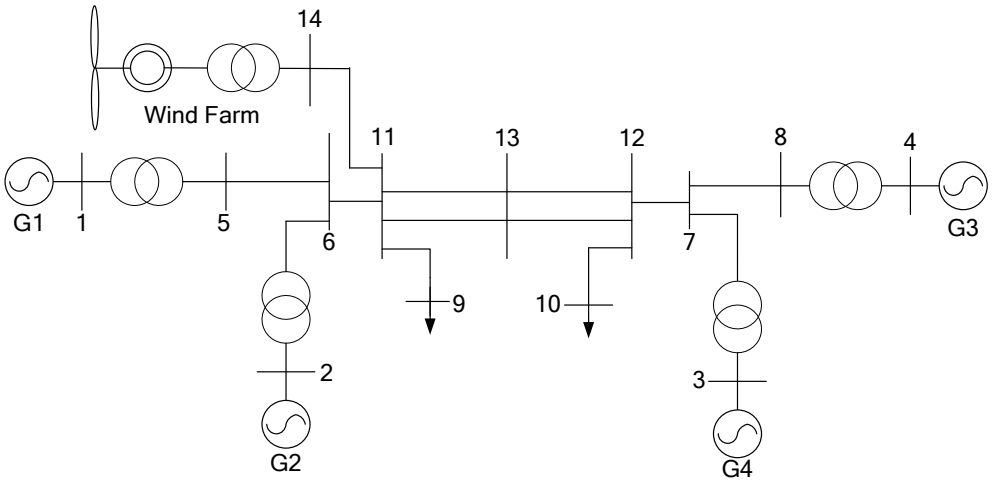

Fig. 3.4 Two-area four-machine system

Table 3.1 Parameters of DFIG-based WECS

Symbol	Meaning	Value
R	Blade length	75m
-	Blade number	3
ρ	Air density	1.225kg/m^3
H	Inertia constant	3s
r	Gearbox ratio	1:89
R_s	Stator resistence	0.01p.u.
R_r	Rotor resistence	0.01p.u.
X_m	Magnetizing reactance	3p.u.
X_s	Stator reactance	0.1p.u.
X_r	Rotor reactance	0.08p.u.
p	Number of poles	4
K_p	Proportional gain	10
K_i	Integral gain	0.1
K	Gain of POD	0.8208p.u.
T_1	Time constant	0.5402s
T_2	Time constant	0.2328s

3.4.1 Small Signal Stability Analysis

According to the objective function Eq. (3.12), the common acceptable damping ratio defined for optimization is 0.1 and the real part is -0.5. During the optimization, MPSO is implemented with MATLAB. The number of particles used in MPSO is 50 and a total of 50 iterations are executed. Values of parameters used in MPSO are: c_1=1.2, c_2=0.12 and w=0.9. There are three parameters to be optimized: gain K and time constants T_1 (T_3) and T_2 (T_4).

The finalized parameters of POD are listed in Table 3.1. Table 3.2 summarizes the system eigenvalues of inherent electromechanical oscillations. It shows three pairs of conjugate eigenvalues based on SSSA under the situation of DFIG-based WECS without installation of POD. Obviously, there is an inter-area mode oscillation with frequency around 0.57Hz in which generators in Area 1 swing against those in Area 2. Moreover, two local modes appear in the system with frequency close to 1Hz in which generators swing against each other in the same area.

Table 3.2 Eigenvalues of electromechanical modes

No	Mode	Eigenvalues	*f*(Hz)	Damping ratio (%)
		Without POD		
1	Inter-area	-0.2013 ± 3.5654i	0.57	**5.6**
2	Local (Area 1)	-0.7492 ± 6.3684i	1.01	11.7
3	Local (Area 2)	-0.6315 ± 6.6736i	1.06	9.4
		With POD		
1	Inter-area	-0.7673 ± 3.3590i	0.53	**22.3**
2	Local (Area 1)	-0.7384 ± 6.3676i	1.01	11.5
3	Local (Area 2)	-0.6372 ± 6.6697i	1.06	9.5

It can be noticed that POD drives the system to a more steady state

effectively by improving damping of inherent electromechanical oscillations, especially in terms of suppressing inter-area oscillation, and the damping ratio of inter-area mode is raised significantly from 5.6% to 22.3%, which is within acceptable levels.

3.4.2 Transient Stability Analysis

In order to obtain more information and to further investigate the performance of the tuned POD on improving system stability, transient stability simulation by software Power System Analysis Tool (PSAT) [Milano, 2005] is also used for evaluation. As the system illustrated in Fig. 3.4, at t=1s, a 100ms three-phase fault is applied at Bus 13. Fig. 3.5 demonstrates the relative power angle dynamics relationship between synchronous generators with Generator 1 as the reference. Obviously, the relative power angle oscillations in the system with the POD (see Fig. 3.5b) can settle down at a much faster rate than in the system without POD (see Fig. 3.5a).

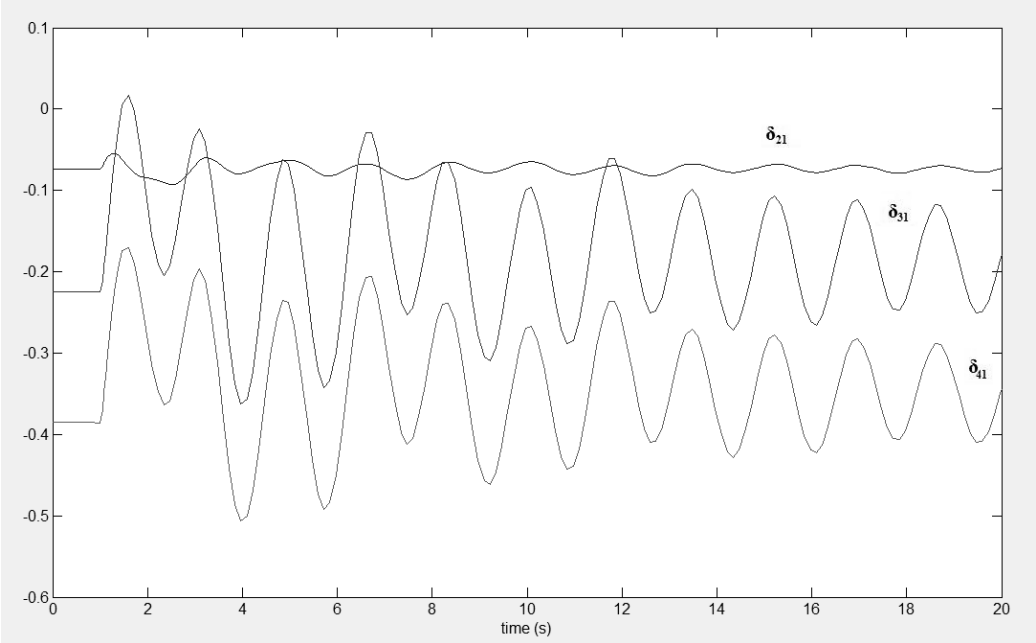

a) Without POD

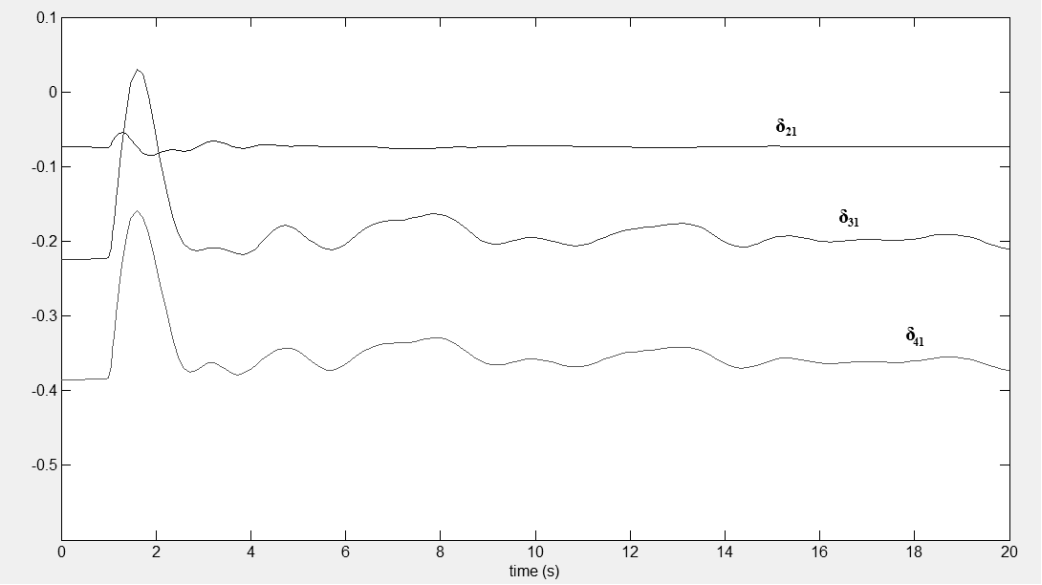

b) With POD

Fig. 3.5 Transient response of generator power angle

Active power supply by all interconnected generations further validates the effectiveness of the proposed POD. It can be observed that with the implementation of POD, fluctuations in active power of the generation are less (Figs. 3.6a and 3.6b). To conclude, POD can guarantee more reliable and stable power supply in the power system.

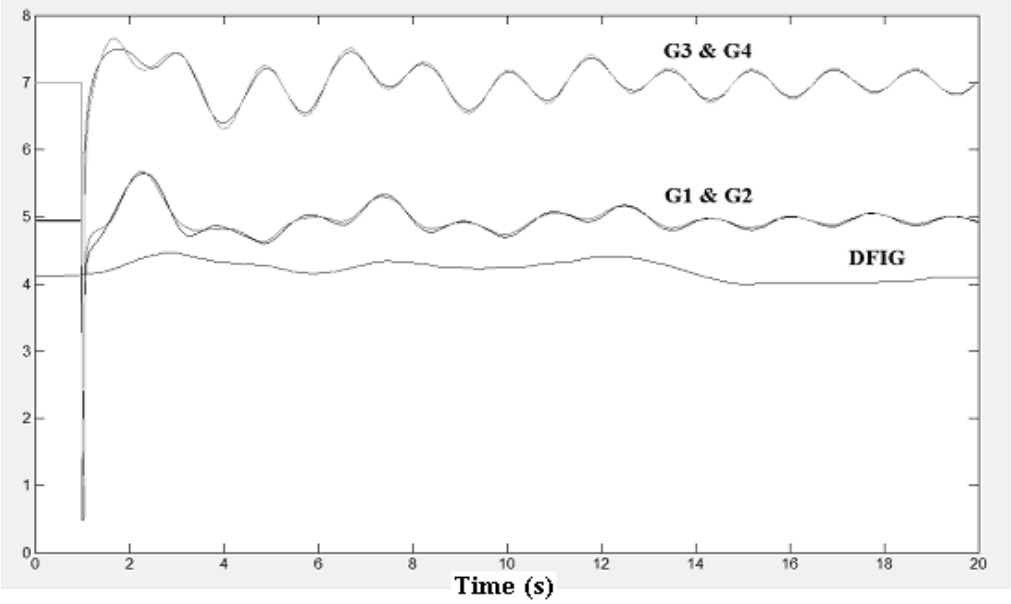

(a) Without POD

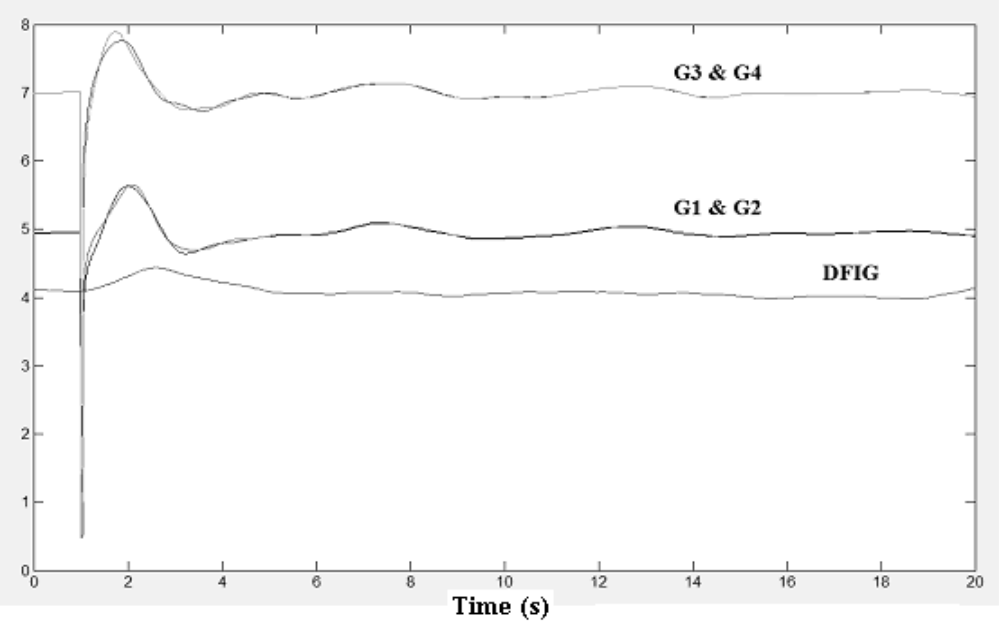

(b) With POD

Fig. 3.6. Transient response of generator active power

To sum up, the above results prove that the tuned POD controller applied in the DFIG-based WECS performs effectively to damp undesirable oscillations in post-fault period. As the oscillations are well-damped, transient stability of the system can be ensured.

3.5 Summary

Based on the eigenvalue analysis and transient stability results, it can be said that the application of MPSO to optimize parameters of the POD is highly efficient and the tuned POD used in the DFIG-based WECS is an effective measure to ensure dynamic performance of the interconnected system.

With the increasing penetration of DFIG-based wind farms into the power network, controllable DFIG-based WECS is necessary for enhancing stability.

Chapter 4 Coordinated Damping Control Design for DFIG-Based Wind Generation Considering Power Output Variation

4.1 Introduction

Wind energy is a kind of stochastic energy, implying that the output of wind farm varies in a certain range due to unstable wind characteristic. Therefore, the operating point of the power system changes from time to time because of integration of wind power. Deterministic SSSA cannot provide adequate security information and so it is necessary to consider the impact of variation of wind farm output in SSSA. The probabilistic theory has been successfully applied to select parameters of PSS, considering a large range of operating conditions [Chung, 2002 & 2003]. Through representing nodal voltage and nodal injection by normal distribution, comprising their expectations and covariance values, probabilistic SSSA can obtain the range of variation of system eigenvalues. Power output of wind farm is a mixed random variable, which is continuous between values of zero and the rated power, but discrete at values of zero and rated power. Therefore, probabilistic SSSA has been further extended in this chapter for handling this kind of distributed variables.

With application of DFIG equipped with PSS, every PSS may affect all electro-mechanical oscillation modes to some extent. Sequential addition of new stabilizers disturbs previously assigned eigenvalues and that may cause destabilization due to lack of coordination, especially in multi-machine systems. Therefore, in this chapter, PSSs for DFIG and conventional synchronous generator are coordinated by MPSO introduced in Chapter 3 which later has been standardized and termed as PSO, while wind farm power output variation is considered by means of probabilistic SSSA.

4.2 Probabilistic Small Signal Stability Analysis Incorporating with Uncertain Wind Generation

Consideration of a wide range of operating points becomes necessary in SSSA due to wind power integration. This section proposes a probabilistic SSSA incorporating uncertain wind generation.

4.2.1 Weibull Distribution for Wind Speed

Generally Weibull distribution is used to describe wind speed probability distribution by two components, shape parameter and scale parameter [Jain, 2011]. Therefore, the PDF and Cumulative Distribution Function (CDF) of wind speed can be obtained by (4.1) and (4.2), as follows:

$$f(V_w) = \frac{K}{C}\left(\frac{V_w}{C}\right)^{K-1} e^{-\left(\frac{V_w}{C}\right)^K}, \quad V_w > 0 \tag{4.1}$$

$$F(V_w) = 1 - e^{-\left(\frac{V_w}{C}\right)^K}, \qquad V_w > 0 \tag{4.2}$$

where constants K and C are shape and scale parameters of Weibull distribution, respectively.

4.2.2 Power Curve of WECS

The power curve model $p=g(V_w)$ needs to be determined to realize the conversion from PDF of V_w to PDF of power output p. Firstly, the candidate models should fit the real statistical data provided by WECS manufacturers as well as possible, and secondly, during the change of PDF variable from V_w to p, both inverse function $V_w=g^{-1}(p)$ and derivative equation $g'(V_w)$ are needed. Then, PDF of p can be obtained by:

$$f(p) = \left| \frac{1}{g'(g^{-1}(p))} \right| \cdot f(g^{-1}(p)) \tag{4.3}$$

In this study, power curve of WECS is modeled with seven widely used mathematical models. In Table 4.1, p_{rated} is the rated power, V_{ci} denotes cut-in speed, V_{rs} is rated speed, V_{co} denotes cut-off speed and a_i are regression constants identified by curve fit tools. Measurements of goodness of fit from M1 to M7 in the range of V_{ci} to V_{rs} are illustrated in Fig. 4.1. Polynomials of M6 and M7 have better goodness of fit, but they cannot provide inverse function to realize the PDF conversion and thus they are not considered to model the power curve. Also, M2 and M5 are eliminated due to the mathematical difficulties in PDF conversion. Between M1, M3 and M4, M1 is the most suitable equation, as the power curve

model.

Table 4.1 Comparison of power curve models

No.	Equations	PDF conversion
M1	$p_{rated} \cdot \left(\frac{V_w - V_{ci}}{V_{rs} - V_{ci}} \right)$	√
M2	$p_{rated} \cdot \left(a_1 V_w{}^2 + a_2 V_w + a_3 \right)$	×
M3	$p_{rated} \cdot \left(\frac{V_w{}^2 - V_{ci}{}^2}{V_{rs}{}^2 - V_{ci}{}^2} \right)$	√
M4	$p_{rated} \cdot \left(\frac{V_w{}^3 - V_{ci}{}^3}{V_{rs}{}^3 - V_{ci}^3} \right)$	√
M5	$p_{rated} \cdot \left(\frac{V_w - V_{ci}}{V_{rs} - V_{ci}} \right)^3$	×
M6	$p_{rated} \cdot \left(a_4 V_w^3 + a_5 V_w{}^2 + a_6 V_w + a_7 \right)$	×
M7	$p_{rated} \cdot \left(a_8 V_w^4 + a_9 \cdot V_w^3 + a_{10} \cdot V_w{}^2 + a_{11} \cdot V_w + a_{12} \right)$	×

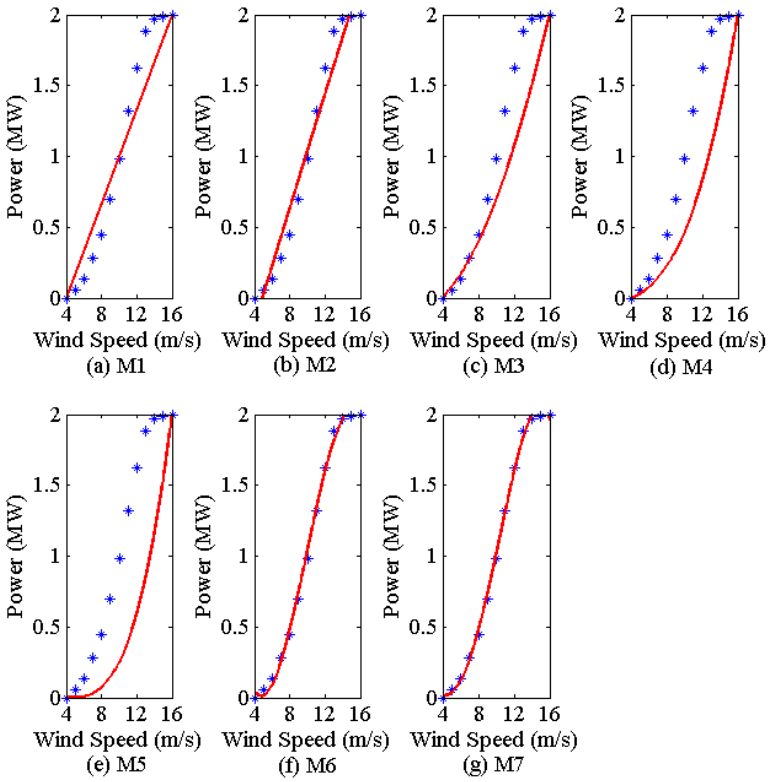

Fig. 4.1 Comparison of real and model power curves

Therefore, the relationship between wind velocity and active output of a WECS can be represented by the following equations:

$$p=\begin{cases} 0, & (0<V_w<V_{ci}, V_w>V_{co}) \\ p_{rated}\cdot\left(\dfrac{V_w-V_{ci}}{V_{rs}-V_{ci}}\right), & (V_{ci}\le V_w\le V_{rs}) \\ p_{rated}, & (V_{rs}\le V_w\le V_{co}) \end{cases} \tag{4.4}$$

All parameters are related to specified features of a WECS, which vary with the manufacturer and the turbine type.

4.2.3 Probabilistic Model for WECS

An aggregated model of a wind farm is preferred when investigating short-term dynamic stability because this simplification can reduce the complexity and time of computation, and it has already included adequate details to represent the dynamics of WECSs [Wang, 2011; Gautam, 2011]. Hence, this section also models the dynamics of a wind farm by a single machine equivalent, i.e. all WECSs operate identically and have the same initial operational state. Besides, a uniform wind speed distribution in the wind farm, i.e. WECSs are receiving similar incoming winds, which is a commonly used assumption for power system studies [Banzo, 2011; Karki, 2010], is also adopted here. For example, a typical 2MW WECS with the following parameters is considered: shape parameter K=2; scale parameter C=20; V_{ci}=4m/s; V_{co}=25m/s; and V_{rs}=16m/s. If the wind speed distribution and characteristics of WECS (i.e. power curve) are known, power output distribution of WECS can be obtained by

Monte-Carlo Simulation (MCS). Then the total power output of a wind farm can be considered as the power output of a WECS, multiplied by the number of WECSs in the wind farm. Fig. 4.2 illustrates the actual distribution of output of a wind farm comprising 100×2MW-WECSs, derived by carrying out MCS 10,000 times.

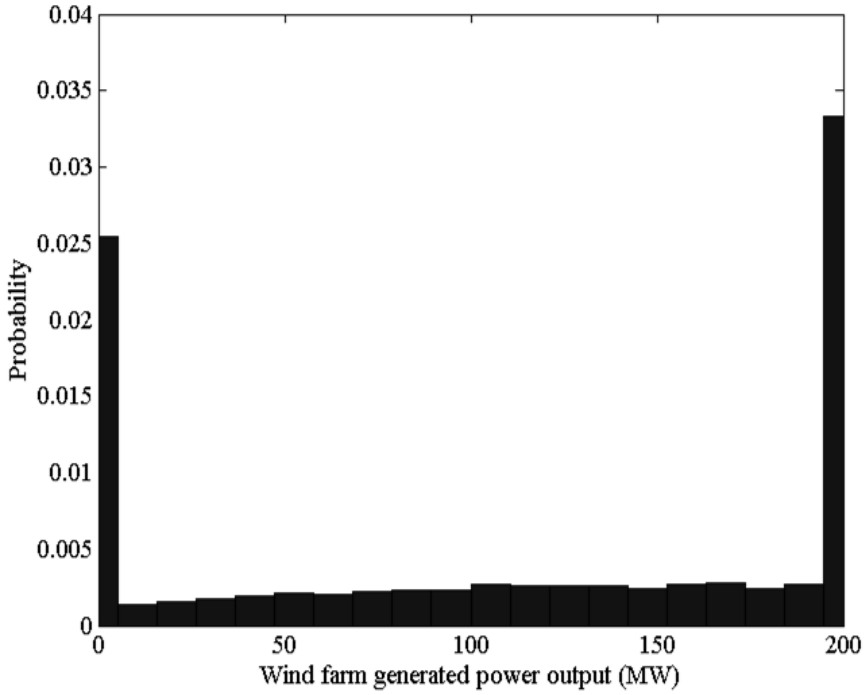

Fig. 4.2 Distribution of wind farm power output

The distribution can be split into three parts, as follows.

1) Generated power at zero

The probability of the power output being zero is the sum of the probability of wind speed being lower than V_{ci} and higher than V_{co}. Values of these probabilities are shown as follows:

$$P(V_w \le V_{ci}) = 1 - e^{-(V_{ci}/C)^K} \tag{4.5a}$$

$$P(V_{co} \le V_w) = e^{-(V_{co}/C)^K} \tag{4.5b}$$

2) Generated power at p_{rated}

The probability of the power output being equal to p_{rated} is the probability of wind speed being between V_{rs} and V_{co}:

$$P(V_{rs} \le V_w \le V_{co}) = e^{-(V_{rs}/C)^K} - e^{-(V_{co}/C)^K} \tag{4.6}$$

3) Generated power between zero and p_{rated}

The probability of the power output being between zero and p_{rated} is the probability of wind speed being between V_{ci} and V_{rs}:

$$P(V_{ci} \le V_w \le V_{rs}) = e^{-(V_{ci}/C)^K} - e^{-(V_{rs}/C)^K} \tag{4.7}$$

In this case, estimation of generated power distribution is approximated and considered as normal distribution represented by expectation μ and variance σ^2, as follows:

$$\mu = \int_{-\infty}^{+\infty} p \cdot f(p) dp, \quad \sigma^2 = \mu^2 - \int_{-\infty}^{+\infty} p^2 \cdot f(p) dp \tag{4.8b}$$

where $f(p)$ is the PDF converted from $f(V_w)$ by (3.3), described as:

$$f(p) = \frac{K'}{C'} \left(\frac{p-\gamma'}{C'}\right)^{K'-1} e^{-\left(\frac{p-\gamma'}{C'}\right)^{K'}} \tag{4.8c}$$

$$C' = \frac{p_{rated} \cdot C}{V_{rs} - V_{ci}} \quad K' = K \quad \gamma' = -\frac{p_{rated} \cdot V_{ci}}{V_{rs} - V_{ci}} \tag{4.8d}$$

4.2.4 Probabilistic SSSA

All nodal voltages (V), nodal injections (S) and eigenvalues (λ) are regarded as random variables. The objective is to determine expectation $\bar{\lambda}$ and covariance values C_λ of system eigenvalues. Since the subset of S (expectation $\bar{S}$ and variance matrix C_S) corresponding to synchronous generators and wind farms is known, it can be used to solve probabilistic power flow instead of conventional

power flow to obtain voltage expectation $\bar{V}$ and covariance matrix C_V. When calculating the power flow, wind power generators are considered as PV nodes [Padron, 2010]. The probabilistic SSSA procedure is described in detail herein below.

Step 1) Based on an initial set of $\bar{V}$ values, mismatches between the specified $\bar{S}_0$. (this vector includes nodal injections of synchronous generators and wind farms; values for wind farms should be *0*, p_{rated}, μ for zero power output, rated power output and output between zero and rated value, respectively) and calculated values of $\bar{S}$ at $\bar{V}$ are called $\Delta\bar{S}$, the same as in conventional load flow.

Step 2) Equation (4.9a) is used to compute a correction $\Delta\bar{V}$ and (4.9b) is used to compute a voltage covariance matrix.

$$\Delta\bar{V} = J_V^{-1}\Delta\bar{S} \tag{4.9a}$$

$$C_V = \overline{\Delta V \Delta V^T} = J_V^{-1}\,\overline{\Delta S \Delta S^T}\,(J_V^{-1})^T = J_V^{-1} C_S (J_V^{-1})^T \tag{4.9b}$$

where J_V is the conventional jacobian matrix calculated at $\bar{V}$. *Cs* includes values of *0*, *0*, σ^2 for zero power output, rated power output and output between zero and rated value, respectively. These values are returned to conventional load flow and the probabilistic power flow is thus iterated until convergence.

Step 3) It is now possible to calculate expectation values $\bar{\lambda}_k$ and covariance matrix C_λ of the eigenvalues. If matrix *A* is the coefficient matrix of the linearized system's dynamics equations, its expectation value $\bar{A}$ can be written as

$$\bar{A} = \bar{A}_0 + \frac{1}{2}\sum_{i=1,j=1}^{2N,2N}\left(\left.\frac{\partial^2 A}{\partial V_i \partial V_j}\right|_{V=\bar{V}} C_{Vi,j} \right) \tag{4.10}$$

And $$C_\lambda = J_\lambda C_V J_\lambda^T \tag{4.11}$$

where $\bar{A}_0$ is determined at $\bar{V}$ and J_λ is the first order derivative matrix $\partial\lambda_k/\partial V_i$ of eigenvalue λ, with respect to voltages, computed at $\bar{V}$.

Step 4) The expectation of a specified eigenvalue $\bar{\lambda}_k = \bar{\alpha}_k + j\bar{\beta}_k$ can be obtained from conventional calculation of $\bar{A}$ and variance from diagonal values of matrix C_λ. In practical calculations, variation of the imaginary part of eigenvalues is sufficiently small to be neglected, so C_λ will be the covariance matrix of the real part C_α. Then the expectation of damping ratio of λ_k can be obtained by $\bar{\xi}_k = -\alpha_k / \sqrt{\alpha_k^2 + \beta_k^2}$ and its variance by $C_\xi(k,k) = \beta_k^4 / \bar{\xi}_k^6 \cdot C_\alpha(k,k)$.

According to the previous descriptions, PDF and CDF of system eigenvalues can be obtained by applying SSSAs to three parts of the probabilistic model for WECS in (4.6)-(4.8), respectively, and then combining them together. When there are N wind farms in a system, the calculation should be done 3^N times; compared to MCS, computational cost of the optimization process will be reduced.

4.3 PSS Parameters Optimization by PSO

This section describes the problem formulation and the solution method for PSS coordinated tuning.

4.3.1 Problem Formulation

The coordination problem is concocted into an optimization problem of a composite set of two eigenvalue-based objective functions, comprising the desired real part and damping ratio of lightly damped and undamped electromechanical modes, as follows:

$P(\xi_k \leq \xi_s)$: The percentage of unacceptable damping ratio ξ_s, which represents that the kth eigenvalue with damping ratio (ξ_k) has not sufficient damping and considerable stability margin.

$P(\alpha_k \geq \alpha_s)$: The percentage of unsatisfied α_k , the real part of the kth eigenvalue, should not be placed in the region that lies on the right-side of a specified value, α_s.

For probabilistic SSSA, the objective function includes CDF of stability constraints, represented as:

$$\min \quad J = PF_1 \cdot \sum_{k=1}^{l} P(\xi_k \leq \xi_s) + PF_2 \cdot \sum_{k=1}^{l} P(\alpha_k \geq \alpha_s) \tag{4.12}$$

The gain and lead-lag time constants of PSS to be coordinated (Fig. 3.2b) are limited by their following physical constraints:

$$\begin{aligned} &K_{i,\min} \leq K_i \leq K_{i,\max} \\ &T_{1i,\min} \leq T_{1i} \leq T_{1i,\max}, T_{3i} = T_{1i} \\ &T_{2i,\min} \leq T_{2i} \leq T_{2i,\max}, T_{4i} = T_{2i} \end{aligned} \tag{4.13}$$

where i=1,2,3,…,*npss*; and *npss* is the total number of PSSs. K_i is in the range of 0.1 p.u. to 100 p.u., so as to increase the damping of electromechanical modes while avoiding making exciter mode unstable; T_{1i} is 0.1s to 1s and T_{2i} is 0.001s

to 0.1s as suggested [Sauer, 1998].

4.3.2 Solution

The optimization is still executed by PSO algorithm as described in detail in Section 3.3.2. Objective functions in (3.12) and (4.12) are used as the fitness functions in PSO optimizations with deterministic and probabilistic SSSA, respectively.

The optimization procedure is similar to Section 3.3.3. Instead, in *step 2*), all parameters of PSSs, is fed into the deterministic or probabilistic SSSA. Then it is possible to obtain the specified eigenvalue $\lambda_k=\alpha_k+j\beta_k$ or CDF $F(\alpha)$ of the real part for each oscillation mode, and its damping ratio ξ_k or CDF $F(\xi)$. Fitness value from (3.12) or (4.12) determines the local best position $pbest\_x_m^{(n)}[]$ and the global best $gbest\_x_m^{(n)}[]$ for each particle.

4.4 Case Study

New England Ten-Generator 39-Bus system is used to validate the effectiveness of the proposed method. This is a widely used test system [Padiyar, 1996]. As shown in Fig. 4.3, three wind farms with aggregate rated capacity of 200MW are connected at Buses 34, 36 and 37, respectively. synchronous generators, except for the equivalent external generator G2 connected at Bus 2, are installed with PSS.

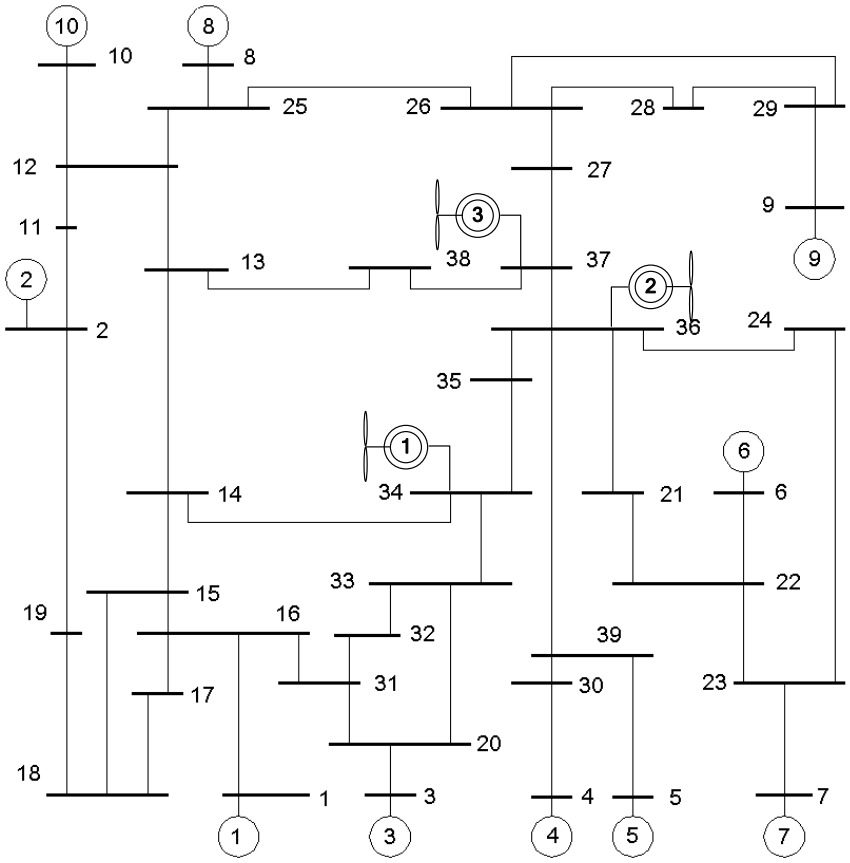

Fig. 4.3 New England ten-generator 39 bus system

4.4.1 Operational Conditions

In order to evaluate the performance of these damping controllers, deterministic SSSA is conducted under different operating conditions of WECS. A DFIG-based WECS can transmit power to the network through both the generator stator and the rotor, with a bidirectional converter, which has a rating typically around 25% of the WECS's rated capacity, simply called the rotor circuit here. Active power of the stator is always supplied to the power grid, independent of wind speed. However, the rotor circuit is able to operate with power flow in both directions (i.e. power absorbing from or injecting into grid), which depends on the variation of wind speed.

1) Sub-synchronous mode:

In light winds, the wind turbine rotor is slow-rotating and slip is positive in sub-synchronous operation; active power is absorbed by the rotor circuit from the power grid. Here wind speed V_w=5m/s is considered.

2) Normal mode:

Active power of the stator is always supplied to the power grid and the rotor circuit does not exchange power with the grid through the converter. Wind speed is assumed to be V_w=8m/s.

3) Super-synchronous mode:

In strong winds, the rotor rotates faster than the synchronous speed and slip is negative in super-synchronous operation of the rotor. Active power is then supplied from the rotor circuit to the power grid and the power output is increased. The wind speed is assumed to be V_w=12m/s.

4.4.2 Control Design

Initially, gains and time constant parameters of PSSs for synchronous generator and WECS (Table 4.2) are determined by the residue method [Pagola, 1989] at normal operation, without coordination. The related eigenvalues are chosen in results of probabilistic SSSA according to frequencies within the typical range of 0.1 to 2.0Hz. To further classify the oscillatory modes obtained, participation factor analysis has been applied to identify dominating states, including deviations of rotor speed and power angle of machines affecting a

given mode or eigenvalue. This system has 9 modes with frequencies ranging from around 0.6Hz to 1.2Hz; eigenvalues associated with different WECS operating conditions are listed in Table 4.3. In this thesis, ξ_s and α_s are chosen to be 0.1 and -0.5, respectively. It is clear that three of these modes do not satisfy these criteria (Modes 3, 4 and 7 are highlighted with boxes), especially when wind power penetration is increasing, i.e. changing from sub-synchronous mode to super-synchronous mode. Therefore, the scenario of wind farm at maximum output is chosen as the worst situation for optimization.

During the optimization, the PSO algorithm is implemented with MATLAB. The number of particles used in PSO is 50 and a total of 50 iterations are executed. Values of parameters used in PSO are: c_1=1.2, c_2=0.12 and w=0.9. There are 60 parameters to be optimized, the time constant T_w is set to be 10s. Firstly, in the condition of maximum output, the deterministic SSSA is applied for optimization and the objective function is Eq. (3.12). Then the method proposed with Eq. (4.12) is used to conduct optimization again. The final values of optimized parameters of damping controllers are listed in Table 4.2.

Table 4.2 Parameters of PSS in ten-generator 39-bus system

PSSs without coordination					
	K	T_1	T_2	T_3	T_4
G1	35	0.3469	0.0557	0.3469	0.0557
G3	4	0.3442	0.0731	0.3442	0.0731
G4	22	0.3104	0.0667	0.3104	0.0667
G5	20.5	0.2934	0.0456	0.2934	0.0456
G6	5	0.3833	0.0422	0.3833	0.0422
G7	25	0.2866	0.0506	0.2866	0.0506
G8	27	0.3083	0.0484	0.3083	0.0484
G9	5.5	0.3277	0.0841	0.3277	0.0841
G10	19.5	0.3124	0.0871	0.3124	0.0871
WECS 1	20	0.5187	0.0391	0.5187	0.0391
WECS 2	20	0.4007	0.0568	0.4007	0.0568
WECS 3	20	0.4020	0.1989	0.4020	0.1989
PSSs coordinated at maximum output					
	K	T_1	T_2	T_3	T_4
G1	16.1	0.4661	0.0681	0.4661	0.0681
G3	51.3	0.9744	0.0518	0.9744	0.0518
G4	5.2	0.6243	0.0654	0.6243	0.0654
G5	24	0.8587	0.0714	0.8587	0.0714
G6	33.4	0.4999	0.0703	0.4999	0.0703
G7	13.3	0.3765	0.0669	0.3765	0.0669
G8	18.8	0.8840	0.0692	0.8840	0.0692
G9	10.3	0.4454	0.0935	0.4454	0.0935
G10	34.5	0.1686	0.0019	0.1686	0.0019
WECS 1	37.2	0.5418	0.0276	0.5418	0.0276
WECS 2	35.3	0.1286	0.0342	0.1286	0.0342
WECS 3	31.7	0.1607	0.0535	0.1607	0.0535
PSSs coordinated by proposed method					
	K	T_1	T_2	T_3	T_4
G1	21.6	0.7885	0.0683	0.7885	0.0683
G3	25.4	0.2609	0.0176	0.2609	0.0176
G4	27.6	0.4214	0.0643	0.4214	0.0643
G5	9.2	0.3614	0.0732	0.3614	0.0732
G6	41.4	0.3287	0.0914	0.3287	0.0914
G7	23.6	0.3139	0.0553	0.3139	0.0553
G8	34.3	0.3612	0.0347	0.3612	0.0347
G9	17.7	0.3438	0.0855	0.3438	0.0855
G10	23.3	0.5067	0.0231	0.5067	0.0231
WECS 1	29.5	0.4329	0.0551	0.4329	0.0551
WECS 2	10.4	0.6192	0.0462	0.6192	0.0462
WECS 3	33.8	0.2057	0.0427	0.2057	0.0427

Table 4.3 Eigenvalues of electromechanical modes

	Sub-synchronous mode	Normal mode	Super-synchronous mode
PSSs without coordination	-1.7083 ±8.3401i	-1.7797 ±8.1490i	-1.6944 ±7.8205i
	-1.4532 ±7.9104i	-1.4623 ±7.9279i	-1.4071 ±8.0388i
	-0.4149 ±6.9432i	-0.4023 ±6.9266i	-0.3839 ±6.9296i
	-0.4751 ±6.5406i	-0.4949 ±6.5562i	-0.2904 ±6.6139i
	-0.7709 ±6.5985i	-0.7118 ±6.5210i	-0.7219 ±6.4788i
	-1.4578 ±6.5795i	-1.4805 ±6.4887i	-1.5515 ±6.4561i
	-0.9888 ±5.0515i	-0.8402 ±5.0829i	-0.3407 ±4.8044i
	-1.8415 ±3.9942i	-1.8873 ±4.0017i	-1.9133 ±4.0255i
	-0.8624 ±3.4328i	-0.9445 ±3.5550i	-0.9360 ±3.8753i
PSSs coordinated at maximum output	-1.3039 ±6.4188i	-1.3239 ±6.4286i	-1.3239 ±6.4906i
	-0.8592 ±6.0804i	-0.8864 ±6.0739i	-0.9120 ±6.0939i
	-2.2110 ±5.6696i	-2.2083 ±5.6630i	-2.2035 ±5.6430i
	-1.2551 ±4.4878i	-1.2819 ±4.4644i	-1.2361 ±4.4464i
	-0.6303 ±4.3324i	-0.6309 ±4.3539i	-0.6339 ±4.3825i
	-1.6819 ±4.1474i	-1.8298 ±4.3135i	-1.9414 ±4.5218i
	-1.7239 ±3.9333i	-1.7279 ±3.9420i	-1.7171 ±3.9487i
	-0.1265 ±3.2409i	-0.3621 ±3.6065i	-0.5135 ±3.4445i
	-0.8347 ±2.6559i	-0.8337 ±2.5963i	-0.7938 ±2.5780i
PSSs coordinated by proposed method	-0.8957 ±8.4534i	-0.9897 ±8.3607i	-1.0004 ±8.3554i
	-1.3013 ±7.3279i	-1.3502 ±7.1023i	-1.3383 ±7.0299i
	-2.0108 ±6.5203i	-2.0477 ±6.8036i	-1.9883 ±7.0485i
	-0.8148 ±6.5195i	-0.9525 ±6.4533i	-1.0158 ±6.4472i
	-0.9697 ±4.8431i	-1.0646 ±4.8375i	-1.1152 ±4.8295i
	-1.4259 ±4.0813i	-1.5789 ±4.0337i	-1.5604 ±4.1233i
	-1.6263 ±3.9721i	-1.3906 ±4.0361i	-1.3521 ±4.0426i
	-0.7258 ±3.8152i	-0.8821 ±3.7840i	-0.9385 ±3.7327i
	-0.6504 ±2.9486i	-0.6461 ±2.8856i	-0.6069 ±2.8598i

4.4.3 Small Signal Stability Analysis

First accuracy of the proposed Probabilistic SSSA is tested. Results obtained by the proposed method are compared with MCS (10,000 times), as shown in Fig. 4.4, the real parts of three poor damping modes 3, 4 and 7 under PSSs without coordination. Effectiveness of the proposed method in handling variation of wind power is clearly confirmed.

Performance under different WECS operating modes is investigated. It can be seen from Table 4.3 that one of the system eigenvalues still lies outside the predefined area (i.e. Mode 8, highlighted with box), when WECS operates in normal or sub-synchronous mode. Also, system eigenvalues distribution results provided by MCS, as shown in Fig. 4.5, confirm that the optimization process at one operating condition cannot shift all eigenvalues to the specified region. On the contrary, both system eigenvalues listed in Table 4.3 and results from MCS confirm that the proposed approach is able to shift all eigenvalues to the predefined area.

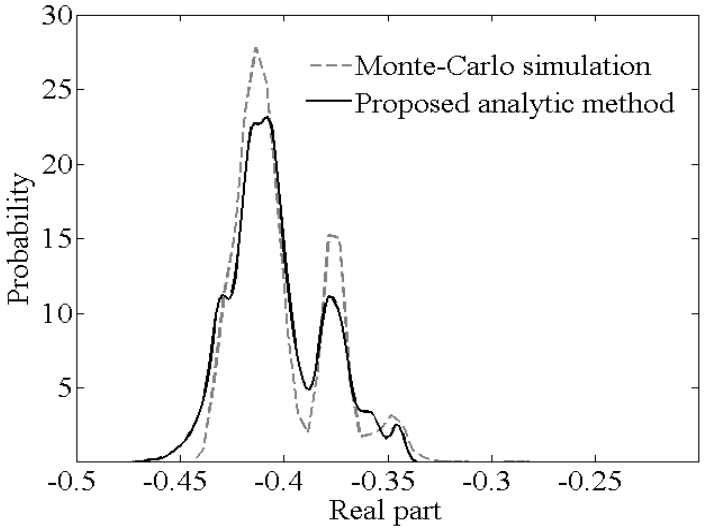

a. Mode 3

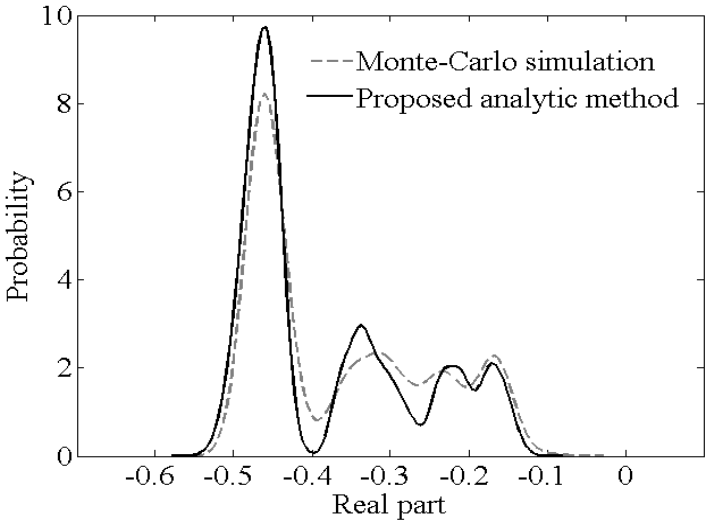

b. Mode 4

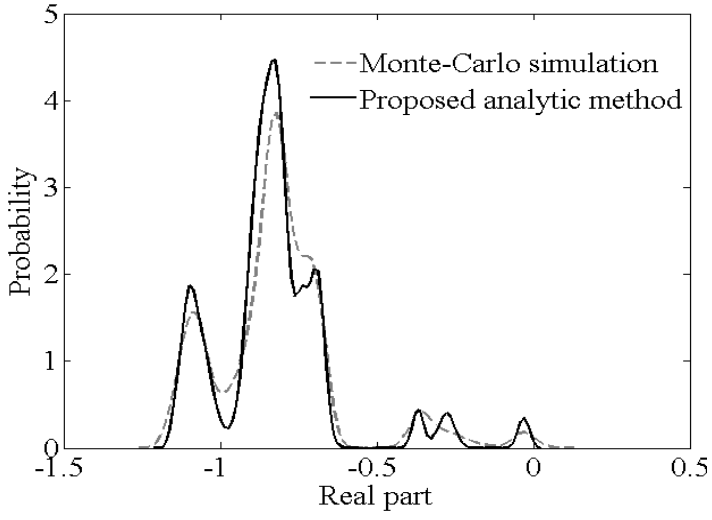

c. Mode 7

Fig. 4.4 PDF of real part of eigenvalues

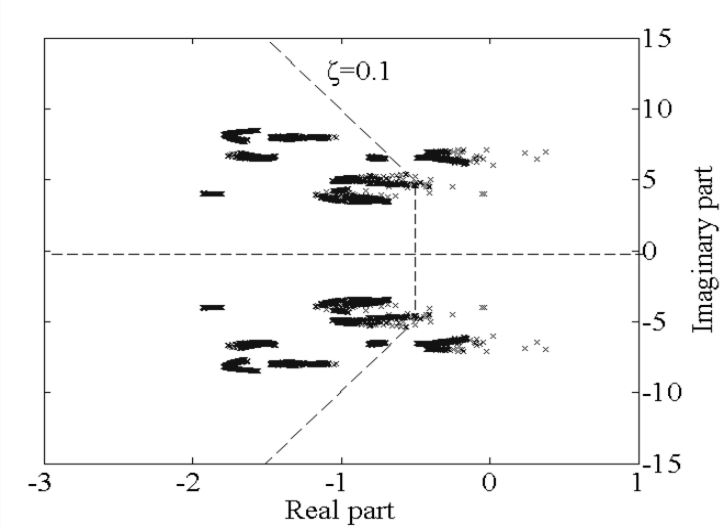

a. PSSs without coordination

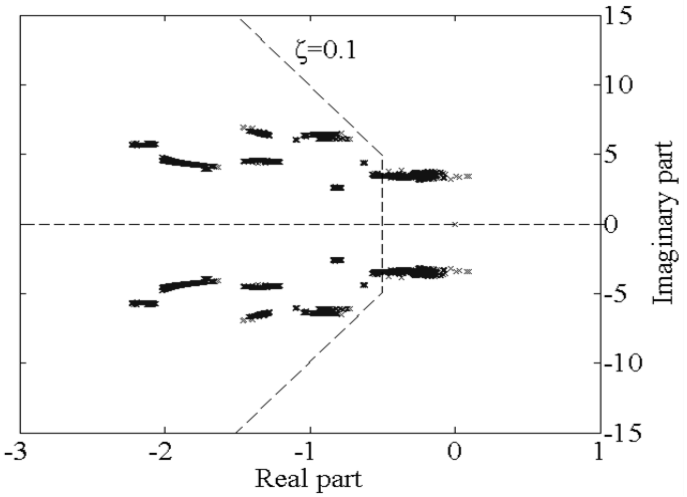

b. PSSs coordinated at maximum output

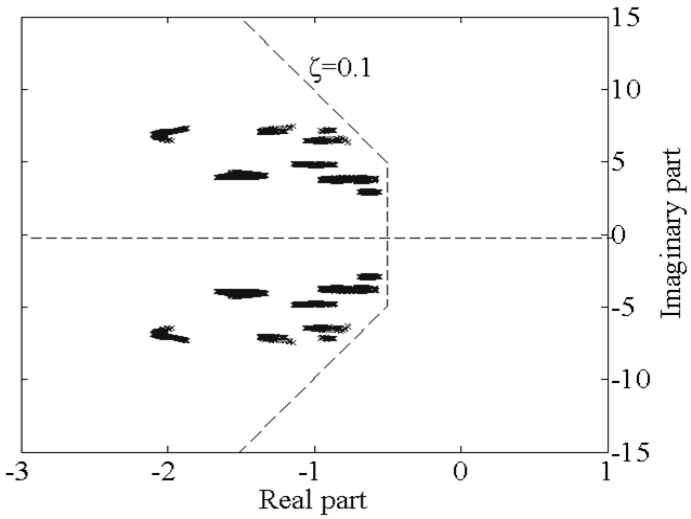

c. PSSs coordinated by proposed method

Fig. 4.5 Eigenvalues distribution under different cases by Monte-Carlo simulation

4.4.4 Transient Stability Simulation

To evaluate the effectiveness of coordinated damping controllers, system transient responses are also considered. Time-domain simulations are carried out by software package PSAT. For time-domain simulations, at t=1s, a 100ms three-phase fault close to Bus 13 is applied at the transmission line between Bus 12 and Bus 13. The fault is cleared by tripping of the faulted line 12-13. The performance of the proposed PSSs is compared to that of the original under sub-synchronous operation of WECS. The power angles compared to G2 under different cases are shown in Fig. 4.6. Transient stability simulation confirms that the system with the proposed coordinated PSS reaches steady state in the shortest time.

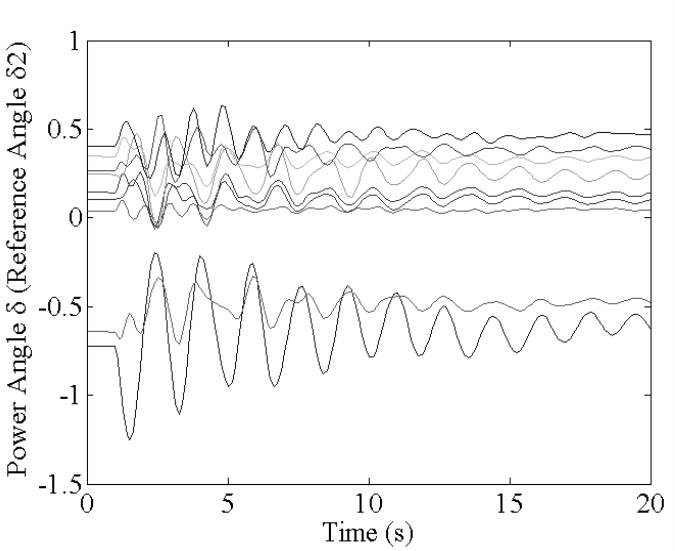

a. PSSs without coordination

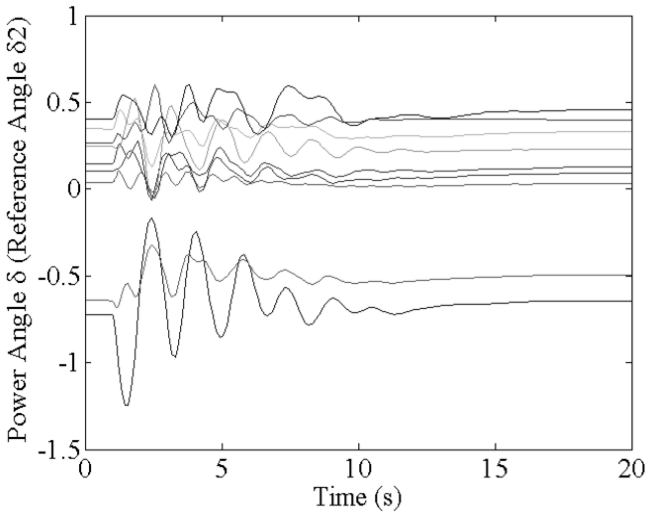

b. PSSs coordinated at maximum output

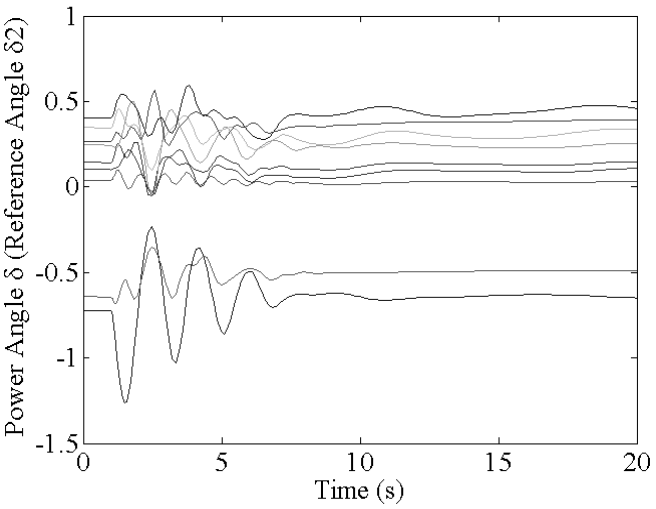

c. PSSs coordinated by proposed method

Fig. 4.6 Transient response of generators (WECS operates under sub-synchronous mode)

Besides, transient responses of WECS operating in sub-synchronous with or without proposed PSS are compared in Fig. 4.7. As shown in Fig. 4.7a, while active power output drops in both conditions, extra reactive power supply can be obtained from WECS to prevent voltage collapse after the fault (Fig. 4.7b). Fig. 4.7c indicates that PSS adds an additional terminal voltage reference signal in voltage control loop, controlling the d-axis rotor current (Fig. 4.7d). WECS has current limiters and their limits are selected depending on the capacity of generators and rating of converter. As shown in Figs. 4.7e and 4.7f, excessive variations of q-axis rotor and stator currents do not occur and then avoid activating the current limiters. The PSS implementation leads to a damping torque which results in slightly increased variation of electrical torque while it is providing damping to the system (Fig. 4.7g). It can be observed from Fig. 4.7h that additional signal will not lead to WECS causing extra loading, i.e. power exchange to the converter rating. After oscillations, WECS can recover to the pre-fault operating state.

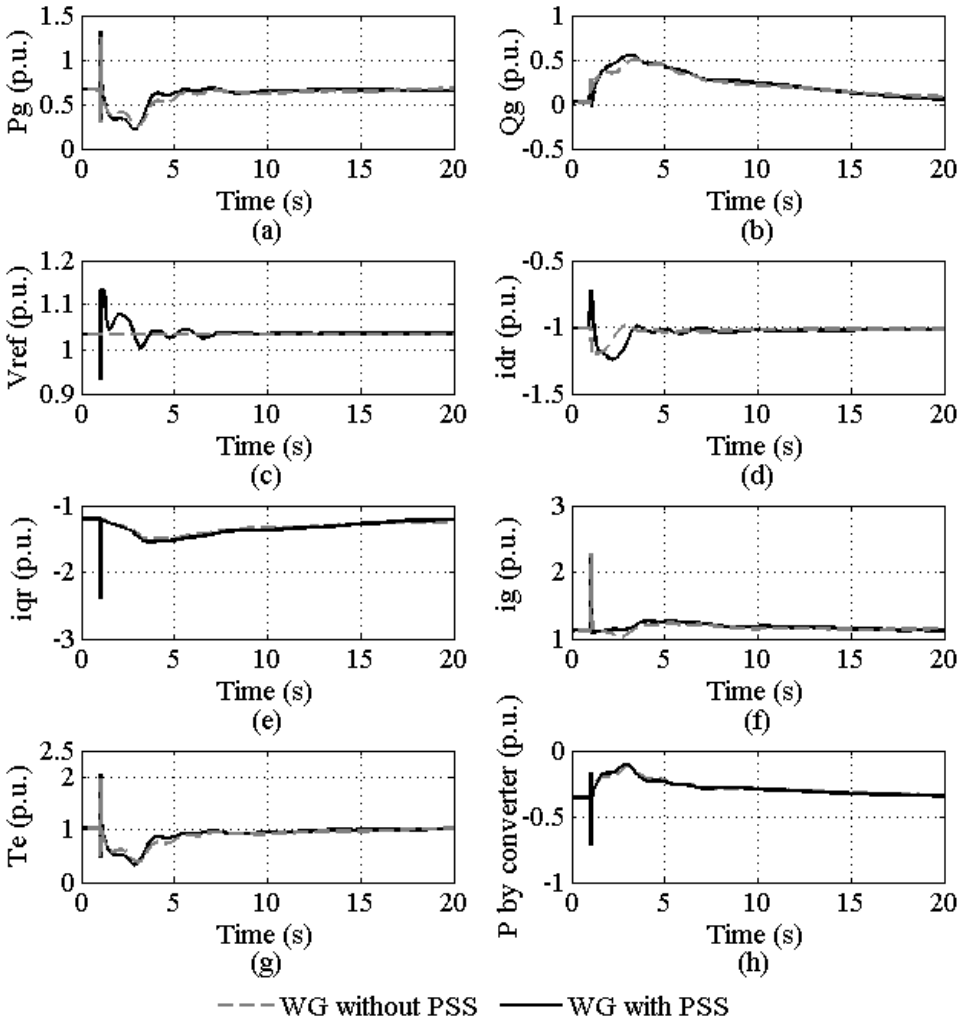

Fig. 4.7 Transient response of WECS

4.5 Summary

The proposed method, based on the probabilistic theory, for coordinating the PSS for DFIG and synchronous generators, has been presented in this chapter. Due to the stochastic characteristic of wind farm output, the system operates under varying conditions. Eigenvalue distribution (PDF or CDF) can be obtained by extended probabilistic SSSA, while considering this stochastic characteristic. Then considering the real part and damping ratio of some lightly-damped

oscillation modes, the objective function and the optimization problem can be established. PSO is used to search the best combination of PSS parameters; computational results and time-domain simulations have proven the efficiency of the proposed method.

This chapter demonstrates that the proposed damping control scheme can consistently enhance network damping with synchronous machines and DFIG-based wind power generation over a range of operating conditions, including sub-synchronous and super-synchronous operating states, depending upon whether the wind farm has encountered light or adequate wind speeds. Application of the proposed method can avoid difficulties of forecasting wind speed accurately. It is also worth recognizing that DFIG can provide an effective network damping control with conventional power generators.

Chapter 5 Quasi-Monte Carlo Based Probabilistic Small Signal Stability Analysis for Power Systems with Plug-in Electric Vehicle and Wind Power Integration

5.1 Introduction

This chapter presents a new QMC based PSSSA method to assess the dynamic effects of PEVs and WECSs in power systems. The detailed dynamic model of PEVs is first proposed for stability study. To account for the stochastic behavior of PEVs and WECSs in load flow studies, the randomized model and PDF representing their nodal power injections are developed. Then with these models, their stochastic injections are sampled by Sobol sequences and the distribution of system eigenvalues can then be obtained by the PSSSA. The proposed QMC-based PSSSA is tested on the modified New England 10-generator 39-bus system. Results show the necessity of modeling of PEVs and WECSs, and efficiency of the proposed QMC is also validated.

5.2 Dynamic Models of PEVs and DFIG-Based WECS

5.2.1 Plug-in Electric Vehicle

The model for a PEV is divided into three parts: the rectifier of the PEV charger, a decoupled controller and the battery of PEV.

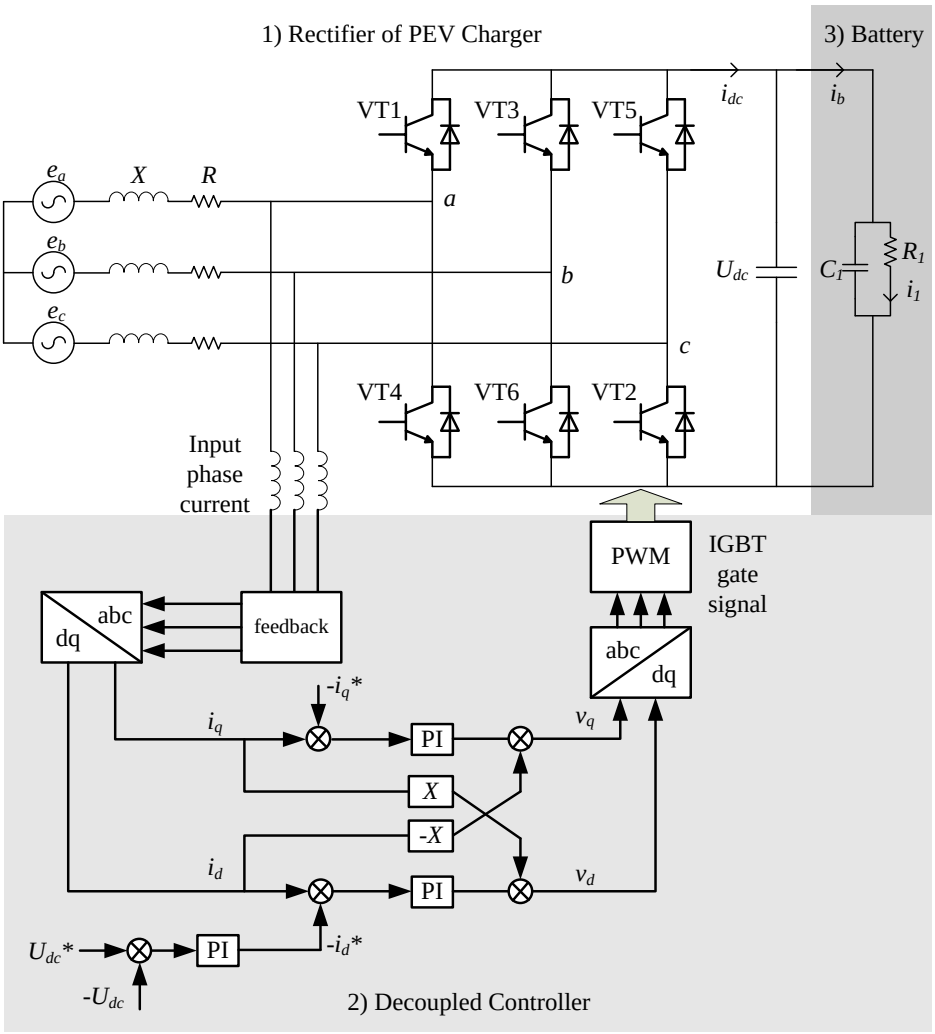

Fig. 5.1 Circuit and control of PEV charger

5.2.1.1 Rectifier of PEV Charger

The voltage-source type pulse-width modulation (PWM) rectifier is illustrated in Fig. 5.1. Here, e_a, e_b and e_c represent the source voltages and R and

X are resistance and reactance, respectively. The system differential equations in *d-q* axis are as follows:

$$\begin{cases} e_d = v_d + Ri_d - Xi_q \\ e_q = v_q + Ri_q + Xi_d \end{cases} \tag{5.1}$$

$$CU_{dc}\frac{dU_{dc}}{dt} + U_{dc}i_b = \frac{3}{2}(v_d i_d + v_q i_q) \tag{5.2}$$

where e_d, e_q and i_d, i_q denote input voltages and input currents in the synchronous rotating frame (SRF) and v_d, v_q are the controlled inputs, denoted by average voltage at the rectifier input in the SRF. Eq. (5.2) represents the power balance between the dc side and the ac side of the rectifier and i_b is the input current of battery. Therefore, the model of the rectifier is represented by (5.1) and (5.2) [Yin, 2009].

5.2.1.2 Decoupled Controller

Due to the strong coupling in the three-phase source, a decoupled control scheme is applied. The controllers in Fig. 5.1 are realized based on the direct current control (DCC) algorithm [Bai, 2011]. First, the magnitude and phase angle of the three-phase alternating current need to be measured directly; second, a *d-q* transformation is used to get the decoupled variables; third, the two decoupled variables are controlled by typical proportional-integral (PI) controllers, as follows:

$$\begin{aligned} i_d^* &= K_{P1}(U_{dc}^* - U_{dc}) + \frac{K_{I1}}{s}(U_{dc}^* - U_{dc}) \\ v_d &= Xi_q + K_{P2}(i_d - i_d^*) + \frac{K_{I2}}{s}(i_d - i_d^*) \\ v_q &= -Xi_d + K_{P3}(i_q - i_q^*) + \frac{K_{I3}}{s}(i_q - i_q^*) \end{aligned} \tag{5.3}$$

where i_d^* and i_q^* are the reference values for the decoupled current variables, i_q^* is zero for unity power factor control; U_{dc}^* is the reference value for dc side voltage; K_{Px} and K_{Ix} are gains in PI controllers. And finally the inverse *d-q* transformation is applied based on the controller output and then PWM to generate the IGBT gate signals for the rectifier.

5.2.1.3 Battery of PEVs

An accurate battery model is to reflect the chemical reaction inside, which is highly nonlinear [Zhang, 2010]; also, the model should indicate characteristics of battery performance with varied temperature. In SSSA, the model should comprehensively reflect the dynamic characteristics of battery. Therefore, a third-order model of lead-acid batteries has been developed and validated for analysis of electrical system in [Ceraolo, 2001].

$$\frac{di_1}{dt} = \frac{1}{C_1 R_1}(i_b - i_1) \tag{5.4a}$$

$$\frac{dQ_e}{dt} = -i_b \tag{5.4b}$$

$$\frac{d\theta}{dt} = \frac{1}{C_\theta}[P_s - \frac{(\theta - \theta_a)}{R_\theta}] \tag{5.4c}$$

where i_1 is current flowing in the resistor R_1 and C_1R_1 is time constant in (5.4a); in (5.4b), Q_e is the extracted charge; in (5.4c) θ is electrolyte temperature, θ_a is ambient temperature, C_θ and R_θ are the battery thermal capacitance and resistance, and P_s is the thermal power generated internally in the battery.

5.2.2 DFIG-Based WECS

The DFIG is controlled by the bidirectional converter, which can be divided into GSC and RSC. The GSC keeps the dc link voltage constant. RSC realizes the decoupled control of rotor speed ω_r and terminal voltage v_s, by series PI controllers. Dynamics of the DFIG can be represented by a third-order model and has been widely used for stability analysis, including transient response of decoupled voltage behind transient reactance e_d and e_q, and electromagnetic torque. Detailed descriptions can be referred to Chapter 3, Section 3.2.

5.3 Randomized Model for Nodal Injection

Randomized models of nodal injections, including thermal plants, load demands, WECSs and PEVs and loads are developed in this section for QMC simulation. Different types of PDF are determined to represent all kinds of power injections.

5.3.1 Thermal Plant and Load

Nodal injections from thermal plants and loads are regards as having normal distribution [Chung, 2003]:

$$P = \mu_P + \sqrt{2} \cdot \sigma_P \cdot erf^{-1}(2r-1) \tag{5.5}$$

where μ_P is expectation selected from data of base case and σ_P is standard deviation, erf^{-1} is the inverse error function and r is uniformly distributed variable. Reactive power of thermal plant and load have similar representation.

5.3.2 Charging Station for PEVs

For a 400V/63A charger, the power demand and related battery state-of-charge of t PEV is shown in Fig. 5.2. In order to determine the power demand of PEVs charging, the initial SOC of PEV is required.

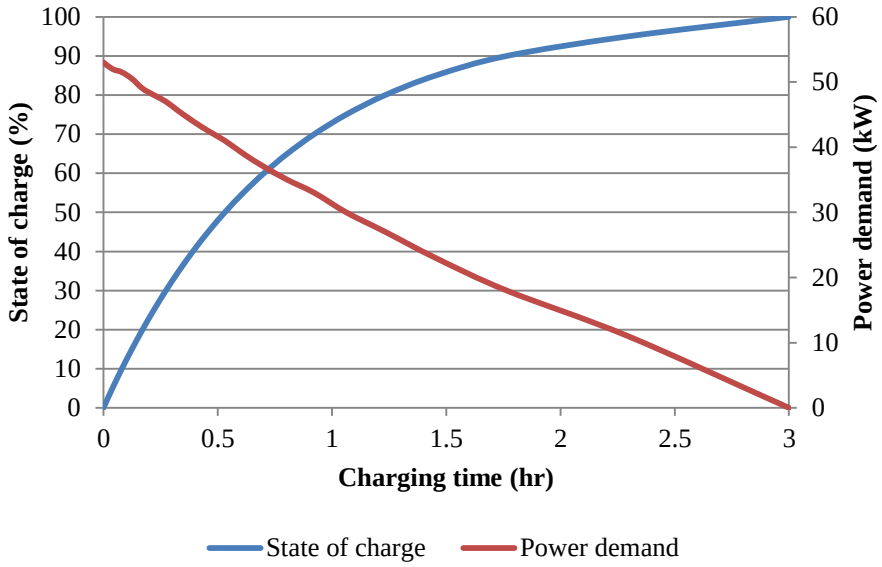

Fig. 5.2 Charging characteristic of PEV

According to the general information of vehicles, the probability distribution of daily driving distance D (in miles) is assumed to have normal distribution and its PDF can be expressed as:

$$f(D|\mu,\sigma)=\frac{1}{\sqrt{2\pi}\sigma}e^{-\frac{(D-\mu)^2}{2\sigma^2}} \tag{5.6}$$

where μ is expectation value and σ is standard deviation; their typical values are 54.1 miles and 15.2 miles, respectively. As normal distribution has tail parts which produce unreasonable values for our study, to avoid this possibility, D have been restricted in the range of zero and maximum distance D_{max}.

Second, assuming that the SOC of battery declines with increase in traveling

distance, with a linear relation, then SOC at the beginning of a recharge cycle can be assessed by [Qian, 2011]:

$$\mathrm{SOC} = (1 - \frac{D}{D_{\max}}) \times 100\% \tag{5.7}$$

where a typical value for D_{max} is 80 miles.

Third, PEVs may arrive at the charging station at different times. In other words, the serviced time t_s of each customer is equal to the time after arrival, which follows exponential distribution with mean T_μ [Li, 2012].

$$f(t_s \mid T_\mu) = \frac{1}{T_\mu} e^{-\frac{t_s}{T_\mu}} \tag{5.8}$$

where T_μ is selected as 1 hour.

Fourth, as the initial value of SOC and the serviced time t_s are determined, instant power demand $P_{EV,i}$ from the network can be obtained in accordance with the charging characteristic (Fig. 5.2).

Finally, total effect of all PEVs in the charging station should be discussed. The number of customer arrivals follows Poisson distribution with expected value λ_μ (900 if the charging station can accommodate a maximum number of 1,000 customers, as an example) and the PDF can be formulated as [Vlachogiannis, 2009]:

$$p(N \mid \lambda_\mu) = \frac{\lambda_\mu^N}{N!} e^{-\lambda_\mu} \tag{5.9}$$

where N is actual number of PEVs in service.

Demand of each PEV can be calculated by (5.7) to (5.9) and demand curve of the charger in Fig. 5.2. The instant power demand of a charging station is the

sum of all PEVs' demand. Total demand distribution is then fitted by a normal distribution. Fig. 5.3 shows comparison of the fitted curve and the original samples. Therefore, similar to thermal plant, the total power demand of a charging station can be obtained by (5.5), according to μ_P and σ_P values of the fitted curve.

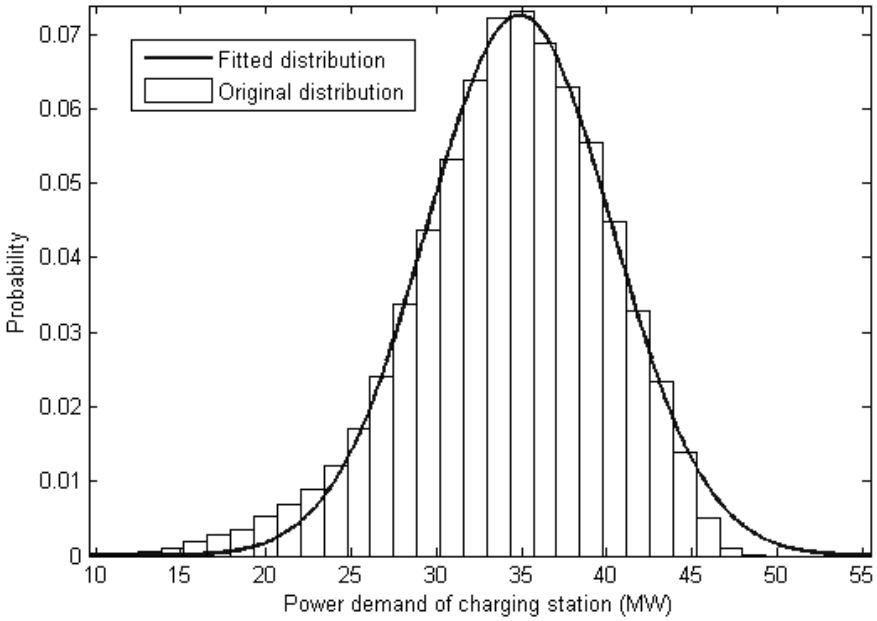

Fig. 5.3 Comparison of original and fitted distribution

5.3.3 Wind Farm

Commonly Weibull distribution is used to describe wind speed probability distribution, by shape and scale parameters [Jain, 2011]. Therefore, PDF of wind speed can be obtained by (5.10), as follows:

$$f(V_w) = \frac{k}{c}\left(\frac{V_w}{c}\right)^{k-1} e^{-\left(\frac{V_w}{c}\right)^k}, \quad V_w > 0 \tag{5.10}$$

where V_w is wind speed, constants k and c are shape and scale parameters, respectively, of Weibull distribution. Then power output of a WECS or a wind

farm, equivalent to one WECS, can be determined by the power curve in (5.11), which is a cubic mathematical model with adequate goodness-of-fit [Huang, 2012]. Therefore, distribution of the wind farm's nodal injection can be calculated by (5.10) and (5.11).

$$P=\begin{cases} 0, & (0<V_w<V_{ci}, V_w>V_{co}) \\ P_{rated}\cdot(a_1V_w^3+a_2V_w^2+a_3V_w+a_4), & (V_{ci}\le V_w\le V_{rs}) \\ P_{rated}, & (V_{rs}\le V_w\le V_{co}) \end{cases} \tag{5.11}$$

where P_{rated} is the rated power, V_{ci} denotes cut-in speed, V_{rs} is rated speed, V_{co} denotes cut-off speed and a_i are regression constants identified by curve fit tools.

5.4 Quasi-Monte Carlo Based Probabilistic Small Signal Stability Analysis

5.4.1 Sobol Sequences in Quasi-Monte Carlo Simulation

QMC simulation is the traditional MCS but using deterministic sequences, i.e. low discrepancy sequences (LDS), instead of pseudorandom numbers. The overall idea is to fill the multi-dimensional unit hypercube with points that are as geometrically and homogeneously equidistant as possible, rather than random sampling. These sequences are used to sample representative data from the inversed CDF of variables that are simulated in the specified problem, as illustrated in Fig. 5.4.

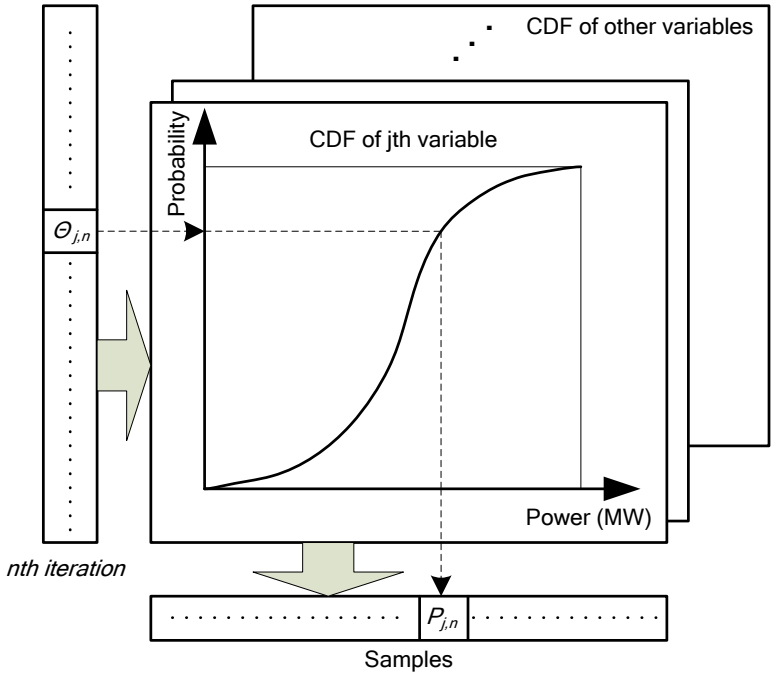

Fig. 5.4 Sampling procedure by QMC

The concept of low discrepancy is associated with the property that successive numbers are added in a position as far away as possible from other numbers, to avoid clustering. This is the main challenge for LDS in handling high-dimensional problems. Halton, Faure and Sobol are the best known LDSs. Halton sequences become unsatisfactory after dimension 14; Faure sequence sampling is slower than Halton and Sobol sequences and suffers degradation at approximately 25 dimensions problem; in Sobol sequence, there is a computational time advantage due to the shorter cycle length, and it outperforms both Faure and Halton sequences for large dimensions problems.

Sobol sequence uses base 2 for all dimensions and starts using van der Corput sequence to represent any decimal number *n* [Fox, 1999]:

$$n = \sum_{k=1}^{M} a_k(n) \cdot 2^k \tag{5.12}$$

where M is the lowest integer that makes $M \geq \log_2(n)$, $a_k(n)$ is either 0 or 1. To generate the nth point in a Sobol sequence, a primitive polynomial of some degree needs to be chosen as $F=x^d+h_1x^{d-1}+h_2x^{d-2}+\ldots+h_{d-1}x+1$, where h_j (j=1,2,…,d-1) is either 0 or 1 and integer d should be selected for solving problems with different dimensions, according to the matching table. A sequence of positive integer m_k (k=1,2,…,M, $M>d$) are defined by the recurrent relation:

$$m_k = 2h_1 m_{k-1} \oplus 2^2 h_2 m_{k-2} \oplus \cdots \oplus 2^d m_{k-d} \oplus m_{k-d} \tag{5.13}$$

where $\oplus$ is the bit-by-bit exclusive-or operator. The initial value m_1, m_2,… can be chosen freely, such that each m_k ($1 \leq k \leq d$) is odd and less than 2^k. The nth point in a Sobol sequence is given by

$$\Theta(n) = a_1(n)v_1 \oplus a_2(n)v_2 \oplus \cdots \oplus a_k(n)v_k \tag{5.14}$$

where v_k (k=1,2,…,M) is the so-called direction number and is equal to $m_k/2^k$.

For a general problem with multi-dimensions, different primitive polynomials F are chosen for the dimension of each case, and Sobol sequences for each case can also be obtained. For the simulation study reported in Section 5.5, there are maximum 55 dimensions, d is chosen as 10 to contain 60 (>55) primitive polynomials for producing sequences according to the matching table [Fox, 1999]. To avoid high-dimensional cluster problem, after producing the low discrepancy points, two procedures are accessed before use in QMC simulations:

a) Skipping: dismiss the length l of contiguous points in the original sequences, this is can be simply achieved by using an alternative start point l+1 on each sequence (e.g., producing vector as $\Theta_{j,l+1}$, $\Theta_{j,l+2}$, …);

b) Leaping: fetch each point with a reasonable interval l from the original sequences (e.g., producing vector as $\Theta_{j,l+1}$, $\Theta_{j,2l+1}$, …).

5.4.2 Probabilistic Small Signal Stability Analysis

After nodal injections are prepared by the sampler in QMC, the load flow analysis is performed to determine the steady state of variables for linearized system models. Fast decoupled load flow (FDLF) [Stott, 1974] method is employed. In our study, PEV is considered as PQ bus with zero reactive power consumption and wind farm as PV bus. Then, the state matrix of the power system is formed by linearized model of each component, including synchronous generators with models in [Kundur, 1994], PEVs and WECSs introduced in Section 5.2. After formulation of state-space equations, eigenvalues λ_i and corresponding left/right eigenvectors Φ_i/Ψ_i can be obtained.

Right eigenvector Φ_i of ith mode gives the mode shape, its angle element gives the phase displacements of state variables (rotor speed $\Delta\omega_k$ in this chapter) with regard to the mode and thus groups of dominators against each other can be revealed. Participation factor (PF), i.e. $PF_{ki}=\Phi_{ki}\cdot\Psi_{ik}$ is a measure of the relative participation of the kth state variable in the ith mode, and vice versa. In this chapter, the joint application of normalized PF_{ki} and angle of Φ_{ik} have been used to determine eigenvalues for specified modes.

When the conjugate eigenvalue $\lambda_i=\alpha_i\pm j\omega_i$ belonging to ith mode is obtained, its damping ratio in (5.15) is used to evaluate the degree of stability:

$$\varsigma_i = \frac{-\alpha_i}{\sqrt{\alpha_i^2 + \omega_i^2}} \times 100\% \tag{5.15}$$

As ς_i is selected as a variable computed by QMC-based PSSSA, CDF of ς_i $F(\varsigma_i)$ will be acquired. Refer to [Rueda, 2009], probabilistic eigenvalue index S_i is formed according to $\varsigma_{i,s}$, where $\varsigma_{i,s}$ is an predefined damping threshold. Distribution of specified modes can be displayed by different fractions: 1) Negative damping or unstable; 2) Lightly damped; 3) Satisfied damped, the relative probability is given by (5.16) respectively:

$$S_i = \begin{cases} S_{i,ND} = F\left(\varsigma_i \mid \varsigma_i \le 0\right) \\ S_{i,LD} = F\left(\varsigma_i \mid 0 \le \varsigma_i \le \varsigma_{i,s}\right) \\ S_{i,SD} = F\left(\varsigma_i \mid \varsigma_i \ge \varsigma_{i,s}\right) \end{cases} \times 100\% \tag{5.16}$$

These indices directly reflect the degree of stability and instability of oscillation modes in the system.

5.4.3 Procedures

The proposed method can be executed following:

Step 1) Data of nodal injections are completely sampled by Sobol sequences in QMC;

Step 2) Acquire one set of nodal injections for each iteration (in MCS-based PSSSA, data will be sampled by pseudorandom sequences randomly);

Step 3) Magnitude and phase of nodal voltage are calculated by FDLF, and form the network admittance matrix;

Step 4) Initial (or steady state) values of devices variables are computed, proposed dynamic models in Section 5.2 are applied to formulate the system state-space matrix;

Step 5) Eigenvalues λ_i and left/right eigenvectors Ψ_i/Φ_i can be obtained and identified for further analysis;

Step 6) Go back to *Step 2)* until iterations are finished, otherwise go to *Step 7)*;

Step 7) Real and imaginary parts of eigenvalues, α_i and ω_i are handling by (5.15) and (5.16) according to selected damping threshold $\varsigma_{i,s}$.

5.5 Case Study

5.5.1 Test System

The proposed methodology is applied on the New England ten-generator 39-bus system, which is widely used in small signal stability study. The diagram and data for this system are taken from [Padiyar, 1996]. Damping enhancement by power system stabilizers (PSS) is neglected here and loads are modeled as constant impedances. As nodal injections are considered as variables, data with a total of 55-dimensions and 10,000-iterations are advance sampled by QMC for scenarios used in Section 5.5.2. The programs are run on a PC with Intel Core2 2.4GHz CPU and 2GB RAM.

5.5.2 Probabilistic Small Signal Stability Analysis

5.5.2.1 Scenario 1: without new establishments

In Scenario 1, assessment is conducted to provide referenced results for identifying dynamic effects from the new establishments. The QMC-based PSSSA is applied to investigate the variation from thermal plants and loads by (5.5).

There are 9 oscillation modes in the system, and related information is listed in Table 5.1.

Table 5.1 Electro-mechanical modes properties

No.	Model type	Mean frequency (in rad/s)	Dominated generators
1	Local mode 1	8.4577	G6⇔G7
2	Local mode 2	8.4774	G1⇔G8
3	Local mode 3	8.6084	G4⇔G5
4	Local mode 4	7.0883	G2⇔G3
5	Local mode 5	7.0413	G1⇔G8⇔G9
6	Local mode 6	7.0869	G4, 5⇔G6, 7
7	Inter-area mode 1	6.1768	G2, 3⇔G4, 5, 6, 7
8	Inter-area mode 2	6.0066	G2 ,3⇔G4, 5, 6, 7⇔G1, 8, 9
9	Inter-area mode 3	3.6845	G2, 3⇔G4, 5, 6, 7⇔G1, 8, 9⇔G10

To illustrate the impacts of the proposed models, ratio of 3% is selected as a damped threshold used in (5.16). The overall stability performance is determined by QMC-based PSSSA (Table 5.2). It can be found that except the system inter-area mode 3, which involves all generators in this system, rest of the modes are almost entirely stable.

Table 5.2 Probabilistic eigenvalue indices

No.	Scenario 1			Scenario 2			Scenario 3		
	$S_{i,ND}$	$S_{i,LD}$	$S_{i,SD}$	$S_{i,ND}$	$S_{i,LD}$	$S_{i,SD}$	$S_{i,ND}$	$S_{i,LD}$	$S_{i,SD}$
1	0	48.1	51.9	0	49.8	50.2	24.9	63.1	12.0
2	0	100	0	0	100	0	0	100	0
3	0	77.9	22.1	0	77.2	22.8	25.2	74.8	0
4	0	100	0	0	100	0	1.6	98.4	0
5	0	100	0	0	100	0	3.4	96.6	0
6	0	99.6	0.4	0	99.7	0.3	31.3	54.6	14.1
7	3.7	96.3	0	3.0	97.0	0	8.0	92.0	0
8	0	100	0	44.2	55.8	0	7.5	92.5	0
9	74.9	25.1	0	100	0	0	25.5	74.5	0

5.5.2.2 Scenario 2: with wind farms and PEVs modeled as constant power load

In Scenario 2, three wind farms consisting of 100×2MW DFIG-based WECS are integrated at bus 27, 28 and 29 in the test system. And five charging stations for PEVs, including 1000×400V/63A chargers are connected at bus 22 to 26. The penetration rates of WECS and PEVs are around 10% and 5%, respectively. Firstly, in this scenario, the dynamic model of PEV is represented by a constant power load in the PSSSA.

Similarly, results from the proposed method are obtained and listed in Table 5.2. It can be noted that inter-area mode 2 and 3 are obviously getting worse in this scenario. In this interconnected power system, power loading of the tie-lines between different areas has been increased by the new establishments. Thus, inter-area mode oscillations become more active in the stressed system in Scenario 2.

5.5.2.3 Scenario 3: with wind farms and detailed PEVs model

In Scenario 3, the original system is also with new establishments mentioned in Scenario 2. Here, the dynamic model of PEVs is represented by the detailed one proposed in Section 5.2.

It can be found that unlike previous results in the two scenarios, just three inter-area modes have disparate degrees of instability. In this scenario, all oscillation modes except local mode 2 demonstrate different degrees of possibility of being unstable. Therefore, PEVs with dynamic behavior can be marked as devices with negative damping effects, which has been illustrated. Moreover, referring to Scenario 2, the proposed detailed model can simulate the impacts of PEVs in PSSSA but constant power load model cannot.

5.5.3 Individual Analysis of PEV Model

In order to further clarify the causes of negative damping efforts from PEV, individual SSSA is taken in the proposed detailed model. Assuming that the charging station is fully-loaded with maximum number of customers, all PEVs begin with zero SOC (to achieve the maximum load demand condition). Then eigenvalues and PFs of all modes are obtained in Table 5.3.

Table 5.3 Oscillation modes of PEV

Mode No.	Eigenvalue	Participation factor
1	0.3792 ±4.3350i	U_{DC}, i_d^*
2	-166.12 ±7.8075i	i_d, i_q
3	-0.0002	i_1
4	-0.0000926	θ

It can be seen that the low frequency oscillation mode, mode 1 with negative damping (-8.7% by (5.15)) which appeared in this analysis, is associated with dc voltage controller This is consistent with results in Section 5.5.2 above that controlling dc voltage to be constant over a fixed load causes instability to the system. The other mode with conjugate eigenvalues is the controller mode, with adequate damping and does not affect the system.

5.5.4 Comparison of QMC and MCS

First the real part α_i of all modes in Scenario 1 is selected as data. The errors calculated by (5.17) and (5.18) are adopted to indicate the accuracy of random variables in the problem.

$$\varepsilon_{x,\alpha_i} = \left| \frac{x_{\alpha_i,simulative} - x_{\alpha_i,correct}}{x_{\alpha_i,correct}} \right| \times 100\% \tag{5.17}$$

$$\bar{\varepsilon}_{x,\alpha} = \frac{1}{z} \sum_{i=1}^{z} \varepsilon_{x,\alpha_i}, z = 9 \tag{5.18}$$

In (5.17), x are μ, σ, s and k, denoting expectation, standard deviation, skewness and kurtosis respectively, which are the measures of probability distribution have been widely used. The results from MCS-based PSSSA with enough time of iterations (50,000 here), are assumed to the correct values $x_{\alpha i,correct}$. Finally, the average errors by (5.18) are defined to indicate the rate of convergence of random variables in the whole system.

As data of MCS-based PSSSA are sampled randomly by pseudorandom sequences, the errors are illustrated as a range with minimum and maximum

values but results of QMC-based PSSSA are totally deterministic. In Table 5.4, indices show that with an identical number of iterations, which are relative small but good in observing the convergent rate [Yu, 2009], PSSSA based on QMC can provide more reliable results than MCS-based one which can be concluded.

Table 5.4 Computation error comparison

Indices (%)	Sample size	MCS-based PSSSA		QMC-based PSSSA
		Minimum	Maximum	
$\bar{\varepsilon}_{\mu,\alpha}$	250	1.5986	2.2258	0.9491
	500	0.9142	1.0632	0.7953
	1,000	0.9247	1.4208	0.7737
$\bar{\varepsilon}_{\sigma,\alpha}$	250	4.8625	6.9909	2.7853
	500	2.9641	5.3660	2.5086
	1,000	2.6318	4.4971	3.1315
$\bar{\varepsilon}_{s,\alpha}$	250	48.3534	79.6226	43.8561
	500	31.0411	51.3518	36.1795
	1,000	30.1070	36.8863	29.7711
$\bar{\varepsilon}_{k,\alpha}$	250	13.8221	30.2599	19.0636
	500	12.3088	23.3579	13.9130
	1,000	12.0336	16.8399	11.8529
$\bar{\varepsilon}_{\mu,\varsigma}$	250	3.2258	8.3621	5.2724
	500	2.4509	4.4173	5.5156
	1,000	2.5015	3.9117	2.2266
$\bar{\varepsilon}_{\sigma,\varsigma}$	250	6.4402	20.8749	11.0486
	500	5.2905	13.0155	6.0148
	1,000	3.6140	7.9883	1.8245
$\bar{\varepsilon}_{s,\varsigma}$	250	39.1135	313.0415	78.3527
	500	21.7417	177.6281	45.4231
	1,000	33.5091	111.6761	39.0674
$\bar{\varepsilon}_{k,\varsigma}$	250	15.1995	73.5185	32.6975
	500	13.0632	52.9816	12.8820
	1,000	8.2142	36.1229	13.8514

Fig. 5.5 shows the distribution of real part of mode 5, which also confirms the accuracy and efficiency of proposed method.

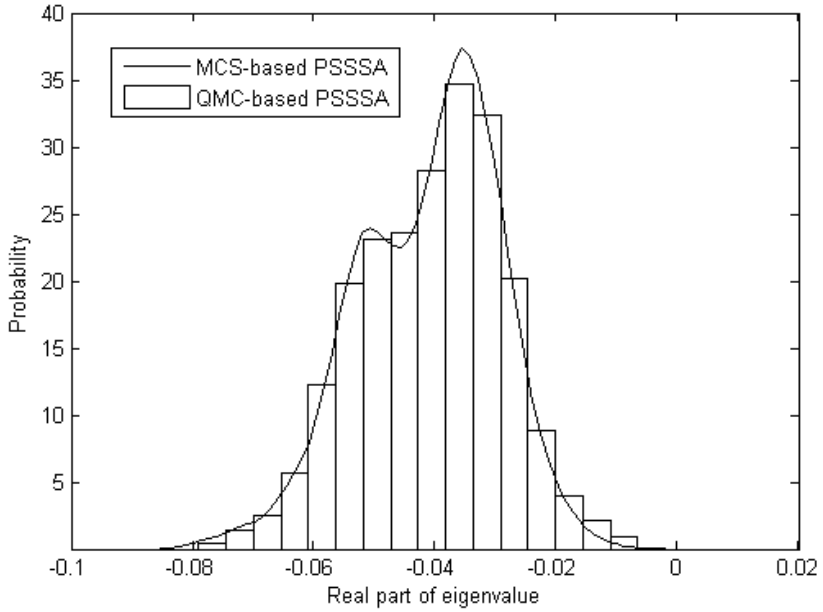

Fig. 5.5 Comparison of MCS and QMC-based PSSSA results. (a. MCS-based PSSSA with sample size N=50,000; b. QMC-based PSSSA with sample size N=250).

Also, another important variables damping ratio ς_i of all the modes in scenario 3 is selected to handle with same procedures. The results listed in Table 5.4 further confirm that QMC is advance over MCS in application with PSSSA.

In the tests, computation time of the two methods did not show a significant gap (Table 5.5). The concerns of complex rules in sampling by Sobol sequences do not increase computational time much over the simulations.

Table 5.5 Computation time comparison (in second)

Sample Size	MCS-based PSSSA	QMC-based PSSSA
N=250	52	54
N=500	114	117
N=1,000	260	253

5.6 Summary

From this chapter, the need for detailed modeling of PEV has been proven by both the different scenarios and individual analysis. The results show that relevant enhancements for stability control are worth further study since more PEVs are likely to come in the future power system.

Compared to other commonly used simulative methods like MCS, this chapter shows the high efficiency of QMC under an identical sampling size, i.e., it obtained a more reliable result with a shorter computational time. This superiority implies that QMC has the potential for use in iterative optimization algorithm with probabilistic problems, which cannot be handled by analytic methods.

Chapter 6 Conclusion and Future Work

6.1 Conclusion

Operating conditions of power systems and the way they are controlled has changed because of increased proportion of renewable energy and PEVs in the systems. This thesis contributes to work on stability and control issues in power systems with renewable energy and fluctuating loads. New methods with advanced intelligent algorithm and probabilistic theory are proposed to enhance the designed damping controller performance and stability of the power system. The following are the conclusions drawn from the work reported in this thesis:

1) Due to the effects of wind shear and tower shadow on mechanical torque of wind turbine, oscillatory behavior in power systems is induced by the WECS itself. By time-domain simulations, the designed controller in SVC with an adaptive theory is shown to have efficiency higher than the conventional lead/lag compensation method.
2) DFIG-based WECS is with high controllable ability and its feasibility of damping enhancement is validated. Advanced optimization algorithms or probabilistic theory are useful approaches to determine the control parameters for enhancing overall system performance.
3) As the proportion of load demand of PEVs in the total demand is increasing, its impact on damping is investigated. The probabilistic

theory is used to extend SSSA and the results reveal that PEVs tend to increase the possibility of instability of power systems. On the other hand, QMC is validated as a sampling tool with higher efficiency compared with pseudorandom MCS. This superiority implies that QMC has the potential for use in iterative optimization algorithm with probabilistic problems, which cannot be handled by analytic methods.

6.2 Future Work

The research work in this thesis is an attempt to develop new methodologies for studying the impact of wind power integration and PEVs. The following issues should be further explored:

1) Charging a large number of PEVs requires large power supply and scheduling wind power is not trivial because of its intermittency. The related coordinated control algorithm is proposed for scheduling PEVs charging and wind power integration. Due to the strong controllability of V2G with bi-directional charger, reasonable scheduling of PEVs charging to accommodate intermittent wind energy should be explored.
2) Measurement and damping control of a power system can be redesigned to achieve better coordination of wind power integration and PEVs and enhance system performance in rotor angle, frequency and voltage stabilities.

Appendix: System Data

Data Format:

Bus.con	Configuration of bus data
SW.con	Configuration of slack generator data
PV.con	Configuration of PV generator data
PQ.con	Configuration of PQ load data
Line.con	Configuration of alternative line data
Syn.con	Configuration of synchronous machine data
Pl.con	Configuration of ZIP load data
Exc.con	Configuration of exciter data
Tg.con	Configuration of turbine governor data
Fault.con	Configuration of fault data
Breaker.con	Configuration of breaker data

Data Format of Each Configuration

Bus.con = [...
1.Bus number 2.Voltage base 3.Voltage amplitude initial guess
4.Voltage phase initial guess];

SW.con = [...
1.Bus number 2.Power rating 3.Voltage rating 4.Voltage magnitude
5.Reference angle 6.Maximum reactive power 7.Minimum reactive power
8.Maximum voltage 9.Minimum voltage 10.Active power guess
11.Loss participation coefficient];

PV.con = [...
1.Bus number 2.Power rating 3.Voltage rating 4.Active power
5.Voltage Magnitude 6.Maximum reactive power 7.Minimum reactive power
8.Maximum voltage 9.Minimum voltage 10.Loss participation coefficient];

PQ.con = [...
1.Bus number 2.Power rating 3.Voltage rating 4.Active power
5.Reactive power 6.Maximum voltage 7.Minimum voltage];

Line.con = [...
1.From bus 2.To bus 3.Power rating 4.Voltage rating
5.Frequency rating 6.Resistance 7.Reactance 8.Susceptance];

Syn.con = [...
1.Bus number 2.Power rating 3.Voltage rating 4.Frequency rating

5.Machine model 6.Leakage reactance Armature resistance
7.d-axis synchronous reactance 8.d-axis transient reactance
9.d-axis subtransient reactance 10.d-axis open circuit transient time constant
11.d-axis open circuit subtransient time constant 12.q-axis synchronous reactance
13.q-axis subtransient reactance 14.q-axis open circuit transient time constant
15.q-axis open circuit subtransient time constant 16.Mechanical start time
17.Damping coefficient 18.Speed feedback gain 19.Active power feedback gain
20.Active power ratio at node 21.Reactive power ratio at node
22.d-axis additional leakage time constant 23.First saturation factor
24.Second saturation factor 25.Center of inertia number];

Pl.con = [...
1.Bus number 2.Power rating 3.Voltage rating 4.Frequency rating
5.Conductance 6.Active current 7.Active power 8.Susceptance
9.Reactive current 10.Reactive power 11.Initialize after power flow];

Exc.con = [...
1.Generator number 2.Exciter type 3.Maximum regular voltage
4.Minimum regular voltage 5.Amplifier gain 6.Amplifier time constant
7.Stabilizer gain 8.Stabilizer time constant 9.Field circuit time constant
10.Measurement time constant 11.1st ceiling coefficient 12.2nd ceiling coefficient];

Tg.con = [...
1.Generator number 2.Turbine governor type 3.Reference speed 4.Droop
5.Maximum turbine output 6.Minimum turbine output
7.Governor time constant 8.Transient gain time constant];

Fault.con = [...
1.Bus number 2.Power rating 3.Voltage rating 4.Frequency rating
5.Fault time 6.Clearance time 7.Fault resistance 8.Fault reactance];

Two-Area Four-Machine System

```
Bus.con = [ ...
    1     1    1.06       0;
    2     1   1.045 -0.08692;
    3     1    1.01    -0.222;
    4     1   1.019   -0.1801;
    5     1    1.02   -0.1532;
    6     1    1.07   -0.2482;
    7     1   1.062   -0.2334;
    8     1    1.09   -0.2334;
    9     1   1.056   -0.2609;
   10     1   1.051   -0.2635;
   11     1   1.057   -0.2583;
   12     1   1.055   -0.2632;
   13     1    1.05   -0.2646;
   14     1   1.038    -0.28];

SW.con = [ ...
```

```
   1      100        1      1.06        0        10       -10        0        0      2.32    1];

PV.con = [ ...
   2      100       22         7     1.01         5        -2      1.1      0.9    1;
  11      100       22      7.16     1.03         5        -2      1.1      0.9    1;
  12      100       22         7     1.01         5        -2      1.1      0.9    1;
 101      100      500         0     1.05        99       -99      1.5      0.5    1];

PQ.con = [ ...
   4      100      115      9.76        1      1.05      0.95    0;
  14      100      115     17.67        1      1.05      0.95    0];

Line.con = [ ...
   1   10      100       22       60        0   0.09565         0    0.0167         0        1        0        0;
   2   20      100       22       60        0   0.09565         0    0.0167         0        1        0        0;
   3   20      100      500       60        0     2.174     0.001      0.01    0.0175        1        0        0;
   3  101      100      500       60        0         0     0.011      0.11    0.1925        1        0        0;
   3  101      100      500       60        0         0     0.011      0.11    0.1925        1        0        0;
  10   20      100      230       60        0         0    0.0025     0.025    0.0437        1        0        0;
  11  110      100       22       60        0   0.09565         0    0.0167         0        1        0        0;
  12  120      100       22       60        0   0.09565         0    0.0167         0        1        0        0;
  13  101      100      500       60        0         0     0.011      0.11    0.1925        1        0        0;
  13  101      100      500       60        0         0     0.011      0.11    0.1925        1        0        0;
  13  120      100      500       60        0     2.174     0.001      0.01    0.0175        1        0        0;
 110  120      100      230       60        0         0    0.0025     0.025    0.0437        1        0        0];

Syn.con = [ ...
   1      900       22       60     6      0.2    0.0025       1.8      0.3     0.25        8     0.03      1.7
0.55     0.25      0.4     0.05    13        0         0         0        1        1        0;
   2      900       22       60     6      0.2    0.0025       1.8      0.3     0.25        8     0.03      1.7
0.55     0.25      0.4     0.05    13        0         0         0        1        1        0;
  11      900       22       60     6      0.2    0.0025       1.8      0.3     0.25        8     0.03      1.7
0.55     0.25      0.4     0.05    13        0         0         0        1        1        0;
  12      900       22       60     6      0.2    0.0025       1.8      0.3     0.25        8     0.03      1.7
0.55     0.25      0.4     0.05    13        0         0         0        1        1        0];

Pl.con = [ ...
   4      100      115       60        0       50        0        0        0        0    1;
  14      100      115       60        0       50        0        0        0        0    1];

Exc.con = [ ...
   1    2      2.5     -2.5       46     0.06      0.1        1        0     0.46     0.01   0.0006      0.9;
   2    3       10      -10     7.04     6.67        1        0        0        0        0        0        0;
   3    3        5       -5      200        0        0        0        0        0     0.01        0        0;
   4    2     4.95     -4.9      300     0.01      0.1    0.675        0     1.33     0.01   0.0006      0.9];

Tg.con = [ ...
   1    1        1     0.04        1        0      0.1      0.5        0     1.25        5;
   2    1        1     0.04        1        0      0.1      0.5        0     1.25        5;
   3    1        1     0.04        1        0      0.1      0.5        0     1.25        5;
   4    1        1     0.04        1        0      0.1      0.5        0     1.25        5];

Fault.con = [ ...
   3      100      500       60      0.1      0.2        0        0];
```

New England Ten-Generator 39-Bus system

```
Bus.con = [ ...
   1   1.00   1.048    -0.1646    1 1;
   2   1.00   1.0505   -0.1203    1 1;
   3   1.00   1.0341   -0.1698    1 1;
   4   1.00   1.0116   -0.1838    1 1;
   5   1.00   1.0165   -0.1637    1 1;
   6   1.00   1.0172   -0.1515    1 1;
   7   1.00   1.0067   -0.1892    1 1;
   8   1.00   1.0057   -0.1979    1 1;
   9   1.00   1.0322   -0.1946    1 1;
```

```
   10    1.00   1.0235   -0.1101    1 1;
   11    1.00   1.0201   -0.1243    1 1;
   12    1.00   1.0072   -0.1246    2 1;
   13    1.00   1.0207   -0.1225    3 1;
   14    1.00   1.0181   -0.1511    4 1;
   15    1.00   1.0194   -0.1581    5 1;
   16    1.00   1.0346   -0.1337    6 1;
   17    1.00   1.0365   -0.1510    7 1;
   18    1.00   1.0343   -0.1656    8 1;
   19    1.00   1.0509   -0.0531    9 1;
   20    1.00   0.9914   -0.0777    1 1;
   21    1.00   1.0337   -0.0918    1 1;
   22    1.00   1.0509   -0.0143    2 1;
   23    1.00   1.0459   -0.0178    3 1;
   24    1.00   1.0399   -0.1316    4 1;
   25    1.00   1.0587   -0.0962    5 1;
   26    1.00   1.0536   -0.1182    6 1;
   27    1.00   1.0399   -0.1532    7 1;
   28    1.00   1.0509   -0.0571    8 1;
   29    1.00   1.0505   -0.0089    9 1;
   30    1.00   1.0475   -0.0780    1 1;
   31    1.00   0.9820         0    1 1;
   32    1.00   0.9831    0.0284    2 1;
   33    1.00   0.9972    0.0380    3 1;
   34    1.00   1.0123    0.0129    4 1;
   35    1.00   1.0493    0.0723    5 1;
   36    1.00   1.0635    0.1192    6 1;
   37    1.00   1.0278    0.0220    7 1;
   38    1.00   1.0265    0.1143    8 1;
   39    1.00   1.0300   -0.1913    9 1];

SW.con = [ ...
   31 100.0    1.00   0.98200    0      8.00000   -5.0000 1.1 0.9   2 1];

PV.con = [ ...
   30 100.0    1.00   2.5000    1.0475   8         -5        1.1 0.9 1;
   32 100.0    1.00   6.5000    0.9831   8         -5        1.1 0.9 1;
   33 100.0    1.00   6.3200    0.9972   8         -5        1.1 0.9 1;
   34 100.0    1.00   5.0800    1.0123   4         -3        1.1 0.9 1;
   35 100.0    1.00   6.5000    1.0493   8         -5        1.1 0.9 1;
   36 100.0    1.00   5.6000    1.0635   8         -5        1.1 0.9 1;
   37 100.0    1.00   5.4000    1.0278   8         -5        1.1 0.9 1;
   38 100.0    1.00   8.3000    1.0265   8         -5        1.1 0.9 1;
   39 100.0    1.00   10.000    1.0300   15        -10       1.1 0.9 1];

PQ.con = [ ...
    1 100.0    1.00   0.0000    0.0000   1.1 0.9 1;
    2 100.0    1.00   0.0000    0.0000   1.1 0.9 1;
    3 100.0    1.00   3.2200    0.0240   1.1 0.9 1;
    4 100.0    1.00   5.0000    1.8400   1.1 0.9 1;
    5 100.0    1.00   0.0000    0.0000   1.1 0.9 1;
    6 100.0    1.00   0.0000    0.0000   1.1 0.9 1;
    7 100.0    1.00   2.3380    0.8400   1.1 0.9 1;
    8 100.0    1.00   5.2200    1.7600   1.1 0.9 1;
    9 100.0    1.00   0.0000    0.0000   1.1 0.9 1;
   10 100.0    1.00   0.0000    0.0000   1.1 0.9 1;
   11 100.0    1.00   0.0000    0.0000   1.1 0.9 1;
   12 100.0    1.00   0.0850    0.8800   1.1 0.9 1;
   13 100.0    1.00   0.0000    0.0000   1.1 0.9 1;
   14 100.0    1.00   0.0000    0.0000   1.1 0.9 1;
   15 100.0    1.00   3.2000    1.5300   1.1 0.9 1;
   16 100.0    1.00   3.2900    0.3230   1.1 0.9 1;
   17 100.0    1.00   0.0000    0.0000   1.1 0.9 1;
   18 100.0    1.00   1.5800    0.3000   1.1 0.9 1;
   19 100.0    1.00   0.0000    0.0000   1.1 0.9 1;
   20 100.0    1.00   6.2800    1.0300   1.1 0.9 1;
   21 100.0    1.00   2.7400    1.1500   1.1 0.9 1;
   22 100.0    1.00   0.0000    0.0000   1.1 0.9 1;
   23 100.0    1.00   2.4750    0.8460   1.1 0.9 1;
```

```
   24 100.0     1.00   3.0860     -0.922    1.1 0.9 1;
   25 100.0     1.00   2.2400     0.4720    1.1 0.9 1;
   26 100.0     1.00   1.3900     0.1700    1.1 0.9 1;
   27 100.0     1.00   2.8100     0.7550    1.1 0.9 1;
   28 100.0     1.00   2.0600     0.2760    1.1 0.9 1;
   29 100.0     1.00   2.8350     0.2690    1.1 0.9 1;
   39 100.0     1.00   11.040     2.5000    1.1 0.9 1];

Line.con = [ ...
    1     2    100.00     1.00 60 0    0.00    0.00350    0.04110    0.69870    1.00000    0.00000 0        0.000        0.000;
    1    39    100.00     1.00 60 0    0.00    0.00100    0.02500    0.75000    1.00000    0.00000 0        0.000        0.000;
    2     3    100.00     1.00 60 0    0.00    0.00130    0.01510    0.25720    1.00000    0.00000 0        0.000        0.000;
    2    25    100.00     1.00 60 0    0.00    0.00700    0.00860    0.14600    1.00000    0.00000 0        0.000        0.000;
    2    30    100.00     1.00 60 0    1.025 0.00000    0.01810    0.00000    1.02500    0.00000 0        0.000        0.000;
    3     4    100.00     1.00 60 0    0.00    0.00130    0.02130    0.22140    1.00000    0.00000 0        0.000        0.000;
    3    18    100.00     1.00 60 0    0.00    0.00110    0.01330    0.21380    1.00000    0.00000 0        0.000        0.000;
    4     5    100.00     1.00 60 0    0.00    0.00080    0.01280    0.13420    1.00000    0.00000 0        0.000        0.000;
    4    14    100.00     1.00 60 0    0.00    0.00080    0.01290    0.13820    1.00000    0.00000 0        0.000        0.000;
    5     8    100.00     1.00 60 0    0.00    0.00080    0.01120    0.14760    1.00000    0.00000 0        0.000        0.000;
    6     5    100.00     1.00 60 0    0.00    0.00020    0.00260    0.04340    1.00000    0.00000 0        0.000        0.000;
    6     7    100.00     1.00 60 0    0.00    0.00060    0.00920    0.11300    1.00000    0.00000 0        0.000        0.000;
    6    11    100.00     1.00 60 0    0.00    0.00070    0.00820    0.13890    1.00000    0.00000 0        0.000        0.000;
    7     8    100.00     1.00 60 0    0.00    0.00040    0.00460    0.07800    1.00000    0.00000 0        0.000        0.000;
    8     9    100.00     1.00 60 0    0.00    0.00230    0.03630    0.38040    1.00000    0.00000 0        0.000        0.000;
    9    39    100.00     1.00 60 0    0.00    0.00100    0.02500    1.20000    1.00000    0.00000 0        0.000        0.000;
   10    11    100.00     1.00 60 0    0.00    0.00040    0.00430    0.07290    1.00000    0.00000 0        0.000        0.000;
   10    13    100.00     1.00 60 0    0.00    0.00040    0.00430    0.07290    1.00000    0.00000 0        0.000        0.000;
   10    32    100.00     1.00 60 0    1.07    0.00000    0.02000    0.00000    1.07000    0.00000 0        0.000        0.000;
   12    11    100.00     1.00 60 0    1.006 0.00160    0.04350    0.00000    1.00600    0.00000 0        0.000        0.000;
   12    13    100.00     1.00 60 0    1.006 0.00160    0.04350    0.00000    1.00600    0.00000 0        0.000        0.000;
   13    14    100.00     1.00 60 0    0.00    0.00090    0.01010    0.17230    1.00000    0.00000 0        0.000        0.000;
   14    15    100.00     1.00 60 0    0.00    0.00180    0.02170    0.36600    1.00000    0.00000 0        0.000        0.000;
   15    16    100.00     1.00 60 0    0.00    0.00090    0.00940    0.17100    1.00000    0.00000 0        0.000        0.000;
   16    17    100.00     1.00 60 0    0.00    0.00070    0.00890    0.13420    1.00000    0.00000 0        0.000        0.000;
   16    19    100.00     1.00 60 0    0.00    0.00160    0.01950    0.30400    1.00000    0.00000 0        0.000        0.000;
   16    21    100.00     1.00 60 0    0.00    0.00080    0.01350    0.25480    1.00000    0.00000 0        0.000        0.000;
   16    24    100.00     1.00 60 0    0.00    0.00030    0.00590    0.06800    1.00000    0.00000 0        0.000        0.000;
   17    18    100.00     1.00 60 0    0.00    0.00070    0.00820    0.13190    1.00000    0.00000 0        0.000        0.000;
   17    27    100.00     1.00 60 0    0.00    0.00130    0.01730    0.32160    1.00000    0.00000 0        0.000        0.000;
   19    33    100.00     1.00 60 0    1.07    0.00070    0.01420    0.00000    1.07000    0.00000 0        0.000        0.000;
   19    20    100.00     1.00 60 0    1.06    0.00070    0.01380    0.00000    1.06000    0.00000 0        0.000        0.000;
   20    34    100.00     1.00 60 0    1.009 0.00090    0.01800    0.00000    1.00900    0.00000 0        0.000        0.000;
   21    22    100.00     1.00 60 0    0.00    0.00080    0.01400    0.25650    1.00000    0.00000 0        0.000        0.000;
   22    23    100.00     1.00 60 0    0.00    0.00060    0.00960    0.18460    1.00000    0.00000 0        0.000        0.000;
   22    35    100.00     1.00 60 0    1.025 0.00000    0.01430    0.00000    1.02500    0.00000 0        0.000        0.000;
   23    24    100.00     1.00 60 0    0.00    0.00220    0.03500    0.36100    1.00000    0.00000 0        0.000        0.000;
   23    36    100.00     1.00 60 0    1.00    0.00050    0.02720    0.00000    1.00000    0.00000 0        0.000        0.000;
   25    26    100.00     1.00 60 0    0.00    0.00320    0.03230    0.51300    1.00000    0.00000 0        0.000        0.000;
   25    37    100.00     1.00 60 0    1.025 0.00060    0.02320    0.00000    1.02500    0.00000 0        0.000        0.000;
   26    27    100.00     1.00 60 0    0.00    0.00140    0.01470    0.23960    1.00000    0.00000 0        0.000        0.000;
   26    28    100.00     1.00 60 0    0.00    0.00430    0.04740    0.78020    1.00000    0.00000 0        0.000        0.000;
   26    29    100.00     1.00 60 0    0.00    0.00570    0.06250    1.02900    1.00000    0.00000 0        0.000        0.000;
   28    29    100.00     1.00 60 0    0.00    0.00140    0.01510    0.24900    1.00000    0.00000 0        0.000        0.000;
   29    38    100.00     1.00 60 0    1.025 0.00080    0.01560    0.00000    1.02500    0.00000 0        0.000        0.000;
    6    31    100.00     1.00 60 0    1.07    0.00000    0.02500    0.00000    1.07000    0.00000 0        0.000        0.000];

Breaker.con = [ ...
3          3          100          1          60          1       1.1          100 ];

Fault.con = [ ...
3          100          1          60          1       1.1          0       0.001 ];

Syn.con = [ ...
   39   100.0    1.0    60    3    0.0030    0.00010    0.0200    0.0060    0    7.000    0    0.019    0.008        0    0.700    0  1000.0
0.000    0.00    0    1    1    0.002;
   31   100.0    1.0    60    4    0.035      0.00270    0.2950    0.0697    0    6.560    0    0.2820    0.170      0    1.500    0  60.600
0.000    0.00    0    1    1    0.002;
   32   100.0    1.0    60    4    0.0304    0.000386  0.2495    0.0531    0    5.700    0    0.2370    0.0531    0    1.500    0  70.600
0.000    0.00    0    1    1    0.002;
```

```
   33   100.0   1.0   60   4   0.0295   0.000222  0.2620   0.0436   0   5.690   0   0.2580   0.0436   0   1.500   0  57.200
0.000   0.00   0   1   1   0.002;
   34   100.0   1.0   60   4   0.0540   0.00014   0.6700   0.1320   0   5.400   0   0.6200   0.1320   0   0.440   0  52.000
0.000   0.00   0   1   1   0.002;
   35   100.0   1.0   60   4   0.0224   0.00615   0.2540   0.0500   0   7.300   0   0.2410   0.0500   0   0.400   0  69.600
0.000   0.00   0   1   1   0.002;
   36   100.0   1.0   60   4   0.0322   0.000268  0.2950   0.0490   0   5.660   0   0.2920   0.0490   0   1.500   0  52.800
0.000   0.00   0   1   1   0.002;
   37   100.0   1.0   60   4   0.0280   0.000686  0.2900   0.0570   0   6.700   0   0.2800   0.0570   0   0.410   0  48.600
0.000   0.00   0   1   1   0.002;
   38   100.0   1.0   60   4   0.0298   0.00030   0.2106   0.0570   0   4.790   0   0.2050   0.0570   0   1.960   0  69.000
0.000   0.00   0   1   1   0.002;
   30   100.0   1.0   60   4   0.0125   0.00014   0.1000   0.0310   0   10.20   0   0.0690   0.0310   0   1.500   0  84.000
0.000   0.00   0   1   1   0.002];

Tg.con = [ ...
   1    1    1    0.02    12      3       0.1    0.45    0.00    12.0    50.0;
   2    1    1    0.02    16.24 1.56    0.1    0.45    0.00    12.0    50.0;
   3    1    1    0.02    7.8    1.95    0.1    0.45    0.00    12.0    50.0;
   4    1    1    0.02    7.56   1.9     0.1    0.45    0.00    12.0    50.0;
   5    1    1    0.02    6.12   1.53    0.1    0.45    0.00    12.0    50.0;
   6    1    1    0.02    8.12   2.03    0.1    0.45    0.00    12.0    50.0;
   7    1    1    0.02    6.72   1.68    0.1    0.45    0.00    12.0    50.0;
   8    1    1    0.02    6.5    1.63    0.1    0.45    0.00    12.0    50.0;
   9    1    1    0.02    9.98   2.5     0.1    0.45    0.00    12.0    50.0;
  10    1    1    0.02    3       0.75   0.1    0.45    0.00    12.0    50.0];

Exc.con = [ ...
   1    2    10.5 -10.5    40.00 0.020      0.03    0.1000    0    1.400    0.001    0.0039    1.555;
   2    2    5      -5          6.20 0.050      0.06    0.0500    0    0.410    0.001    0.0039    1.555;
   3    2    5      -5          5.00 0.060      0.08    0.1000    0    0.500    0.001    0.0039    1.555;
   4    2    5      -5          5.00 0.060      0.08    0.1000    0    0.500    0.001    0.0039    1.555;
   5    2    30     -10        40.00 0.020      0.03    0.1000    0    0.785    0.001    0.0039    1.555;
   6    2    5      -5          5.00 0.020      0.08    0.125     0    0.471    0.001    0.0039    1.555;
   7    2    6.5    -6.5      40.00 0.020      0.03    0.1000    0    0.730    0.001    0.0039    1.555;
   8    2    5      -5          5.00 0.020      0.09    0.1260    0    0.528    0.001    0.0039    1.555;
   9    2    10.5 -10.5      5.00 0.020      0.03    0.1000    0    0.500    0.001    0.0039    1.555;
  10    2    5      -5          5.00 0.060      0.04    0.1000    0    0.25     0.001    0.0039    1.555];
```

Reference

Abido M.A., "Optimal design of power-system stabilizers using particle swarm optimization," *IEEE Trans. Energy Convers.*, vol. 17, no. 3, pp. 406-413, Sep. 2002.

Akhmatov Vladislav, *Induction generators for wind power*. Brentwood: Multi-Science, 2005.

Almeida R.G. de, Lopes J.A.P., and Barreiros J.A.L., "Improving power system dynamic behavior through doubly fed induction machines controlled by static converter using fuzzy control," *IEEE Trans. Power Syst.*, vol. 19, no. 4, pp. 1942- 1950, Nov. 2004.

Atwa Y.M., El-Saadany E.F., Salama M.M.A., and Seethapathy R., "Optimal renewable resources mix for distribution system energy loss minimization," *IEEE Trans. Power Syst.*, vol. 25, no. 1, pp. 360- 370, Feb. 2010.

Bai Hua and Mi Chris, *Transients of Modern Power Electronics*. Chichester: Wiley, 2011.

Banzo M. and Ramos A., "Stochastic optimization model for electric power

system planning of offshore wind farms," *IEEE Trans. Power Syst.*, vol. 26, no. 3, pp. 1338- 1348, Aug. 2011.

Barsali Stefano and Ceraolo M., "Dynamical models of lead–acid batteries: implementation issues, " *IEEE Trans. Power Syst*., vol. 17, no. 1, pp. 16-23, Mar. 2000.

Bomfim A.L.B. Do, Taranto G.N. and Falcao D.M., "Simultaneous tuning of power system damping controllers using genetic algorithms," *IEEE Trans. Power Syst.*, vol. 15, no. 1, pp. 163-169, Feb. 2000.

Buller S., Thele M., De Doncker R.W.A.A., and Karden E., "Impedance-based simulation models of supercapacitors and Li-ion batteries for power electronic applications," *IEEE Trans. on Industry Application*, vol. 41, pp. 742-747, May 2005.

Burchett R.C. and Heydt G.T., "Probabilistic methods for power system dynamic stability studies," *IEEE Trans. Power App. Syst.*, vol. PAS-97, no. 3, pp. 695-702, May 1978.

Cai Li-Jun and Erlich I., "Simultaneous coordinated tuning of PSS and FACTS damping controllers in large power systems," *IEEE Trans. Power Syst.*, vol. 20,

no. 1, pp. 294- 300, Feb. 2005.

Carlos F., Gallardo Q., and Ledesma L.P., “Damping of inter-area mode oscillations with high penetration of the Power System in Wind,” in *34th Annual Conference of IEEE Industrial Electronics*, pp. 2137- 2142 , Nov. 2008.

Cartwright P., Holdsworth L., Ekanayake J.B., and Jenkins N., "Co-ordinated voltage control strategy for a doubly-fed induction generator (DFIG)-based wind farm," *IEE Proc.- Generat. Transmiss. Distrib.*, vol. 151, no. 4, pp. 495- 502, Oct. 2004.

Ceraolo M., "New dynamical models of lead–acid batteries," *IEEE Trans. Power Syst*., vol. 15, no. 4, pp. 1184-1190, Nov. 2000.

Chen Chern-Lin and Hsu Yuan-Yih, "Coordinated synthesis of multimachine power system stabilizer using an efficient decentralized modal control (DMC) algorithm," *IEEE Trans. Power Syst.*, vol. 2, no. 3, pp. 543-550, Aug. 1987.

Chen Min and Rincon-Mora G.A., "Accurate electrical battery model capable of predicting runtime and I-V performance," *IEEE Trans. Energy Convers*., vol. 21, no. 2, pp. 504-511, June 2006.

Chung C.Y., Wang K.W., Tse C.T., and Niu R., "Power-system stabilizer (PSS)

design by probabilistic sensitivity indexes (PSIs)," *IEEE Trans. Power Syst.*, vol. 17, no. 3, pp. 688- 693, Aug. 2002.

Chung C.Y., Wang K.W., Tse C.T., Bian X.Y., and David A.K., "Probabilistic eigenvalue sensitivity analysis and PSS design in multimachine systems," *IEEE Trans. Power Syst.*, vol. 18, no. 4, pp. 1439- 1445, Nov. 2003.

Chung C.Y., Wang L., Howell F. and Kundur P., "Generation rescheduling methods to improve power transfer capability constrained by small-signal stability," *IEEE Trans. Power Syst.*, vol. 19, no. 1, pp. 524-530, Feb. 2004.

Cidras J., and Feijoo A.E., "A linear dynamic model for asynchronous wind turbines with mechanical fluctuations," *IEEE Trans. Power Syst.*, vol.17, no.3, pp.681-687, Aug. 2002.

Cidras J., Feijoo A.E., and Carrillo Gonzalez C., "Synchronization of asynchronous wind turbines," *IEEE Trans. Power Syst.*, vol.17, no.4, pp.1162-1169, Nov. 2002.

Das T. and Aliprantis D.C., "Small-signal stability analysis of power system integrated with PHEVs," in *Proc. IEEE Energy 2030 Conf.*, Altanta, GA, Nov. 17-18, 2008, pp. 1-4.

Demuth H. and Beale M., *Neural Network Toolbox User's Guide*. Natick, MA: The Math Works, Inc., 1998.

Dolan D.S.L., and Lehn P.W., "Simulation model of wind turbine 3P torque oscillations due to wind shear and tower shadow," *IEEE Trans. Energy Convers.*, vol. 21, no. 3, pp. 717-724, Sept. 2006.

Eberhart R. and Kennedy J., "A new optimizer using particle swarm theory," in *Proc. 6th Int. Symp. Micromachine and Human Science*, Nagoya, Oct. 1995, pp.39-43.

Ekanayake J.B., Holdsworth L., Wu Xue Guang, and Jenkins N., "Dynamic modeling of doubly fed induction generator wind turbines," *IEEE Trans. Power Syst.*, vol. 18, no. 2, pp. 803- 809, May 2003.

Fadaeinedjad R., Moschopoulos G., and Moallem M., "The impact of tower shadow, yaw error, and wind shears on power quality in a wind–diesel system," *IEEE Trans. Energy Convers.*, vol.24, no.1, pp.102-111, March 2009.

Feng X. and Sun Z., "A battery model including hysteresis for state-of-charge estimation in Ni-MH battery," in *Proc. IEEE Vehicle Power and Propulsion*

Conference (*VPPC*), 2008, pp. 1-5.

Fox Bennett L., *Strategies for Quasi-Monte Carlo*, Massachusetts: Kluwer, 1999.

Gautam D., Vittal V., Harbour T., "Impact of increased penetration of DFIG-based wind turbine generators on transient and small signal stability of power systems," *IEEE Trans. Power Syst.*, Vol.24, no.3, pp. 1426- 1434, Aug. 2009.

Gautam D., Goel L., Ayyanar R., Vittal V., and Harbour T., "Control strategy to mitigate the impact of reduced inertia due to doubly fed induction generators on large power systems," *IEEE Trans. Power Syst.*, vol. 26, no. 1, pp. 214- 224, Feb. 2011.

Gould C.R., Bingham C.M., Stone D.A., and Bentley P., "New battery model and state-of-health determination through subspace parameter estimation and state-observe techniques," *IEEE Trans. Vehicular Technology*, vol. 58, no. 8, pp. 3905-3916, Oct. 2009.

Gurrala G. and Sen I., "Power system stabilizers design for interconnected power systems, " *IEEE Trans. Power Syst.*, vol. 25, no. 2, pp. 1042-1051, Feb. 2010.

Hadley S.W. and Tsvetkova A.A., *Potiential Impact of Plug-in-Hybrid Electric Vehicles on Regional Power Generation*, Minnesota pollution control Agency, March 2007.

Han Sekyung, Han Soohee and Sezaki K., "Development of an optimal vehicle-to-grid aggregator for frequency regulation," *IEEE Trans. Smart Grid*, vol. 1, no. 1, pp. 65-72, June 2010.

Han Sekyung, Han Soohee and Sezaki K., "Estimation of achievable power capacity from plug-in electric vehicles for V2G frequency regulation: case studies for market participation," *IEEE Trans. Smart Grid*, vol. 2, no. 4, pp. 632-641, Dec. 2011.

Heier S., *Grid Integration of Wind Energy Conversion System*. New York: Wiley, 1998.

Holdsworth L., Wu X.G., Ekanayake J.B., and Jenkins N., "Comparison of fixed speed and doubly-fed induction wind turbines during power system disturbances," *IEE Proc.- Generat. Transmiss. Distrib.*, vol. 150, no. 3, pp. 343-352, May 2003.

Huang Huazhang and Chung C.Y., "Coordinated damping control design for

DFIG-based wind generation considering power output variation," *IEEE Trans. Power Syst*., vol. 27, no. 4, pp. 1916-1925, Nov. 2012.

Hughes F.M., Anaya-lara O., Jenkins N., and Strbac G., "Control of DFIG-based wind generation for power network support," *IEEE Trans. Power Syst.*, vol. 20, no. 4, pp. 1958-1966, Nov. 2005.

Hughes F.M., Anaya-lara O., Jenkins N., and Strbac G., "A power system stabilizer for DFIG-based wind generation," *IEEE Trans. Power Syst.*, vol. 21, no. 2, pp. 763-772, May 2006.

Hughes F.M., Anaya-lara O., Ramtharan G., Jenkins N., and Strbac G., "Influence of tower shadow and wind turbulence on the performance of power system stabilizers for DFIG-based wind farms," *IEEE Trans. Energy Convers.*, vol. 23, no. 2, pp. 519-528, June 2008.

Islam F.R., Pota H.R., Mahmud M.A., and Hossain M.J., "Impact of PHEV loads on the dynamic performance of power system, " in *20th Australasian Universities Power Engineering Conference* (*AUPEC*), Dec. 2010, pp. 1-5.

Jain Pramod, *Wind Energy Engineering*. New York: McGraw-Hill, 2011.

Jang J.-S.R., “ANFIS: adaptive-network-based fuzzy inference system,” *IEEE Trans. Systems, Man and Cybernetics*, vol.23, no.3, pp.665-685, May-June 1993.

Karki R., Hu Po, and Billinton R., "Reliability evaluation considering wind and hydro power coordination," *IEEE Trans. Power Syst.*, vol. 25, no. 2, pp. 685- 693, May 2010.

Ke D.P. and Chung C.Y., “An inter-area mode oriented pole-shifting method with coordination of control effects for robust tuning of power oscillation damping controllers”, *IEEE Trans. on Power Syst., accepted*.

Ke D.P., Chung C.Y. and Xue Y., “An eigenstructure-based performance index and its application to control design for damping inter-area oscillations in power systems”, *IEEE Trans. on Power Syst.*, Vol. 26, No. 4, November 2011, pp. 2371-2380.

Kempton W. and Tomi J., "Vehicle-to-grid power implementation: from stabilizing the grid to supporting large-scale renewable energy, " *Journal of Power Sources*, 144(1): 280-294, 2005.

Kennedy J. and Eberhart R., "Particle swarm optimization," in *Proc. IEEE Int. Conf. Neural Network*, vol.4, Perth, Australia, Nov. 1995, pp. 1942-1948.

Kshatriya N., Annakkage U.D., Hughes F.M., and Gole A.M., "Optimized partial eigenstructure assignment-based design of a combined PSS and active damping Controller for a DFIG," *IEEE Trans. Power Syst.*, vol. 25, no. 2, pp. 866-876, May 2010.

Kundur P., *Power System Stability and Control*. New York: McGraw-Hill, 1994.

Larsen E., Chandrashekhara D.K., and Østergård J., "Electric vehicles for improved operation of power systems with high wind power penetration," in *Proc. IEEE Energy 2030 Conf.*, Altanta, GA, Nov. 17-18, 2008, pp. 1-6.

Larsson A., "Flicker emission of wind turbines during continuous operation," *IEEE Trans. Energy Convers.*, vol.17, no.1, pp.114-118, March 2002.

Ledesma P. and Gallardo C., "Contribution of variable-speed wind farms to damping of power system oscillations," *Power Tech, 2007 IEEE Lausanne*, pp. 190-194, July 2007.

Li C.-T., Ahn C., Peng H., and Sun J., "Integration of plug-in electric vehicle charging and wind energy scheduling on electricity grid," in *Proc. IEEE PES Innovate Smart Grid Technologies* (*ISGT*), MI, USA, Jan. 16-20, 2012, pp. 1-7.

Li G. and Zhang Xiao-ping, “Modeling of plug-in hybrid electric vehicle charging demand in probabilistic power flow calculations,” *IEEE Trans. Smart Grid*, vol. 3, no. 1, pp. 492-499, Mar. 2012.

Liu Xian and Xu Wilsun, "Minimum emission dispatch constrained by stochastic wind power availability and cost," *IEEE Trans. Power Syst.*, vol. 25, no. 3, pp. 1705- 1712, Aug. 2010.

Lopez Y.U., Antonio J., and Navarro D., “Small signal stability analysis of wind turbines with squirrel cage induction generators,” in *Transmission and Distribution Conference and Exposition: Latin America, 2008 IEEE/PES*, Aug. 2008.

McSwiggan D., Littler T., Morrow D.J., and Kennedy J., "A study of tower shadow effect on fixed-speed wind turbines," *UPEC 2008*, Padova, Italy, Sept. 2008.

Mendonca A., Lopes J.A.P., “Impact of large scale wind power integration on small signal stability,” *Future Power Systems, 2005 International Conference on*, pp.1-5, 18 Nov. 2005.

Miao Z., Fan L., and Osborn D., “Control of DFIG-based wind generation to

improve interarea oscillation damping," *IEEE Trans. Energy Convers.*, vol. 24, no. 2, pp. 415-422, June 2009.

Milano F., "An open source power system analysis toolbox," *IEEE Trans. Power Syst.*, vol. 20, no. 3, pp. 1199- 1206, Aug. 2005.

Mishra Y., Mishra S., Tripathy M., Senroy N., and Dong Z.Y., "Improving stability of a DFIG-based wind power system with tuned damping controller," *IEEE Trans. Energy Convers.*, vol. 24, no. 3, pp. 650-660, Sept. 2009.

Mishra Y., Mishra S., Li F., Dong Z.Y., and Bansal R.C., "Small-signal stability analysis of a DFIG-based wind power system under different modes of operation," *IEEE Trans. Energy Convers.*, vol. 24, no. 4, pp. 972-982, Dec. 2009.

Mohagheghi S., Venayagamoorthy G.K., and Harley R.G., "Optimal neuro-fuzzy external controller for a STATCOM in the 12-bus benchmark power system," *IEEE Trans. Power Delivery*, vol.22, no.4, pp.2548-2558, Oct. 2007.

National Staticstics, Department for Transport, Transport Statistics Bulletin-National Travel Survey: 2008, Apr. 9, 2009.

Padiyar K. R., *Power system dynamics: stability and control*. Singapore: Wiley,

1996.

Padron J.F.M. and Lorenzo A.E.F., "Calculating steady-state operating conditions for doubly-fed induction generator wind turbines," *IEEE Trans. Power Syst.*, vol. 25, no. 2, pp. 922- 928, May 2010.

Pagola F.L., Perez-Arriaga I.J., and Verghese G.C., "On sensitivities, residues and participations: applications to oscillatory stability analysis and control," *IEEE Trans. Power Syst.*, vol. 4, no. 1, pp. 278-285, Feb. 1989.

Patten J., Christensen N., Nola G., and Srivastava S., "Electric vehicle battery-wind storage system," in *Proc. IEEE Vehicle Power and Propulsion Conference* (*VPPC*), MI, USA, Sept. 6-9, 2011, pp. 1-3.

Qian K., Zhou C., Allan M., and Yuan Y., "Modeling of load demand due to EV battery charging in distribution systems," *IEEE Trans. Power Syst*., vol. 26, no. 2, pp. 802-810, May 2011.

Ramakrishna G., and Malik O.P., "Radial basis function identifier and pole-shifting controller for power system stabilizer application," *IEEE Trans. Energy Convers.*, vol.19, no.4, pp.663 – 670, Dec. 2004.

Rueda J.L., Colome D.G., and Erlich I., “Assessment and enhancement of small signal stability considering uncertainties,” *IEEE Trans. Power Syst.*, vol. 24, no. 1, pp. 198-207, Feb. 2009.

Sanchez-Gasca J.J., Miller N.W., and Price W.W., “A modal analysis of a two-area system with significant wind power penetration,” *Power Systems Conference and Exposition, 2004. IEEE PES*, pp. 1148- 1152 vol.2, 10-13 Oct. 2004.

Sauer P.W. and Pai M.A., *Power system dynamics and stability*. Englewood Cliffs, NJ: Prentice-Hall, 1998.

Shi Y. and Eberhert R., “A modified particle swarm optimization.” In *IEEE World Congress on Computational Intelligence*, 69-73, 1998.

Singhee A. and Rutenbar R.A., “Why quasi-monte carlo is better than monte carlo or latin hypercube sampling for statistical circuit analysis,” *IEEE Trans. Computer-Aided Design of Integrated Circuits and Systems*, vol. 29, no. 11, pp. 1763-1776, Nov. 2010.

Slootweg J.G. and Kling W.L., “The impact of large scale wind power generation on power system oscillations,” *Electric Power Systems Research*, Vol.67, no.1,

pp. 9-20, Oct. 2003.

Stott B. and Alsac O., “Fast decoupled load flow,” *IEEE Trans. Power App. Syst.*, vol. PAS-93, no. 3, pp. 859-869, May 1974.

Strachan Peter A., Toke David, and Lal David, *Wind Power and Power Politics*. New York: Routledge, 2010.

Thiringer T., and Dahlberg J.-A., “Periodic pulsations from a three-bladed wind turbine,” *IEEE Trans. Energy Convers.*, vol.16, no.2, pp.128-133, June 2001.

Tremblay Oliver, Dessaint Louis-A., and Dekkiche Abdel-Illah, "A generic battery model for the dynamic simulation of hybrid electric vehicles, " in *Proc. IEEE Vehicle Power and Propulsion Conference* (*VPPC*), Arlington, Texas, USA, Sept., 2007, pp. 284-289.

Trudnowski D.J., Pierre D.A., Smith J.R., and Adapa A., "Coordination of multiple adaptive PSS units using a decentralized control scheme," *IEEE Trans. Power Syst.*, vol. 7, no. 1, pp. 294-300, Feb. 1992.

Tsourakis G., Nomikos B. M., and Vournas C. D., “Contribution of doubly fed wind generators to oscillation damping,” *IEEE Trans. Energy Convers.*, vol. 24,

no. 3, pp. 783-791, Sept. 2009.

Villanueva D., Pazos J. L., and Feijoo A., “Probabilistic load flow including wind power generation,” *IEEE Trans. Power Syst*., vol. 26, no. 3, pp. 1659- 1667, Aug. 2011.

Vlachogiannis J.G., “Probabilistic constrained load flow considering integration of wind power generation and electric vehicles,” *IEEE Trans. Power Syst*., vol. 24, no. 4, pp. 1808-1817, Nov. 2009.

Vowles D.J., Samarasinghe C., Gibbard M.J., Fellow L., and Ancell G., “Effect of wind generation on small-signal stability-a New Zealand example,” in 2008 *IEEE Power and Energy Society General Meeting*, pp. 1-8, July 2008.

Wang Li and Hsiung Chia-Tien, "Dynamic stability improvement of an integrated grid-connected offshore wind farm and marine-current farm using a STATCOM," *IEEE Trans. Power Syst.*, vol. 26, no. 2, pp. 690- 698, May 2011.

Wang M.Q., and Gooi H.B., "Spinning reserve estimation in micro grids," *IEEE Trans. Power Syst.*, vol. 26, no. 3, pp. 1164- 1174, Aug. 2011.

Yang H.M., Chung C.Y. and Zhao J.H., “Application of plug-in electric vehicles

to frequency regulation based on distributed signal acquisition via limited communication", *IEEE Trans. Power Syst., Early Access*.

Yang N., Liu Q., and McCalley J.D., "TCSC controller design for damping interarea oscillations," *IEEE Trans. Power Syst.*, vol.13, no.4, pp. 1304-1310, Nov. 1998.

Yin B., Oruganti R., Panda S.K., and Bhat A.K.S., "A simple single-input -single-output (SISO) model for a three-phase PWM rectifier," *IEEE Trans. Power Electronics*, vol. 24, no. 3, pp. 620-631, Mar. 2009.

Yin H., Fan L., and Miao Z., "Reactive power modulation for inter-area oscillation damping of DFIG-based wind generation," in *2010 IEEE Power and Energy Society General Meeting*, Minnesota, USA, July 2010.

You Ruhua, Eghbali H.J., and Nehrir M.H., "An online adaptive neuro-fuzzy power system stabilizer for multimachine systems," *IEEE Trans. Power Syst.*, vol.18, no.1, pp. 128 – 135, Feb. 2003.

Yu H., Chung C.Y., Wong K.P. and Zhang J.H., "A chance constrained transmission network expansion planning method with consideration of load and wind farm uncertainties, " *IEEE Trans. Power Syst.*, vol. 24, no. 3, pp.

1568-1576, Aug. 2009.

Yu H., Chung C.Y., Wong K.P., Lee H.W., and Zhang J.H., “Probabilistic load flow evaluation with hybrid latin hypercube sampling and cholesky decomposition,” *IEEE Trans. Power Syst*., vol. 24, no. 2, pp. 661-667, May. 2009.

Zhao B., Guo C.X., and Cao Y.J., "A multi agent-based particle swarm optimization approach for optimal reactive power dispatch," *IEEE Trans. Power Syst.*, vol. 20, no. 2, pp. 1070- 1078, May 2005.

Zhang Hanlei and Chow Mo-Yuen, "Comprehensive dynamic battery modeling for PHEV application," in 2010 *IEEE Power and Energy Society General Meeting*, pp. 1-6, Aug. 2010.

Zhang J.B., Chung C.Y., and Han Y.D., “A novel modal decomposition control and its application to PSS design for damping inter-area oscillations in power systems”, *IEEE Trans. on Power Syst., accepted*.

Zhang P. and Coonick A.H., "Coordinated synthesis of PSS parameters in multi-machine power systems using the method of inequalities applied to genetic algorithms ," *IEEE Trans. Power Syst.*, vol. 15, no. 2, pp. 811-816, May 2000.